EXPERIMENTAL INVESTIGATION OF REPAIR TECHNIQUES FOR DETERIORATED END REGIONS OF PRESTRESSED CONCRETE BRIDGE GIRDERS

by

William B. Rich

A Thesis

Submitted to the Faculty of Purdue University

In Partial Fulfillment of the Requirements for the degree of

Master of Science in Civil Engineering

Lyles School of Civil Engineering

West Lafayette, Indiana

May 2021

THE PURDUE UNIVERSITY GRADUATE SCHOOL

STATEMENT OF COMMITTEE APPROVAL

Dr. Christopher S. Williams, Chair

Lyles School of Civil Engineering

Dr. Robert J. Frosch

Lyles School of Civil Engineering

Dr. Mark D. Bowman

Lyles School of Civil Engineering

Approved by:

Dr. Dulcy Abraham

To all my family and friends.

Those past, present, and yet to come.

ACKNOWLEDGMENTS

To begin, I would like to sincerely thank my advisor, Dr. Christopher Williams, for his unwavering support, unending patience, and exemplary guidance throughout this project. Thank you for providing me the opportunity to work as a research assistant on this project. It has been a pleasure working on this project with you. Your mentorship has not only made me a better engineer, but a better person as well. I would also like to thank Dr. Robert Frosch for helping develop and guide this research project. Your willingness to share your knowledge and expertise was a critical component for the successful completion of this study. I also extend my appreciation to Dr. Mark Bowen for taking the time to serve on my committee and providing valuable research perspectives and knowledge.

I owe a great debt of gratitude to my project partners, Bobby Jacobs and Jon Pevey, who provided me with a solid research foundation to build upon. Their knowledge and assistance were vital to the successful completion of this research. Additionally, it would be remiss of me if I did not thank Dan Mochen and David Derks for all their hard work in assisting me over the course of this experimental program.

I would also like to thank the Indiana Department of Transportation (INDOT), in cooperation with the Federal Highway Administration (FHWA), through the Joint Transportation Research Program (JTRP) for sponsoring this project. Specifically, I would like to extend my deepest gratitude to the members of the Study Advisory Committee: Greg Klevitsky, Jennifer Hart, Jeremy Hunter, Jose Ortiz, Pete White, Prince Baah, and Stephanie Wagner. Thank you for so generously lending your time and expertise, without which, this research could not have been completed.

While at Purdue, I have been incredibly fortunate to learn from, work alongside, and grow close with a great many friends and colleagues including Ahmed Alimran, Andi Vicksman, Ata Taghipour, Eric Fleet, Farida Mahmud, Herta Montoya, Hwa Ching (Dennis) Wang, Jacob Witte, Josh Harmon, Mackenzie Davies, Morgan Broberg, Ryan Whelchel, Sarah Bowlin, Scott Grier, Ting-Wei Wang, Tom Bradt, and Yen-Chen Chiang. Thank you all for the extraordinary patience, mentorship, support, and friendship you provided me along the way. You all played an integral role in the completion of this research, and I wish you good fortune in the wars to come.

The successful completion of this research program required the coordination and support of many departments around the university, especially the staff at Bowen Laboratory. As such, I would like to thank Harry Tidrick, Kevin Brower, and Molly Stetler for their assistance throughout this research initiative.

Words fail to describe how grateful I am for the unbridled love, support, and encouragement of my parents, Karen and Greg Rich. Thank you for always believing in and supporting me; I would never have accomplished my goals without you. I am also eternally thankful for the friendship of my sister, Abby Rich, who provided an everlasting source of joy and love throughout this journey. Lastly, I would like to thank my Wyoming friends and family including Brendan McKinney, Eric Young, Jesse Chavez, Josh Messer, and Ryan Kobbe for their continuing and ever-present support, encouragement, and friendship.

TABLE OF CONTENTS

LIST OF TABLES

LIST OF FIGURES

ABSTRACT

Due to harsh environmental conditions, the deterioration of prestressed concrete bridge girders is a commonly observed phenomenon in Indiana and much of the Midwest. Concordantly, one widely observed damage scenario is deteriorated end regions of prestressed concrete girders. Damaged or failed expansion joints expose prestressed concrete girder end regions to chloride-laden water, resulting in a corrosive environment in which reinforcement section loss and concrete spalling can occur. For bridges experiencing this type of deterioration, action is needed to ensure the structure remains safe and serviceable. As such, an experimental program was developed to investigate the effectiveness of three repair techniques in restoring the structural behavior of prestressed concrete bridge girders with end region deterioration. The three examined repair techniques are (i) an externally bonded fiber reinforced polymer (FRP) system, (ii) a near-surface-mounted (NSM) FRP system, and (iii) a concrete supplemental diaphragm. Additionally, installation procedures for the three end region repair techniques were developed. Results, conclusions, and recommendations from the experimental program are presented to help advise best practices for implementing end region repair techniques in the field.

CHAPTER 1. INTRODUCTION

1.1 Overview

There are over 600,000 bridges in the United States, and a large percentage of these bridges are nearing the end of their 50-year design life according to the American Road and Transportation Builders Association (ARTBA 2020). The average age of a non-deficient bridge is 44 years old while the average age of structurally deficient bridges is 69 years old (ARTBA 2020). As a result, many of these bridges are currently, or soon will be, in need of structural repair or replacement. ARTBA (2020) estimates that 37% of all bridges are currently in need of some type of repair work. While replacing some of these bridges will be necessary, structural repairs are often preferred due to the high economic costs associated with total bridge replacement. The development of efficient and cost-effective repair techniques capable of counteracting a wide variety of structural damage is critically important to the short- and long-term health of America's infrastructure.

Considering that over 480,000 bridges in the U.S. are classified as having reinforced or prestressed concrete as the material for the main span (Federal Highway Administration 2020), the identification of best practices for the repair of regions or components of concrete bridges that commonly experience deterioration is essential in this effort. One repair technique that has proven to be viable for concrete bridges is the implementation of fiber reinforced polymer (FRP) systems. Despite past significant efforts to study and implement FRP systems for the repair of in-service structures, additional research is needed to develop more detailed design guidelines and installation procedures.

1.2 Background and Motivation

A major area of concern for bridges in Indiana and the Midwest is the deterioration of prestressed concrete bridge girders. Due to harsh environmental conditions in the region, the use of deicing salt is required during the winter months. This produces an environment in which chloride-laden water is present, greatly increasing the possibility of corrosion. One damage scenario caused by this phenomenon that is widely observed in Indiana is the deterioration of girder end regions. The Indiana Bridge Inspection Application System (BIAS) currently lists 172 prestressed concrete stringer/multi-beam/girder bridges in the state system with a superstructure

condition rating of six or less (condition ratings range from zero to nine, with a rating of nine indicating the element is in excellent condition). A condition rating of six indicates that the structural element is in satisfactory condition, but minor deterioration is present (Federal Highway Administration 1995). Of these 172 bridges, approximately 55% (96 bridges) either have or show signs of end region deterioration. Failed, leaking expansion joints in the deck or between the deck and approach slab expose girder end regions to the chloride-laden water, leading to a corrosive environment in which reinforcement section loss and concrete spalling can occur. This process is illustrated in Figure 1.1, and an example of a bridge girder with end region deterioration caused by this mechanism is shown in Figure 1.2.

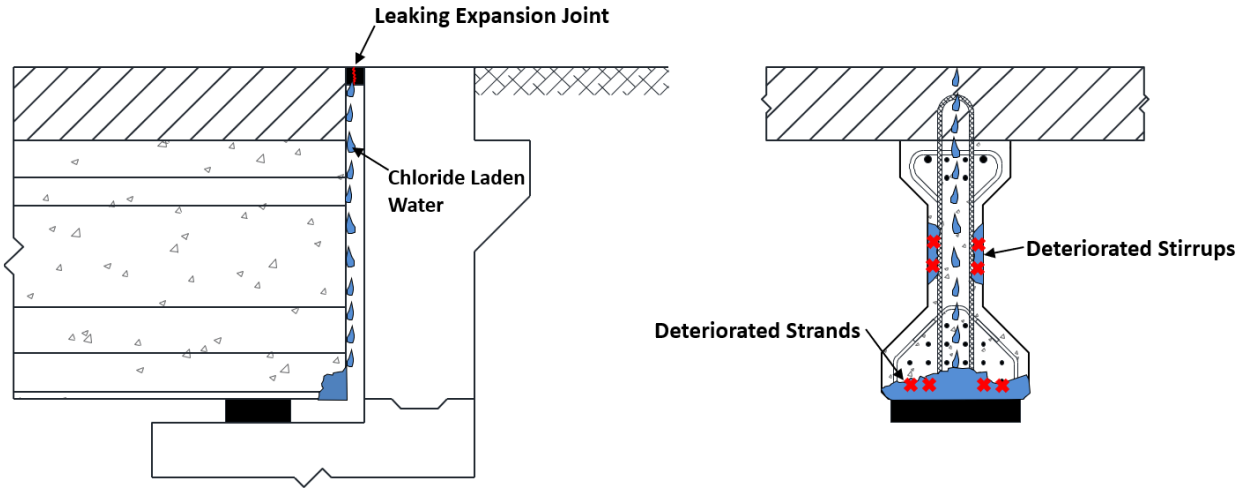

Figure 1.1 Process of Deterioration at Girder End Regions

(a) Bottom Flange Deterioration **(b) Web Deterioration**

Figure 1.2 Bridge Girders with End Region Deterioration (INDOT Asset Name I469-01-07020, near Fort Wayne, Indiana)

With the high volume of bridges requiring end region repair, it is necessary to develop techniques that can extend the service life of these bridges. One repair technique which could contribute to this effort is fiber reinforced polymer (FRP) systems. FRP systems are rapidly gaining popularity in the concrete infrastructure repair industry due to the many advantages they offer. FRP systems have a high strength-to-weight ratio, are naturally corrosion resistant, come in a variety of materials, have installation flexibility, and can be used for different types of strengthening and repair applications, including shear strengthening, flexural strengthening, and column confinement. Furthermore, FRP systems can typically be installed relatively quickly, minimizing or eliminating bridge closures (ACI 440R-07). These characteristics make FRP an appealing material for concrete bridge girder repair.

1.3 Scope and Objectives

This thesis presents details of an experimental program conducted to better understand the effectiveness and practicality of using FRP, and specifically carbon FRP (CFRP) systems to repair prestressed concrete bridge girders with end region deterioration. While glass FRP (GFRP) systems have historically been used in Indiana to provided confinement for patched concrete members and environmental protection, CFRP systems are often considered more suitable for structural applications due to their ultimate strengths, stiffnesses, and durability (Kim et al. 2012). As part of this effort, an alternative repair technique that does not include FRP was also explored. More specifically, the experimental program consisted of the development and testing of three repair techniques for bridge girders with damaged end regions. These techniques are (i) an externally bonded FRP system, (ii) a near-surface-mounted (NSM) FRP system, and (iii) a concrete supplemental diaphragm. The main objectives of the experimental program included:

1. Evaluate the effects of end region deterioration on the behavior of prestressed concrete bridge girders.
2. Determine effective repair techniques for restoring the behavior of prestressed concrete bridge girders with end region deterioration.
3. Evaluate anchorage details for externally bonded FRP sheets applied to an I-shaped girder.

4. Develop and verify installation procedures and recommendations for end region repair techniques.

The experimental program described in this thesis is the final portion of a larger research initiative conducted for the Indiana Department of Transportation (INDOT). The information gathered from each component of the research contributed to the development of an FRP guidebook for application to Indiana bridges. Previous portions of this study include a state-of-the-art review of FRP and its uses in bridge strengthening and repair systems (Pevey 2018) in addition to an experimental investigation of the use of FRP systems for flexural strengthening with a specific focus on adjacent box beam bridges (Jacobs 2020).

1.4 Organization

The following chapters include relevant background information and details of the experimental program focused on end region repair. Chapter 2 provides an overview of different repair techniques used for the rehabilitation of end regions of prestressed concrete bridge girders. This includes an introduction to externally bonded and NSM FRP systems and a discussion of past research programs with a similar focus. An examination of supplemental diaphragm and end block repair techniques is included. The repair details and installation procedures developed for the experimental program are discussed in Chapter 3 along with the testing procedures. The results of the experimental program are then presented in Chapter 4. To determine the effectiveness of each repair technique, an analysis of each individual test is provided along with comparisons between experimental baseline specimens and repaired test specimens. Chapter 5 summarizes conclusions and recommendations gathered from this research, including the effectiveness of the repair techniques considered in the study and repair details and installation procedures recommended for end region repair of prestressed concrete bridge girders.

CHAPTER 2. OVERVIEW OF REPAIR TECHNIQUES FOR END REGIONS OF PRESTRESSED CONCRETE BRIDGE GIRDERS

2.1 Introduction

As the infrastructure in the United States continues to age and bridges approach the end of their design life, the need to develop repair techniques is critical. One area of concern for bridges in Indiana is the deterioration of the end regions of prestressed concrete girders. Due to the local climate, the use of deicing salts is a necessity. This produces an environment in which chloride-laden water is present. When expansion joints between bridge components fail, the concrete girders, and eventually the steel reinforcement, are exposed to chlorides, leading to corrosion of the reinforcement and concrete spalling. As such, repair techniques capable of counteracting damage caused by this mechanism are needed. This study examines three potential repair solutions for such damage: (i) externally bonded fiber reinforced polymers (FRP), (ii) near-surface-mounted (NSM) FRP, and (iii) a concrete supplemental diaphragm. This chapter provides an introduction to each of these repair strategies.

2.2 FRP Repair Systems

2.2.1 Overview

One potential technique for repairing deteriorated end regions of prestressed concrete bridge girders is using fiber reinforced polymer (FRP) systems. FRP systems are rapidly gaining popularity for concrete infrastructure repair due to the many advantages they provide over conventional repair methods. FRP systems are corrosion resistant, easy to install, and provide a high strength-to-weight-ratio (ACI 440R-07). FRP systems are also a more versatile repair method, as they can be made from different materials, are commercially available in many different forms, and can be applied via multiple installation methods.

FRP is a two-part composite material composed of high-strength reinforcing fibers within a resin matrix. The reinforcing fibers are impregnated with resin, and after the resin cures, form an FRP laminate. Commonly available types of FRP laminates included sheets, meshes, strips, and bars as shown in Figure 2.1. FRP sheets and meshes are utilized in externally bonded FRP systems,

while FRP strips and bars are used for near-surface mounted (NSM) FRP applications (Pevey 2018). Externally bonded and NSM FRP repair systems are discussed in more detail in Sections 2.2.3 and 2.2.4, respectively.

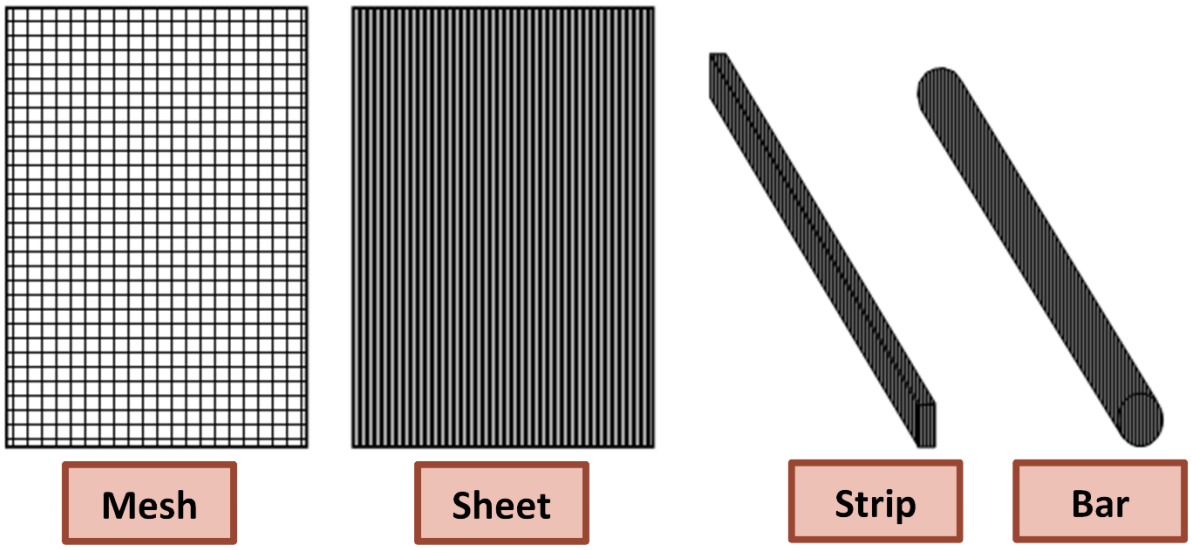

Figure 2.1 Common FRP Laminate Types (from Pevey 2018)

Depending upon the required characteristics and properties of the FRP system, different types of reinforcing fibers and resins can be selected. Reinforcing fibers are typically made of aramid, carbon, or glass; however, steel and hybrid fibers are also manufactured (ACI 440R-07). Table 2.1 shows some of the mechanical properties of aramid, carbon, and glass FRP laminates. The most widely used resins are epoxy products, but polyester, phenolics, and vinyl ester resins are also available (ACI 440R-07, *fib* Task Group 9.3 2001). A detailed review of FRP materials and systems, as well as case studies involving FRP repairs, can be found in a study completed by Pevey (2018).

Table 2.1 Material Properties of FRP Laminates (adapted from ACI 440.2R-17, as presented in Kim et al. 2012)

FRP Laminate Material	Ultimate Tensile Strength (ksi)	Elastic Modulus (ksi)	Rupture Strain (%)
Aramid (high-performance)	100 to 250	7,000 to 10,000	2.0 to 3.0
Carbon (high-strength)	150 to 350	15,000 to 21,000	1.0 to 1.5
Glass (E-glass)	75 to 200	3,000 to 6,000	1.5 to 3.0
Properties shown are for laminates with fiber volumes of 40% to 60% and unidirectional fiber orientations.			

2.2.2 FRP System Failure Behaviors

The failure behavior of FRP strengthened systems is generally governed either by FRP rupture or debonding. FRP rupture results from the fibers of an FRP laminate reaching their ultimate strain limit and failing at the location of maximum stress (Quinn 2009). This failure mechanism is preferred, as the FRP system develops its ultimate capacity prior to failure (Pevey 2018). However, as shown by the stress-strain curve in Figure 2.2, FRP displays linear-elastic behavior up to rupture. This results in a brittle failure mode and is associated with an abrupt drop in load-carrying capacity (Chennareddy et al. 2017). This resulting structural behavior should be considered when designing FRP systems.

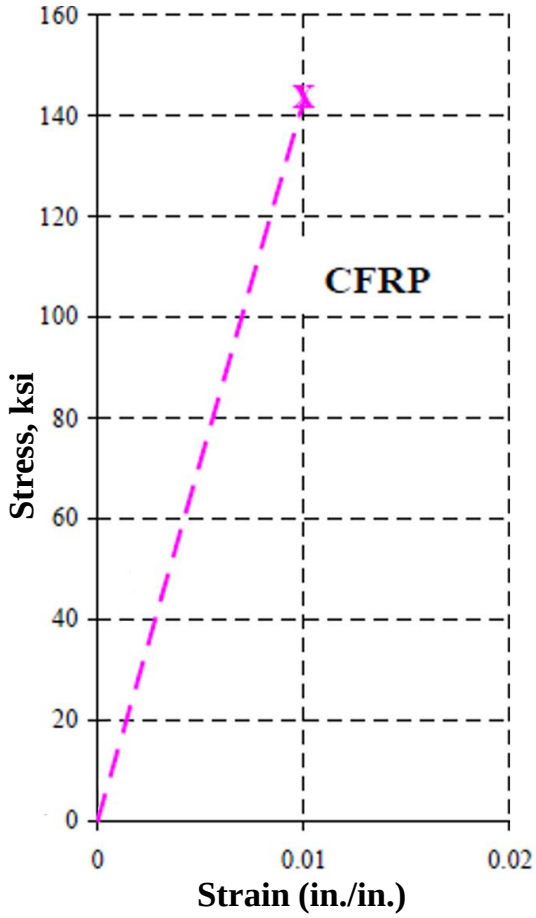

Figure 2.2 Example Stress-Strain Curve of CFRP Laminate (adapted from Kim 2008)

Another failure mechanism associated with FRP systems is debonding. Debonding, which is generally considered to include both FRP debonding and concrete cover delamination (ACI 440.2R-17), results in the FRP laminate and/or concrete cover separating from the concrete member due to high stress concentrations within the FRP system or concrete cover. These stress concentrations occur at either the termination points of FRP laminates or at locations where cracks in the concrete substrate appear (Kang et al. 2012). As Figure 2.3 demonstrates, the location of the stress concentration dictates the debonding behavior. Stress concentrations at the termination of the FRP laminate result in a delamination of the concrete cover, while stress concentrations developed by the formation of cracks result in a debonding of the FRP laminate (ACI 440.2R-17). When compared to failure due to FRP rupture, debonding occurs at lower levels of strain and thus does not develop the full tensile capacity of the FRP laminate (ACI 440.2R-17). Therefore, preventing the debonding failure mode is desirable. This is most commonly achieved by using different anchorage techniques, which are discussed in Section 2.2.3.1. Proper anchorage systems

can prevent FRP debonding from occurring and allow for the full tensile capacity of the FRP laminate to develop.

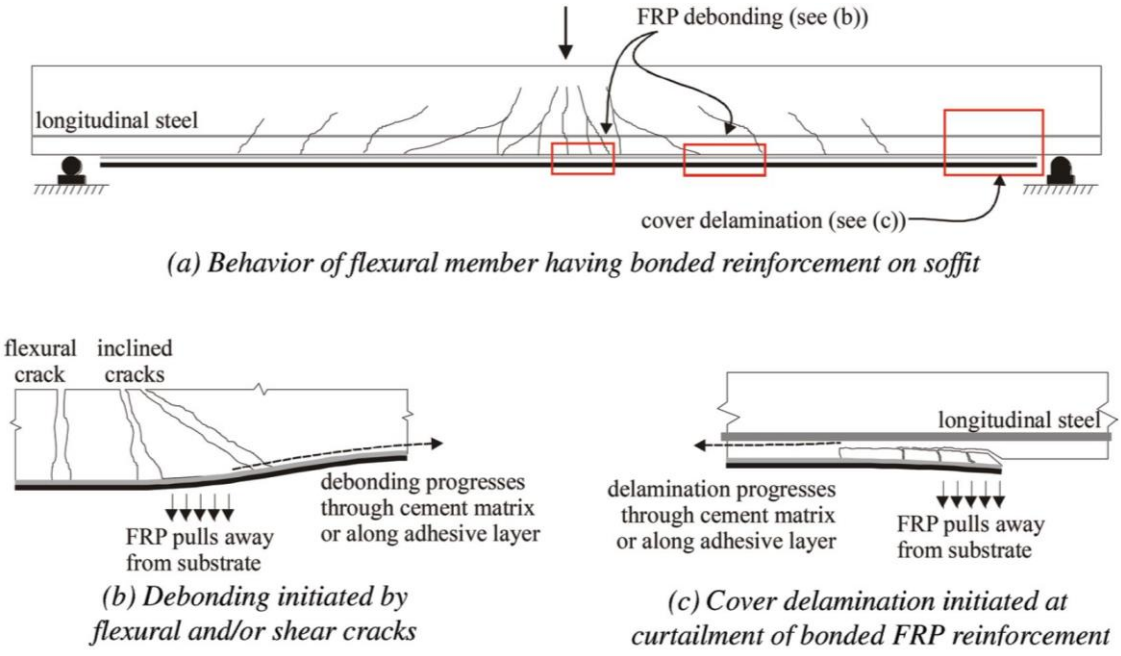

Figure 2.3 Debonding Failure Mechanisms of Externally Bonded FRP Systems (from ACI 440.2R-17)

2.2.3 Externally Bonded FRP Repair Systems

Externally bonded FRP systems are installed by adhering the FRP laminate to the concrete surface using an adhesive. Externally bonded FRP sheets can either be pre-saturated with epoxy by the manufacturer or field saturated. Field-saturated sheets can either be installed using a wet- or dry-layup procedure. Wet-layup applications require the FRP sheets to be saturated with epoxy prior to placement on the primed concrete surface (Quinn 2009, Kim et al. 2012, Garcia et al. 2014). In dry-layup installations, the epoxy used to prime the concrete surface is pressed into the dry fabric upon application, eliminating the need to saturate the sheet prior to placement (Kim et al. 2012, Garcia et al. 2014, Shekarchi 2016).

Externally bonded FRP systems used for flexural and shear strengthening applications are typically categorized as bond-critical applications. As such, ensuring that the repair area has an appropriate surface profile to enhance the bond with the FRP laminate is critically important to the success of the FRP system. According to guides from the International Concrete Repair Institute

(ICRI) and the American Concrete Institute (ACI) (ICRI 330.2-2016 and ACI 440.2R-17), the minimum acceptable concrete surface profile (CSP) for FRP applications is CSP 3. ICRI 310.2R-2013 correlates CSP 3 to a "light shotblast" and provides the example shown in Figure 2.4 as a reference profile. Molded replicas of CSPs 1-10 can be acquired through ICRI if further reference is needed to ensure that the proper surface preparation is achieved. Table 2.2 shows the surface preparation methods, and their CSP range, which ICRI suggests for obtaining a CSP of 3.

Figure 2.4 Example of CSP 3 (from ICRI 310.2R-2013)

Table 2.2 Appropriate Surface Preparation Methods for FRP Systems (adapted from ICRI 310.2R-2013)

	Concrete Surface Profile (CSP)									
Surface Preparation Method	CSP 1	CSP 2	CSP 3	CSP 4	CSP 5	CSP 6	CSP 7	CPS 8	CPS 9	CPS 10
Acid Etching	■	■	■							
Needle Scaling		■	■	■						
Abrasive Blasting		■	■	■	■	■	■			
High- and ultra-high-pressure water jetting			■	■	■	■	■	■	■	■

Flexibility in application is a major advantage of externally bonded FRP systems. Externally bonded systems can be used for flexural strengthening, shear strengthening, and axial confinement applications. As a result of past research conducted on these systems, there are readily available guidelines and suggestions pertaining to the design and installation of externally bonded FRP. However, externally bonded systems are highly susceptible to premature debonding failures. Thus, proper anchorage is needed for efficient use of these systems.

2.2.3.1 Anchorage Systems

As discussed in Section 2.2.2, FRP systems are susceptible to failing prior to developing their full tensile capacity due to the debonding phenomenon. As a result, many anchorage techniques have been developed to prevent this undesirable failure behavior.

2.2.3.1.1 FRP Spike Anchors

FRP spike anchors, also known as FRP fan anchors or simply FRP anchors, are one anchorage system which has been developed to prevent debonding. As shown in Figure 2.5, spike anchors consist of individual FRP fibers that have been bound together. Spike anchors can either be manufactured and pre-assembled or field-assembled by separating individual fibers from an FRP sheet. The anchor is then saturated with resin and inserted through the externally bonded FRP sheet into a pre-drilled hole in the concrete substrate. As suggested in ICRI 310.2R-2013, the edges of the pre-drilled anchor holes should be rounded to a 0.50-in. radius. The individual fibers are then splayed out in an arch shape on the externally bonded sheet. The splayed portion of the anchor is then saturated. Two FRP patch sheets are then place over the splayed anchors. The fibers of the first patch sheet should be orientated perpendicular to the fibers of the externally bonded sheet, while the fibers of the second patch sheet should be orientated parallel with the fibers of the externally bonded sheet (Orton 2007, Quinn 2009, Kim et al. 2012, Pudleiner 2016, Shekarchi et al. 2020). Figure 2.6 provides an example of this installation procedure.

Figure 2.5 FRP Spike Anchor

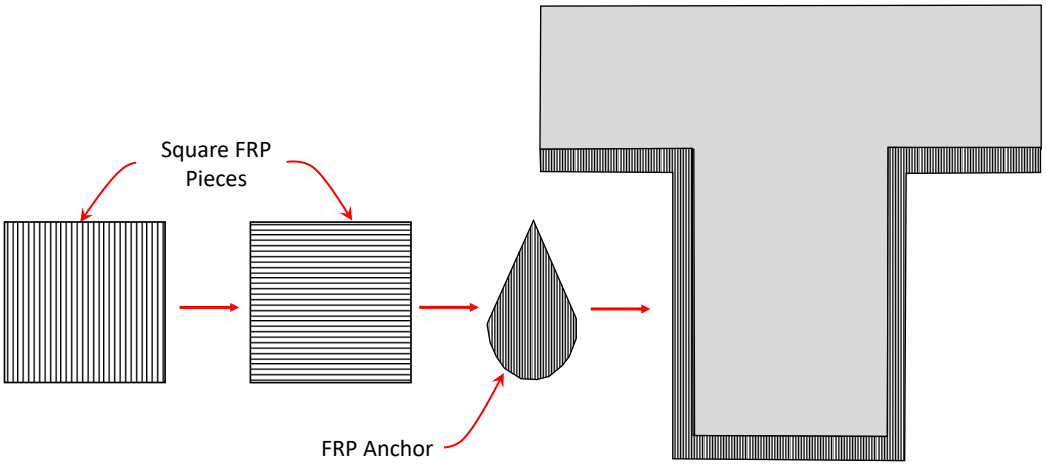

Figure 2.6 FRP Spike Anchor Installation (from Pevey 2018)

Spike anchors have been extensively studied and have shown to be effective at preventing debonding (Orton 2007, Quinn 2009, Pham 2009, Kim et al. 2012, Pudleiner 2016, Jacobs 2020, Shekarchi et al. 2020). One of the major advantages of this anchorage system is that material continuity is maintained. This can eliminate material compatibility concerns, including those related to corrosion (Grelle and Sneed 2013). Additionally, spike anchors can easily be applied to a variety of structural members and geometries (Grelle and Sneed 2013, Kalfat et al. 2013). However, spike anchors do require a hole to be drilled into the structural member. Correct detailing

of these holes can become difficult if the reinforcement pattern is tightly congested within the repair area, such as within the end regions of bridge girders.

2.2.3.1.2 Longitudinal FRP Strip Anchors

Longitudinal FRP strip anchors are applied by placing a saturated FRP sheet, often cut into narrower "strips," over a vertically orientated externally bonded FRP sheet. Figure 2.7 shows an example of a longitudinal strip-anchored FRP system. Like spike anchors, longitudinal strip anchors have all the benefits associated with maintaining material compatibility but have the additional advantage of not requiring drilling for installation. However, comparatively little research has been conducted on longitudinal FRP strip anchors. Additionally, repair detailing and results from the available studies vary. Petty et al. (2011) examined different FRP anchorage systems on I-shaped prestressed concrete bridge girders with end region deterioration. The authors concluded that longitudinal FRP strip anchors orientated at 90° relative to externally bonded FRP sheets were an effective anchorage method. In addition to resulting in satisfactory shear performance, this anchorage system was also simple in terms of both design and installation. Andrawes et al. (2018) examined the effectiveness of longitudinal strip-anchored FRP shear-strengthening systems on prestressed concrete bridge girders with end region deterioration and concluded that "longitudinal FRP anchors proved to be effective in preventing the overall debonding of FRP laminates." In contrast to the conclusions reached by Petty et al. (2011) and Andrawes et al. (2018), Ortega (2009) found that longitudinal FRP strip anchors did not prevent debonding of externally bonded FRP laminates.

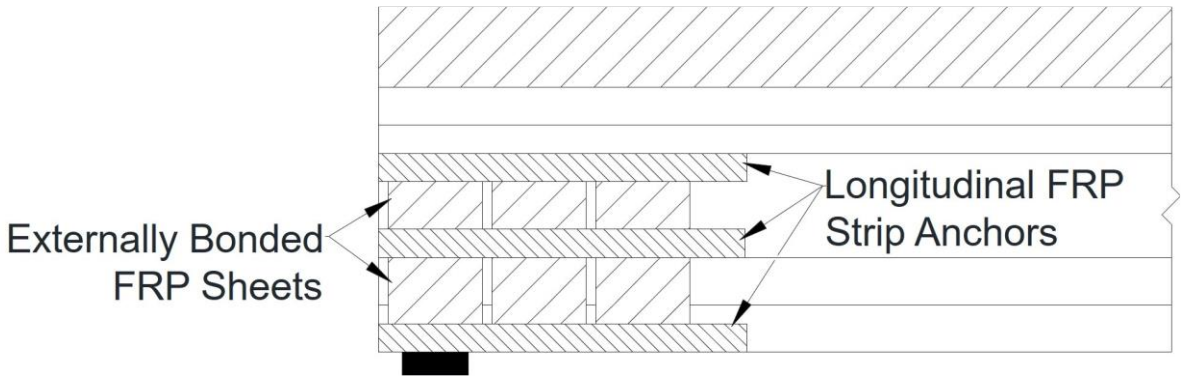

Figure 2.7 Longitudinal FRP Strip Anchor System

2.2.3.1.3 Other Anchorage Systems

Another type of anchorage system which has been developed to prevent debonding of externally bonded FRP laminates used for shear applications is the U-anchor system. This system was established by Khalifa et al. (1999). Prior to the installation of the shear strengthening system, a groove is cut into the concrete substrate where the FRP sheet will terminate. The FRP sheet is then installed onto the concrete surface with the ends of the FRP sheet recessed into the groove. Next, the groove is filled halfway with epoxy before an FRP bar is inserted. The groove is then filled the remainder of the way with epoxy. Figure 2.8 shows a completed installation of the U-anchor system. Khalifa et al. (1999) saw a 145% increase it shear capacity and no debonding was observed. While these results do indicate that the U-anchor system is effective, it does require significant labor to install.

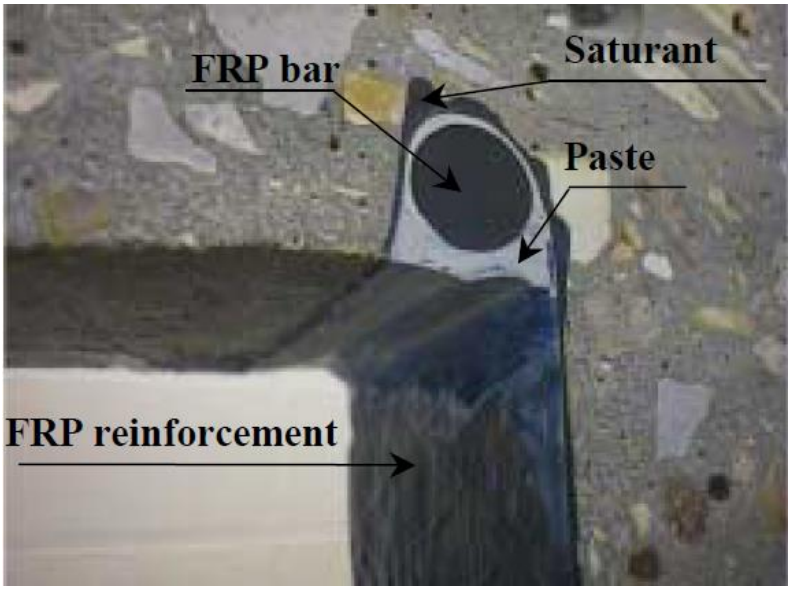

Figure 2.8 Installed U-anchor System (from Khalifa et al. 1999)

Many forms of mechanical anchorage systems have also been developed. These include, but are not limited to, threaded anchor rod systems, modified anchor bolt systems, and anchored metal plates. More information on these systems can be found in Grelle and Sneed (2013), Kalfat et al. (2013), and Pevey (2018).

2.2.4 Near-Surface-Mounted FRP Repair Systems

Near-surface-mounted (NSM) systems are a type of FRP strengthening system in which a pre-cured FRP laminate, usually in the form of a strip/tape or bar, is embedded directly into the concrete substrate. The installation procedure begins by cutting a groove in the concrete substrate. After the groove is cut, epoxy is inserted into the groove followed by the selected FRP laminate. More epoxy is then placed into the groove to fully cover the FRP laminate. Figure 2.9 displays the minimum groove dimensions recommended by ACI 440.2R-17.

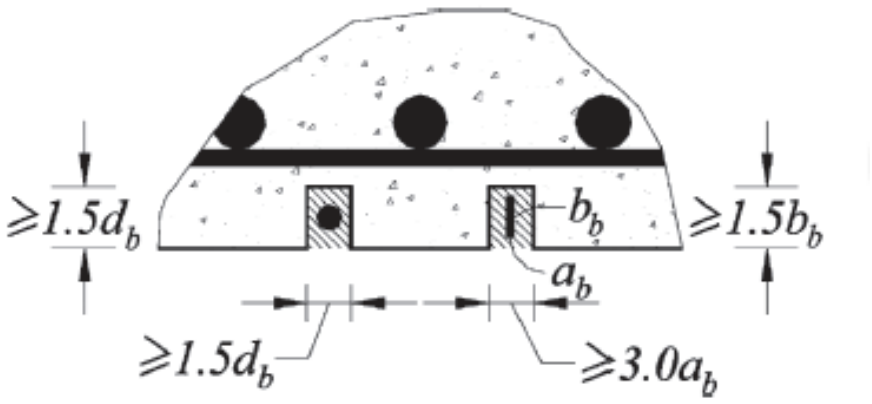

Figure 2.9 Minimum Recommended Groove Dimensions for NSM Systems (from ACI 440.2R-17)

Near-surface-mounted systems have many advantages which make them an attractive repair option. Unlike externally bonded systems, NSM systems do not require surface preparation other than cutting the groove. NSM systems are also less susceptible to debonding failures and, due to the protection provided by the concrete cover, are less vulnerable to vandalism, fire, accidental impact, and mechanical damage (De Lorenzis and Teng 2006). However, less research has been conducted for NSM systems, resulting in fewer available guidelines for designers.

2.2.5 Past Research on End Region Repairs Using FRP Systems

While the use of FRP as a repair and strengthening system has been widely researched, only a few studies have been conducted to examine the use of FRP systems for repairing deteriorated end regions of bridge girders. As the damage in these scenarios is largely concentrated at bridge supports, arch action, not beam action, is of primary focus. Research by Kim (2011) and

NASEM (2011) concluded that the effectiveness of externally bonded FRP systems decrease as the shear span-to-depth (a/d) ratio decreases. Kim (2011) found that externally bonded CFRP-strengthened T-beams with a/d ratios of 3.0 achieved shear strength increases up to 50%. In contrast, Kim (2011) also found that identically detailed CFRP-strengthened T-beams with a/d ratios of 1.5 only achieved strength increases up to 15%. Therefore, more research is needed to better understand the behavior of FRP repair systems when arch action controls. The following studies fall into this category, as they examine the behavior of FRP systems used to repair the end region of prestressed concrete bridge girders.

2.2.5.1 Ramseyer and Kang (2012)

Ramseyer and Kang (2012) examined the effectiveness of glass and carbon FRP repair systems for prestressed concrete bridge girders with deteriorated end sections. Type II AASHTO bridge girders were artificially damaged by failing the girder ends in shear. This damage was meant to simulate in-field corrosion. The end regions were then repaired by (1) removing delaminated concrete, (2) restoring the section using rapid set mortar, (3) epoxy-injecting cracks (only on select specimens), (4) cutting anchorage grooves at the top of the web, (5) applying externally bonded FRP U-wraps onto the repair section, and (6) inserting a metal rod into the groove to anchor the U-wrap. Figure 2.10 illustrates the repair process. As Table 2.3 shows, the only repair system to regain the shear strength of the undamaged end region was the system with glass FRP U-wraps and epoxy-injected cracks. However, the authors concluded that the carbon FRP systems recovered more stiffness than the glass FRP systems (Ramseyer and Kang 2012).

(a) Delaminated Concrete Removed

(b) Cross Section Restored

(c) Epoxy-Injected Cracks

(d) Groove Cut

(e) Primed Concrete

(f) FRP Repair

Figure 2.10 Repair Procedure for Damaged End Regions (from Ramseyer and Kang 2012)

Table 2.3 Shear Test Results (adapted from Ramseyer and Kang 2012)

Repair System	Initial Ultimate Shear Load (kip)	Ultimate Shear Load Post-Repair (kip)
GFRP U-Wraps without Epoxy Injection	97.9	84.1
GFRP U-Wrap with Epoxy Injection	106.3	108.0
CFRP U-Wrap without Epoxy Injection	99.1	81.4
CFRP U-Wrap with Epoxy Injection	123.5	87.9

2.2.5.2 Andrawes et al. (2018)

Another study that examined the effectiveness of FRP repair systems for prestressed concrete bridge girders with deteriorated end sections was conducted by Andrawes et al. (2018). The end regions of laboratory-fabricated, half-scale AASHTO Type II I-shaped girders were artificially damaged by removing 0.5 in. of the concrete cover from the webs. Rapid set cement was then used to restore the cross sections of the members. Both glass and carbon side-bonded FRP systems were examined. The side-bonded sheets were anchored using longitudinal FRP strips. As shown in Figure 2.11, the anchorage detailing consisted of a single layer of longitudinal strip anchors located at the top and bottom of the web and at the bottom flange. The longitudinal strip anchors were continuous around the end of the member. An NSM repair system was also tested. Experimental results showed that the carbon FRP system exceeded the stiffness and ultimate shear capacity of the control specimen (19.5% and 6.0% increases, respectively), while the glass FRP system exceeded the ultimate shear capacity of the control specimen (2.0% increase) but was unable to restore the stiffness (25.6% decrease). The NSM repair system did not restore the stiffness or the shear capacity of the undamaged specimen (21.4% and 7.5% decrease, respectively).

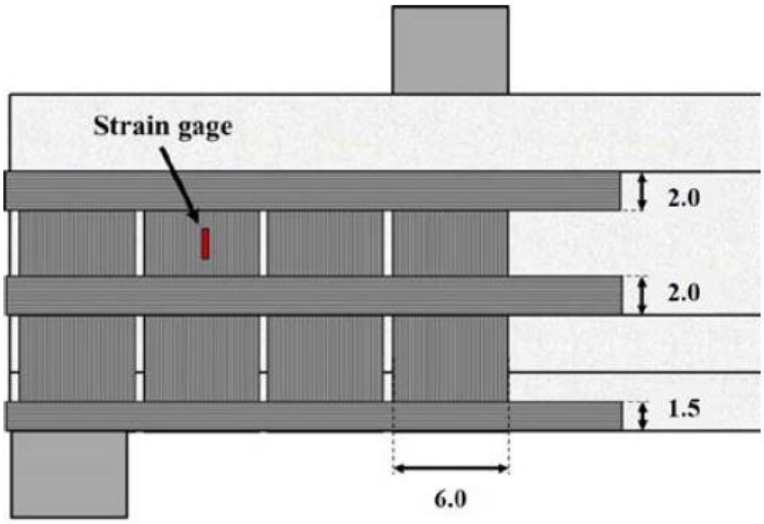

Figure 2.11 Longitudinal FRP Strip Anchorage Detailing for Half-Scale Specimens (from Andrawes et al. 2018)

Based upon the results of the half-scale test specimens, the carbon FRP repair system was selected for full-scale testing on AASHTO Type II I-shaped girders. The full-scale AASHTO Type II I-shaped girders were damaged in a similar manner as the half-scale specimens except that the imposed damaged was continued into the bottom flange. The repair procedure for the full-scale specimens was identical to that of the half-scale specimens except for the FRP detailing. For the full-scale tests, the longitudinal strip anchors were placed at the same locations as the half-scale specimens, but the widths of the anchors were increased to 3 in. each. Additionally, the longitudinal strip anchors were not wrapped around the end of the girder. Instead, each side of the girder was anchored with longitudinal strips. Figure 2.12 displays the anchorage detailing for the full-scale test specimens. As with the half-scale specimens, the carbon FRP repair system was able to exceed the shear capacity of the control specimen (2.6% increase) but did not fully regain the control stiffness (2.3% decrease) (Andrawes et al. 2018).

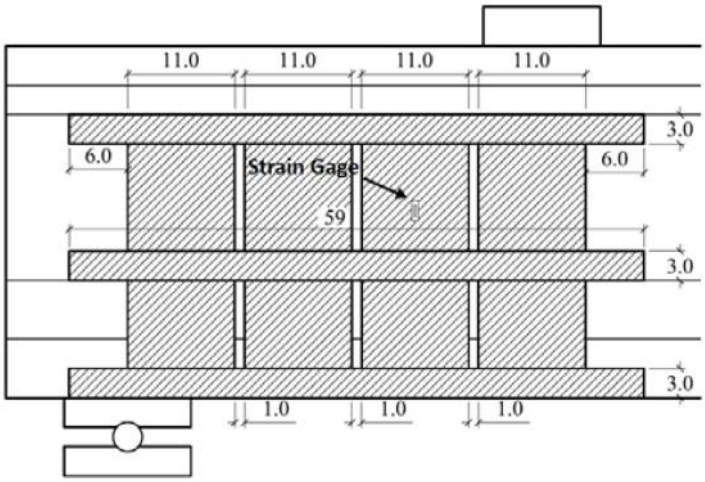

Figure 2.12 Longitudinal FRP Strip Anchorage Detailing for Full-Scale Specimens (from Andrawes et al. 2018)

2.2.5.3 Petty et al. (2011)

Petty et al. (2011) examined the effectiveness of different FRP strengthening systems on deteriorated end regions of I-shaped prestressed concrete bridge girders. Eight AASHTO Type II girders were salvaged from a bridge replacement project for load testing. The following five CFRP repair configuration were implemented: (1) four vertical U-wrap sheets (20-in. wide) anchored at the top and bottom web-flange interfaces with embedded CFRP laminate, as shown in Figure 2.13, (2) six discontinuous, 45° oriented sheets (10-in. wide) with two layers of longitudinal strip anchors (15-in. wide) along the web of the girder, (3) six discontinuous, 45° oriented sheets (10-in. wide) without anchorage, (4) four vertical U-wrap sheets (10-in. wide) anchored with two layers of longitudinal strip anchors (15-in. wide) along the web of the girder, as shown in Figure 2.14, and (5) six discontinuous, 45° oriented sheets (10-in. wide) anchored with the detail shown in Figure 2.13. Table 2.4 shows the results of the experimental program. The authors concluded that the CFRP configuration of vertical U-wrap sheets and longitudinal strip anchors was the most effective design due to its consistent strength increase, ease of installation, and simplistic design. As such, this configuration was used for two additional ultimate shear tests. These tests resulted in strength increases of 16.2% and 15.1%, further displaying the effectiveness of the repair system (Petty et al. 2011).

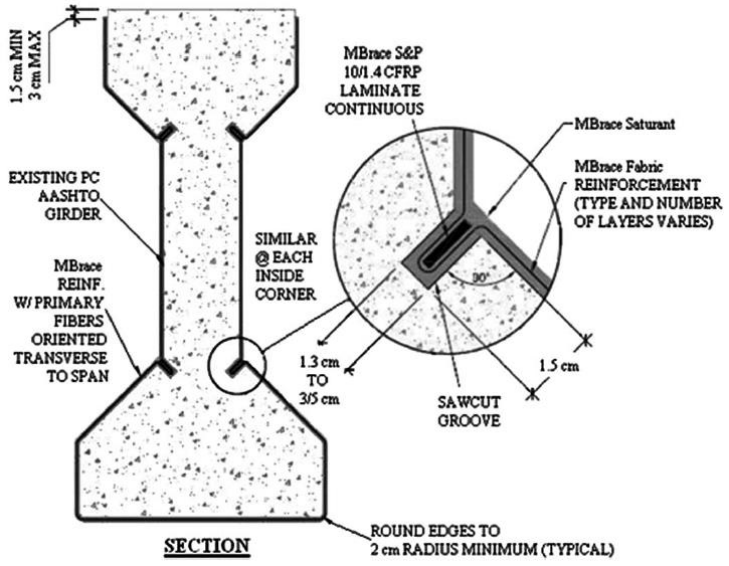

Figure 2.13 Embedded CFRP Laminate Anchorage System Detail (from Petty et. al 2011)

Figure 2.14 CFRP Repair System with Vertical U-Wrap and Longitudinal Strip Anchorage (from Petty et. al 2011)

Table 2.4 Results from Experimental Program (adapted from Petty et. al 2011)

CFRP System	Test	Increase in Shear Capacity
Vertical U-Wrap with Embedded Anchorage	A	36.0%
	B	-0.5%
Diagonal Sheets with Longitudinal Strip Anchorage	A	17.0%
	B	21.9%
Diagonal Sheets without Anchorage	A	8.9%
	B	6.4%
Vertical U-Wrap with Longitudinal Strip Anchorage	A	27.3%
	B	27.3%
Diagonal Sheets with Embedded Anchorage	A	34.1%
	B	-7.8%

2.3 Past Research on End Block/Supplemental Diaphragm Repair Systems

Two studies in the literature (Needham 2000, Shield and Bergson 2018) examined the use of end blocks to repair deteriorated end regions of bridge girders. End block repairs increase the original cross section of the girder and rely on supplemental reinforcement to redistribute stresses from the original member into the repair. As part of the current study described in this thesis, a similar detail, referred to as a supplemental diaphragm, was considered. The two end block studies served as the design basis for the supplemental diaphragm repair method developed in the current study.

In 2000, the Michigan Department of Transportation (MDOT) published the results of a research project focusing on the repair of I-shaped prestressed concrete bridge girder end regions (Needham 2000). The project included the development of an end block repair procedure, load testing of the repaired girder, and field installation of the repair on in service girders. The repair procedure was conducted as follows:

1. Deteriorated concrete was removed using either a 15-kg pneumatic chipping hammer or a 7-kg pneumatic chipping hammer around the prestressing strands.
2. The repair limits on the bottom flange of the beam were saw cut to prevent featheredging of the repair material.

3. A 7-kg chipping hammer was used to lightly roughen the surface of the existing sound concrete within the repair limits to improve the bond between the existing concrete and the repair material.
4. Three 13-mm by 25-mm keyways were created in each side of the existing concrete to improve the shear performance of the interface between the existing concrete and the patch material.
5. The supplemental reinforcement was placed, and the concrete forms were set.

A latex modified concrete was used as the patch material. While the repaired girder did not reach the expected shear capacity, it was determined that this was a result of the residual effects of impact damage caused by a vehicle collision when the girder was in service. Additionally, it was concluded that use of the 7-kg pneumatic hammer to roughen the surface of the existing concrete caused too much micro-cracking, and thus an alternative method should be used to prepare the surface. Figure 2.15 shows the end block repair details utilized in the study. The repair performed well for six months, at which time the report was written. Only two minor cracks, caused during the construction of the end block, had appeared despite experiencing several issues during construction. These included accidental cutting of the prestressing strands in the bottom flange, mixing problems with the latex modified concrete, and featheredging at the bottom of the repair area (Needham 2000).

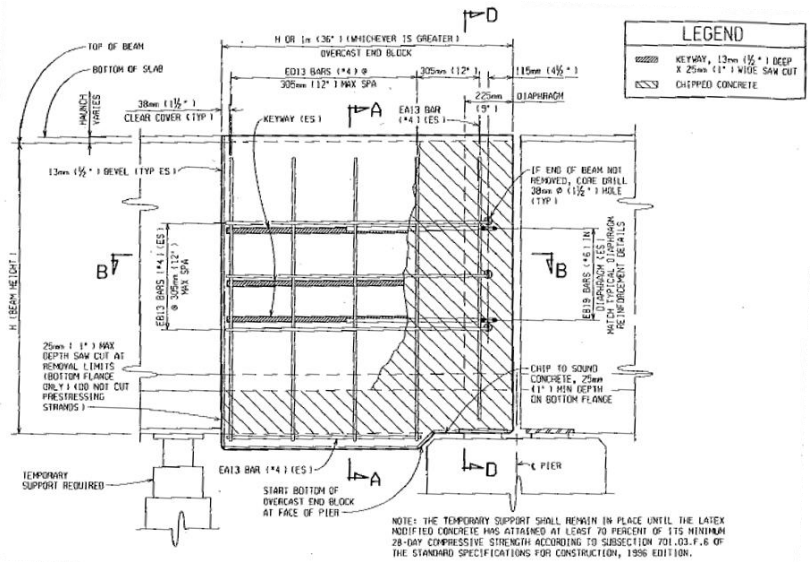

(a) End Block Repair Elevation Detail

Figure 2.15 End Block Repair Details (from Needham 2000)

Figure 2.15 continued

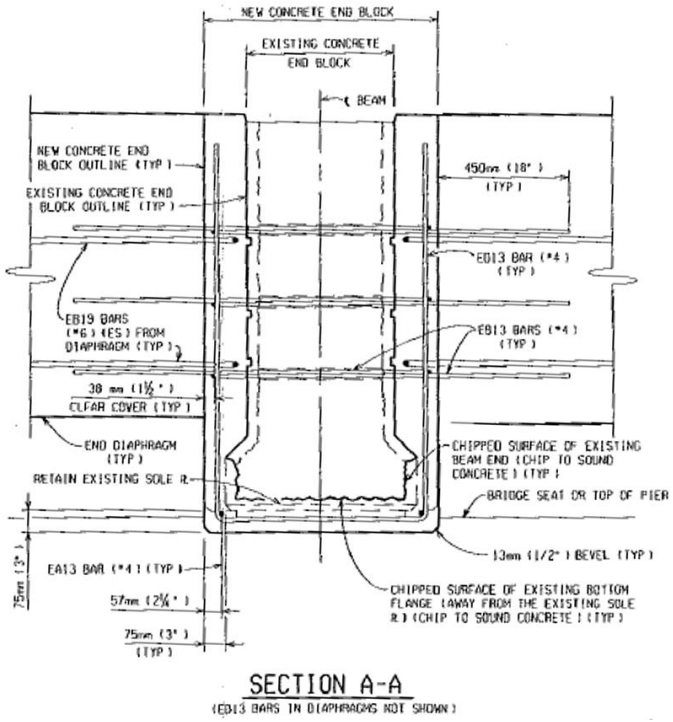

(b) End Block Repair Cross-Sectional Detail

Another end block study that influenced the development of the supplemental diaphragm repair was conducted by Shield and Bergson (2018) at the University of Minnesota in collaboration with the Minnesota Department of Transportation (MnDOT). The study examined the performance of shotcrete end block repairs MnDOT performed in 2013 on I-shaped prestressed concrete bridge girders with significant end region deterioration. Figure 2.16 shows the condition of the girders prior to and after the repair, and Figure 2.17 shows the shotcrete repair details. The shotcrete repair was conducted as follows (Shield and Bergson 2018):

1. The concrete was sounded to locate hollow sounding areas.
2. Delaminated concrete was removed.
3. Supplemental reinforcement was added to the repair area.
4. The supplemental reinforcement was encased in the shotcrete end block.

In 2017, the bridge which received the shotcrete repair was replaced, and the girders which received the repairs were transported to the University of Minnesota for load testing. Two

unrepaired specimens were also tested as control specimens. The end block repaired girders failed at marginally higher loads (1.2% and 3%) than the unrepaired specimens, establishing the effectiveness of the repair (Shield and Bergson 2018).

(a) Condition of the Girder Following Removal of Delaminated Concrete

(b) Complete Shotcrete Repair

Figure 2.16 Girder Condition Prior to and Following Shotcrete Repair (from Shield and Bergson 2018)

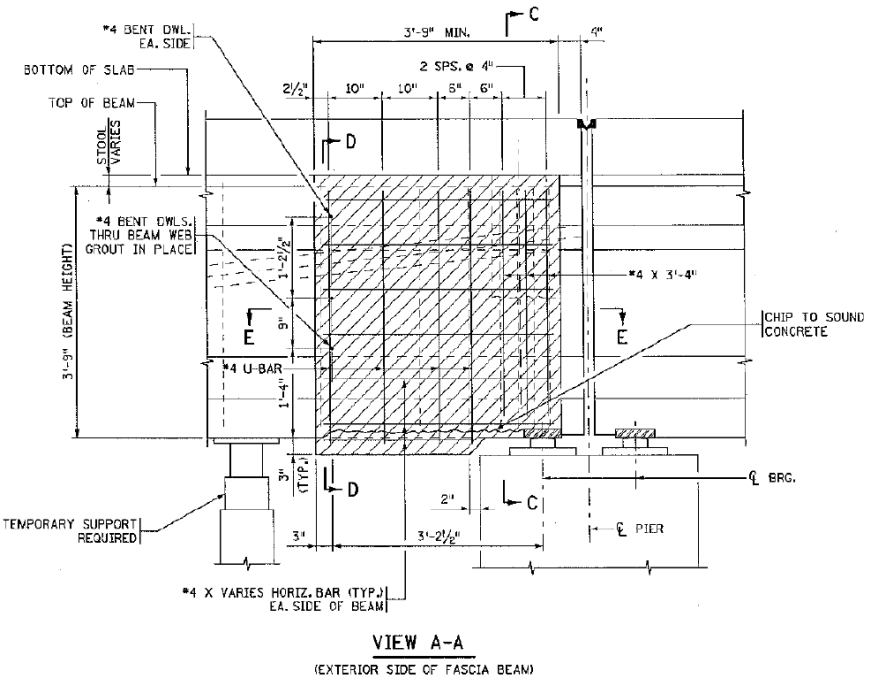

(a) Shotcrete Repair Elevation Detail

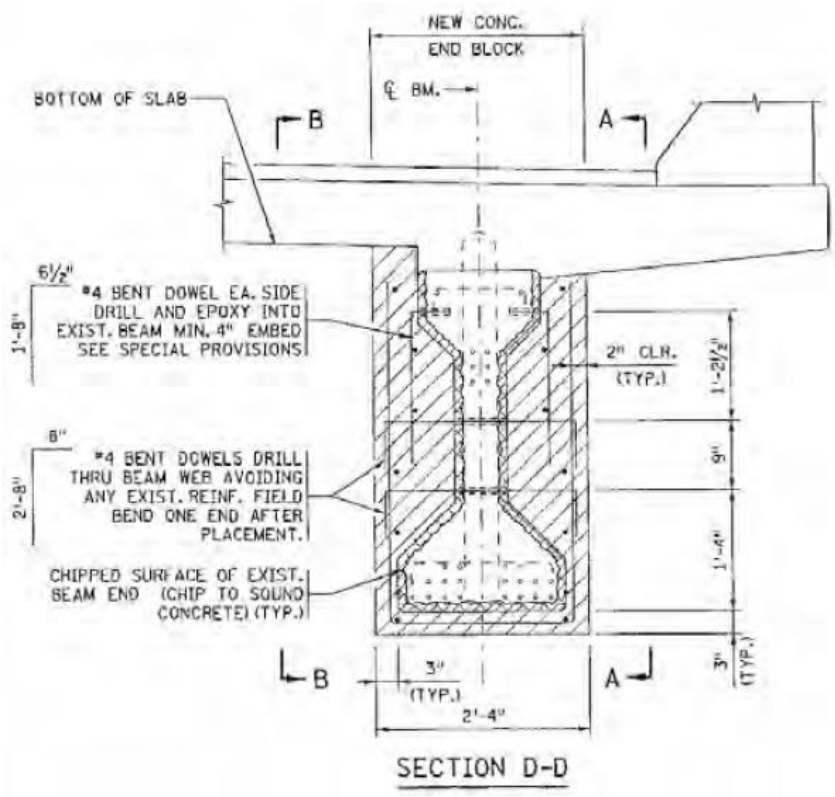

(b) Shotcrete Repair Cross-Sectional Detail

Figure 2.17 Shotcrete Repair Details (from Shield and Bergson 2018)

2.4 Summary of Examined Repair Systems

The above sections highlight previously conducted studies examining different repair techniques for end regions of prestressed concrete bridge girders. Ramseyer and Kang (2012), Andrawes et al. (2018), and Petty et al. (2011) examined the effectiveness of different FRP strengthening techniques. Ramseyer and Kang (2012) concluded that the glass FRP U-wrap system with embedded steel rods for anchorage in combination with epoxy-injected cracks was the most effective system for restoring lost shear capacity. However, Andrawes et al. (2018) and Petty et al. (2011) concluded that the carbon FRP systems with longitudinal strips for anchorage provided the best retrofit solution. End block repair solutions were also examined by Needham (2000) and Shield and Bergson (2018). Needham (2000) concluded that the latex modified concrete end block repair provided a cost-effective solution for the repair of prestressed concrete bridge girder end regions, while Shield and Bergson (2018) concluded that the shotcrete end block repair technique that was implemented was also an effective system. Table 2.5 summarizes the strength increases achieved by each of these systems. However, caution should be taken when directly comparing the performance of the systems due to differences in repair procedures, repair system detailing, and test specimen configurations.

Table 2.5 Strength Increase for Recommended Repair Techniques from Examined Studies

Study	Recommended Repair Technique	Average % Increase in Ultimate Shear Capacity
Ramseyer and Kang (2012)	GFRP U-Wrap with Epoxy Injected Cracks	1.6%
Andrawes et al. (2018)	CFRP Side-Bonded Sheets with Longitudinal FRP Strip Anchorage	2.6%
Petty et al. (2011)	CFRP U-Wrap with Longitudinal FRP Strip Anchorage	21.5%
Shield and Bergson (2018)	Shotcrete End Block	2.1%
Strength data not available for Needham (2000) study.		

2.5 Research Needed

As FRP becomes a more popular construction material, opportunities will arise to conduct research that can fill current gaps in the knowledge base. One area of future research should be the development of anchorage guidelines for FRP spike anchors. As of the completion of this study, there are no standardized guidelines for spike anchors. Furthermore, as discussed in Section 2.2.5, there is limited research pertaining to the use of FRP shear strengthening systems in applications with low shear-span-to-depth ratios, such as the repair of deteriorated end sections. The controlling behavior in these applications switches from beam action to arch action. Preliminary research has shown that this change in behavior decreases the effectiveness of FRP systems. More research is needed to better understand this phenomenon.

2.6 Summary

Across the United States, aging infrastructure is in need of repair due to a variety of factors. In Indiana and many Midwestern states, one area of growing concern is the deterioration of the end regions of prestressed concrete bridge girders. This chapter introduced three potential repair solutions: (i) externally bonded FRP, (ii) near-surface-mounted FRP, and (iii) a concrete supplemental diaphragm.

FRP is a two-part composite material composed of high-strength reinforcing fibers within a resin matrix. The reinforcing fibers are most commonly made of carbon, aramid, and glass. After these reinforcing fibers are impregnated with resin and given time to cure, an FRP laminate is formed. The most common types of FRP laminates are fabrics, meshes, strips/tapes, and bars. The failure of FRP laminate systems are generally characterized by either FRP rupture or debonding.

Externally bonded FRP systems are installed by directly adhering the FRP laminate to the concrete surface and can be installed using either a wet- or dry-layup procedure. Externally bonded FRP systems used for flexural and shear strengthening applications are usually classified as bond critical applications. As a result, these externally bonded systems are sensitive to debonding failures, and thus require additional considerations to ensure proper anchorage. Different methods of anchorage include FRP spike anchors, FRP strip anchors, FRP U-anchors, and various mechanical anchorage systems. In near-surface-mounted (NSM) FRP systems, the FRP laminate is embedded directly into the concrete substrate. This eliminates the need for additional anchorage.

A supplemental diaphragm repair solution was developed for the experimental program described in Chapter 3 as an alternative to FRP repair systems and was influenced by end block repairs described in the literature. In addition to a description of the experimental program, Chapter 3 includes information about the test specimens; test setup and procedure descriptions; and the repair details, implementation, and rationale for the three proposed repair techniques.

CHAPTER 3. EXPERIMENTAL PROGRAM

3.1 Introduction

An experimental program was developed to evaluate the effectiveness of the three repair techniques discussed in Chapter 2: externally bonded FRP, NSM FRP, and a concrete supplemental diaphragm. To this end, five decommissioned prestressed concrete bridge girders acquired from the field were tested. Three of the girders were tested after being repaired using the aforementioned repair techniques. Each girder was loaded in shear with a short shear span-to-depth ratio. This chapter provides a description of the repair details, repair procedures, and the test setup used to conduct the experimental program.

3.2 Specimen Background and Details

Five AASHTO Type I prestressed concrete bridge girders were salvaged from a bridge located on Interstate 469 (I-469) in Allen County near Fort Wayne, Indiana (INDOT Asset Name I469-01-07020, NBI Number 032823). The bridge was constructed in 1988 and received only minimal substructure maintenance until the girders were transported to Bowen Laboratory at Purdue University during the summer of 2018 for the experimental program. However, as shown in Figure 3.1, many of the bridge girders showed signs of significant end region deterioration. Due to the condition of these girders, the bridge superstructure was replaced in 2018. A simple plan view of the original superstructure is shown in Figure 3.2. The girders transported to the laboratory for testing are indicated in Figure 3.2.

(a)

(b)

Figure 3.1 Typical In-Service Condition of Girder End Regions Prior to Removal

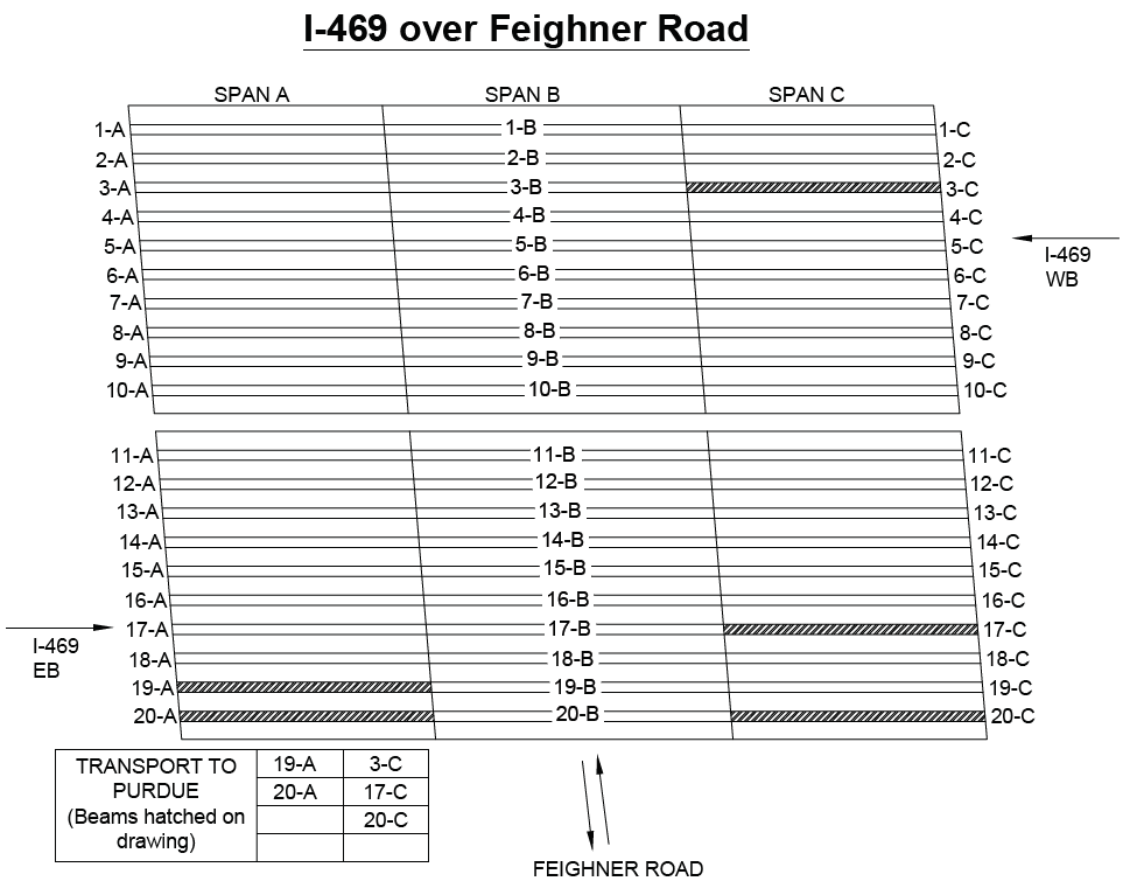

Figure 3.2 Girders of I-469 Bridge Selected for Experimental Program

Each of the five test specimens were 38.5 ft long. The cross-sectional dimensions of the girders were in accordance with the standard AASHTO Type I beam, as shown in Figure 3.3 and Figure 3.4. The reinforced concrete composite deck on top of the girders was 8-in. thick as indicated in Figure 3.4. A thin epoxy overlay had been applied to the top surface. As specified in the bridge plans (INDOT 1987), the girders were prestressed with eight 0.5-in. diameter seven-wire prestressing strands with an ultimate tensile strength, f_{pu}, of 270 ksi. As shown in Figure 3.5, four of the eight prestressing strands were straight and were located 2 in. from the bottom surface of the beam. The remaining four strands were harped with harping points located at 1/3 of the girder length from each end. All prestressing strands were initially stressed to 189 ksi, or $0.7f_{pu}$, according to the bridge plans (INDOT 1987). The stirrups were fabricated from deformed reinforcing bars. The stirrup spacing is shown in Figure 3.5. According to the bridge plans (INDOT 1987), the specified 28-day concrete compressive strength, f'_c, was 5000 psi. However, after 30 years of service, the actual concrete strength was unknown. As such, 4-in. by 6-in. concrete cores

were taken from the webs of the test specimens following testing. The average compressive strength of the cores obtained from each girder is provided in Table 3.1.

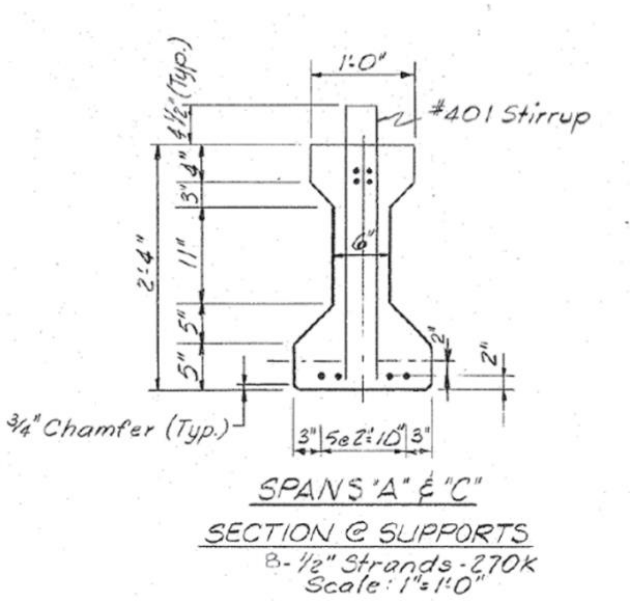

Figure 3.3 Cross Section of Test Specimens at the Original Supports (from INDOT 1987)

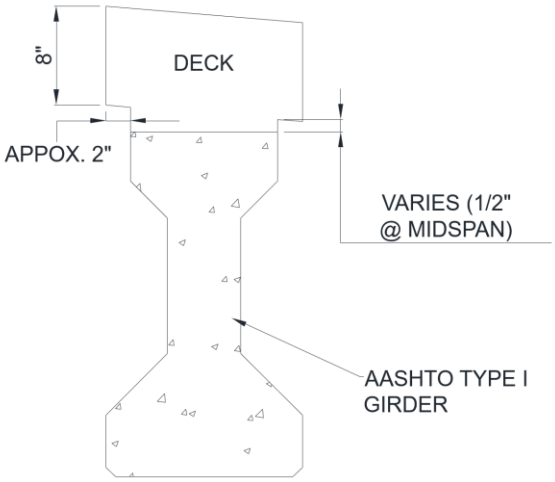

Figure 3.4 Cross Section of Test Specimens (adapted from INDOT 1987)

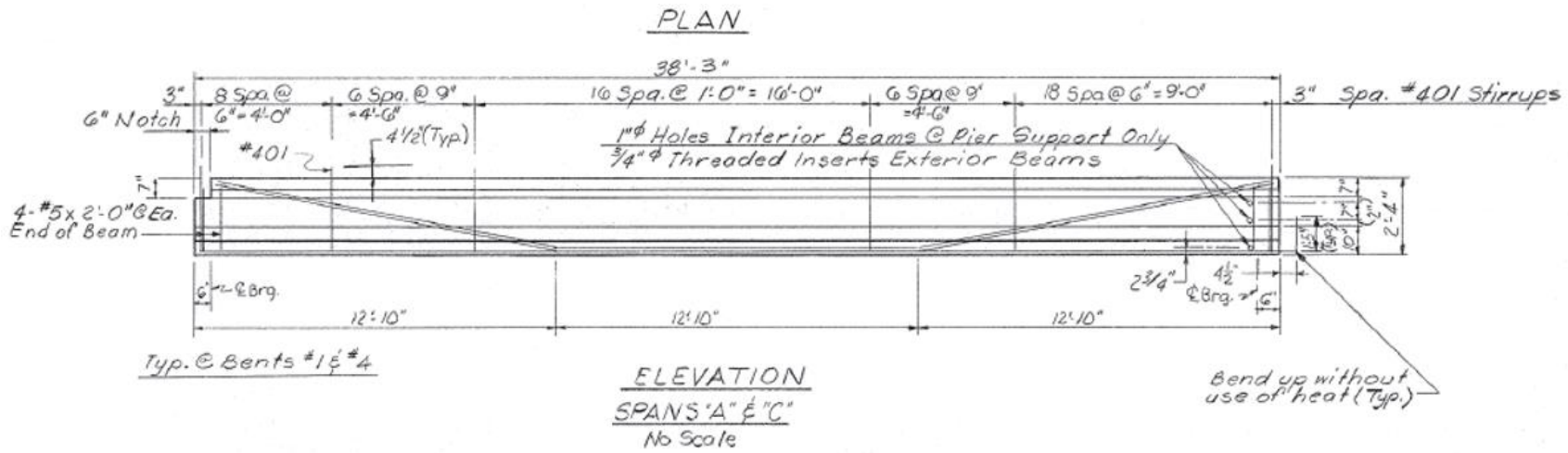

Figure 3.5 Elevation of Test Specimens (from INDOT 1987)

Table 3.1 Average Concrete Compressive Strength Obtained from Concrete Cores

Girder	Average Compressive Strength (psi)
3-C	7270
20-C	9240
19-A	7440
17-C	9070
20-A	7850

When extracting the girders from the bridge, longitudinal cuts were made approximately 2 in. from the edge of the top flange as indicated Figure 3.4. The portion of the deck that remained on the girder was kept in place through the completion of the experimental program. A transverse edge beam was cast along the ends of the girders that were detailed with the 6-in. notch noted in Figure 3.5. A portion of this edge beam remained on all of the test girders except for Girder 17-C as discussed in Section 4.2.4. As observed in Figure 3.1(b), a patch material was applied to the deteriorated end of Girder 20-A while in service. This measure is assumed to have been performed in an effort to mitigate corrosion. Additionally, one side of Girders 20-A and 20-C had been painted. Any paint or patch material remaining on the girders after being transported to the laboratory was removed prior to repairing the specimen.

3.3 Repair Details and Rationale

The test matrix for the five girder specimens is shown in Table 3.2. One of the five test girders (Girder 3-C) had an end region in good condition and was used as a control specimen. The other four girders exhibited severe end region deterioration. Girder 20-C received minimal repairs prior to testing as described in Section 3.4.2 and was tested to evaluate the performance of a deteriorated girder in its field condition. This girder is referred to herein as the damaged specimen. The remaining three test specimens were repaired using the three techniques indicated in Table 3.2. Repair details are described in Sections 3.3.2 through 3.3.4. Rationale for the selection of each repair technique is provided along with justification for the repair details. First, however, the behavior of the control girder and the girder tested in its deteriorated condition is briefly discussed as the rationale for the repairs is related to the test results of these two specimens. Complete details of the test results for all specimens are provided in Section 4.2.

Table 3.2 Test Matrix

Girder	End Region Condition	Repair Technique
3-C	Good	Control
20-C	Deteriorated	Tested in Deteriorated Condition
19-A	Deteriorated	Externally Bonded FRP
17-C	Deteriorated	NSM FRP
20-A	Deteriorated	Supplemental Diaphragm

3.3.1 Failure Behavior of Control and Damaged Specimens

Testing of the control and damaged specimens provided insight into the change in behavior caused by the deterioration of girder end regions. As previously described, for each test of the experimental program, load was applied to the girder at a distance of 45 in. from the support located at the end of the girder (further details of the test setup are provided in Section 3.5). For a girder in good condition, the loading was expected to cause the development of a diagonal strut between the applied load and the support. As shown in Figure 3.6, a diagonal strut did develop within the test region of the control specimen. The damaged specimen, however, exhibited a different behavior. The failure behavior of this specimen was controlled by the inability of the prestressing strands to develop tensile forces along the bottom flange. The primary failure crack of the damaged specimen, shown in Figure 3.7, was nearly vertical. A diagonal strut did not form within the test region due to the inability of the corroded prestressing strands to develop adequate tensile capacity in the bottom flange at the end of the member. The behaviors of the control and damaged specimens led to the observation that restoring the tensile capacity along the bottom flange is key to a successful repair. This observation influenced the details of the repair techniques included in the experimental program.

Figure 3.6 Control Specimen After Failure

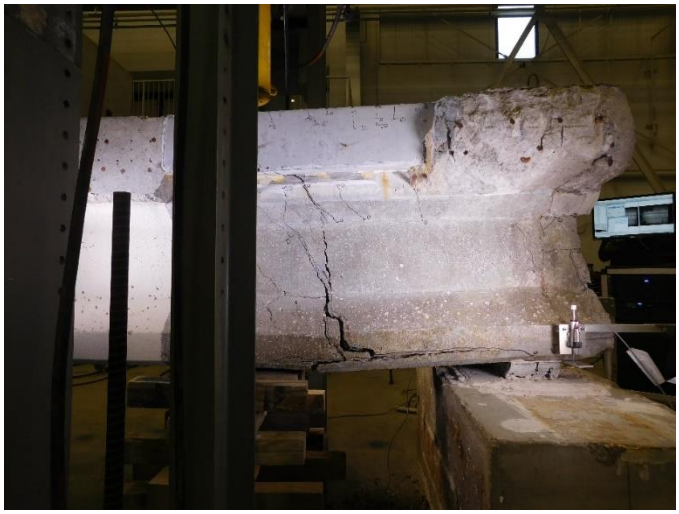

Figure 3.7 Damaged Specimen After Failure

3.3.2 Externally Bonded FRP Repair System

For the externally bonded FRP repair of the experimental program, carbon fiber sheets were used. Carbon reinforcing fibers were selected because they offer a greater ultimate tensile strength and elastic modulus than either glass or aramid fibers (ACI 440.2R-17). As a result, carbon fibers are often chosen for strengthening applications (Pevey 2018). Furthermore, carbon fiber spike anchors were used to ensure that the FRP sheets were properly anchored to the concrete. For the FRP sheets, a wet-layup installation method was used. After considering both pre-saturated sheets and dry sheets that are saturated by the installer, the latter option was chosen due to concerns about the interaction between pre-saturated FRP sheets and FRP spike anchors saturated in the field. Based upon the above decisions, an FRP sheet product (SikaWrap® 103C) was selected, which requires saturation by the installer using the wet-layup procedure. The resin specified by the manufacturer for saturating sheets of this type is an epoxy resin (Sikadur® 300). To improve the tack of the concrete surface during vertical and overhead applications, the manufacturer suggested using a different epoxy resin (Sikadur® 330) to prime and seal the concrete. The FRP spike anchors used for the end region repair were cut from a premanufactured FRP rope (SikaWrap® FX-50 C Unidirectional Carbon Fiber Rope). The applicable design properties of the externally bonded FRP sheets and rope, both in the form of a cured laminate, as reported by the manufacturer are provided in Table 3.3.

Table 3.3 Externally Bonded FRP Repair System Components and Design Values

Repair System	Constituent Materials	Nominal Ply Thickness/Cross-Sectional Area	f_{fu}^* (ksi)	ε_{fu}^*	E_f (ksi)
Externally Bonded FRP Sheet	FRP Fabric[1] + Epoxy[3]	0.04 in.	160.9	0.0145	10,390
FRP Anchor	FRP Rope[2] + Epoxy[3]	0.1 in.[2]	304	0.016	33,300

[1]SikaWrap® Hex-103 C
[2]SikaWrap® FX-50 C Unidirectional Carbon Fiber Rope
[3]Sikadur® 300 Impregnating Resin

The details of the externally bonded FRP system for the end region repair are shown in Figure 3.8. The repair system is composed of three layers of FRP. The first layer consists of FRP sheets that were cut into strips and applied with the fibers running longitudinally (Figure 3.8(a)). The ends of the strips are anchored with spike anchors as shown. The second layer consists of FRP sheets with fibers oriented vertically on the side surfaces of the girder (Figure 3.8(b)). Spike anchors are also used to anchor these sheets. Two of these sheets are U-wraps as indicated. The third layer of FRP consists of externally bonded FRP patch sheets (Figure 3.8(c)). Detailed drawings of the externally bonded system with complete dimensions are provided in Appendix A.

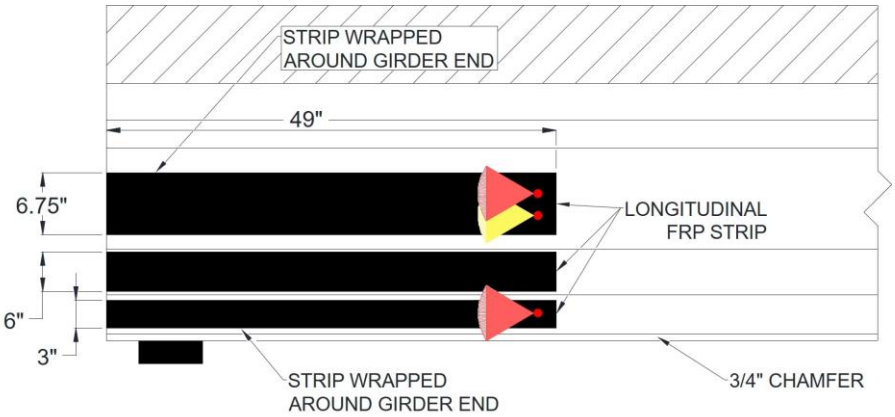

(a) Layer 1 Detail

Figure 3.8 Externally Bonded CFRP Detail

Figure 3.8 continued

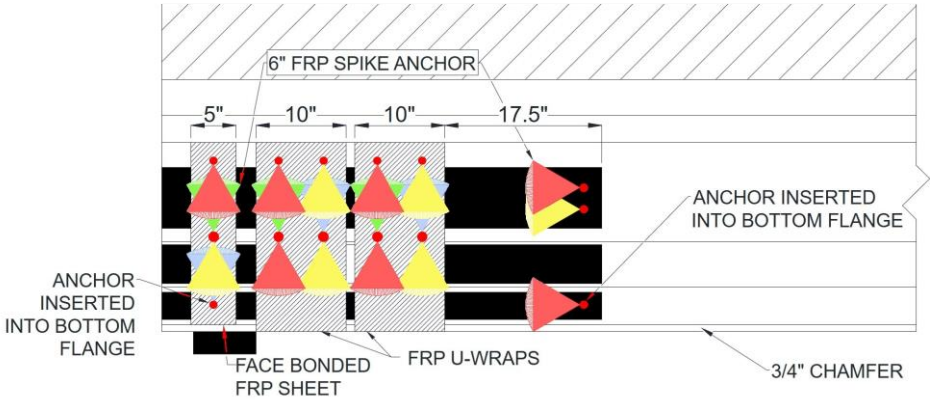

(b) Layer 2 Detail

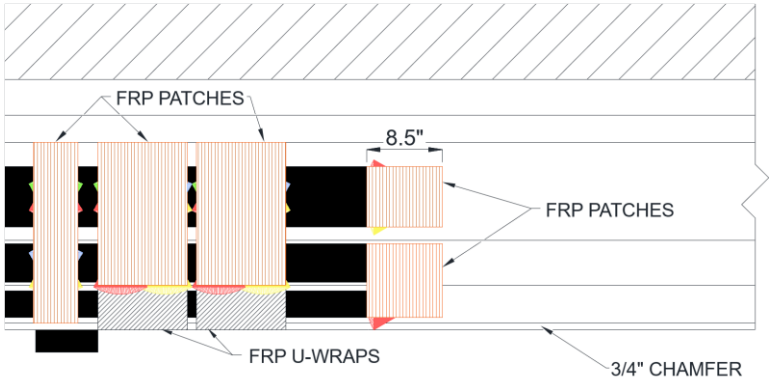

(c) Layer 3 Detail

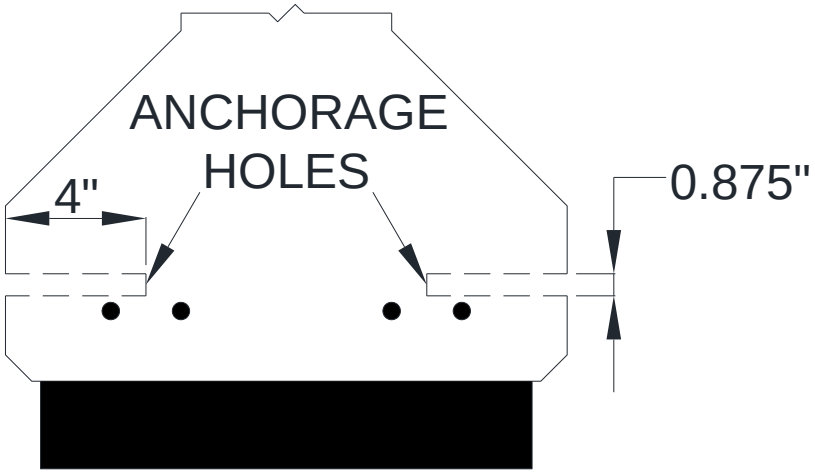

(d) Location of Anchor Holes within Cross Section of Bottom Flange

Because of the importance of restoring the tensile capacity of the girder along the bottom flange as explained in Section 3.3.1, the longitudinal FRP strips were installed as the first layer of FRP with the second layer aiding in the anchorage of these strips. As shown in Figure 3.8(a), one longitudinal strip was applied directly to the web of the specimen. Longitudinal strips were also applied directly to both the vertical and sloped surfaces of the bottom flange of the girder. The primary purpose of the longitudinal strips applied to the bottom flange was to regain the tensile capacity lost due to the deteriorated condition of the member. In contrast, the primary purpose of the longitudinal FRP strips in the studies examined in Sections 2.2.5.2 and 2.2.5.3 (Andrawes et al. 2018, Petty et al. 2011) was to provide anchorage to vertically-oriented FRP sheets. The longitudinal strip applied to the vertical surface of the bottom flange and the strip applied to the girder web each consisted of one continuous strip, wrapping around the end of the girder, providing improved anchorage for the longitudinal strip. These strips also provided additional confinement to the mortar used to the repair the end region (see Section 3.4.3). The longitudinal strips applied to the sloped surface of the bottom flange were two discrete strips on either side of the girder. Due to the surface being sloped, wrapping the strip around the end of the test specimen was not possible. The longitudinal FRP strips were extended 17.5 in. past the termination of the vertically-oriented FRP sheets. The longitudinal strips applied to the vertical surface of the bottom flange and the strip applied to the girder web were anchored at the ends using FRP spike anchors, as discussed later in this section. The longitudinal strips installed along the sloped surface of the bottom flange were not anchored, as there would be a high risk of hitting prestressing stands when drilling the anchor holes perpendicular to the surface.

The second FRP layer of the repair system consists of sheets with fibers oriented vertically on the side surfaces of the girder (Figure 3.8(b)). The sheet closest to the end of the girder is a face-bonded sheet (i.e., not a U-wrap) to simulate limitations during in-field installations near the support bearing. The second and third FRP vertically-oriented sheets from the end of the member were installed in a U-wrap configuration, as access to the bottom surface of the girder would not be limited in the field. Per the recommendations of the manufacturer, a space was left between all the externally bonded FRP sheets. A space of at least 1 in. was selected based on the research conducted by Andrawes et al. (2018). The vertically-oriented U-wrap sheets were 10-in. wide. This sheet width was selected based on practical limits. While narrower sheets result in a more uniform strain profile over the width of the sheet (Pudleiner 2016), they require more sheets to be

installed along the repair area, thus increasing the labor required for installation. However, increasing the sheet width over 10 in. can make handling the sheet during installation difficult. Because the layout of the internal steel at the end of the girder dictated the locations of the spike anchors, the width of the face-bonded sheet was reduced to 5 in. and the space between the face-bonded sheet and the first U-wrap was increased to 2.25 in. This FRP layout allowed the spike anchors to be located concentrically on the vertical FRP sheets.

A total of 19 FRP spike anchors were used on each side of the girder to anchor the externally bonded strips/sheets as shown in Figure 3.8(b). Two of these anchors were inserted into 0.875-in. diameter holes drilled horizontally into the bottom flange of the girder. The nominal area of these anchors, in the form of a cured laminate, was approximately 0.31 in.^{2}. This area was achieved by combining and folding in half (see Section 3.4.3) 1.6 20-in. long segments of the SikaWrap® FRP rope specified in Table 3.3. However, as presented in Appendix B, the amount of material used for each anchor was determined by weight, not by area. The location of the holes relative to the strands in the bottom flange is shown in Figure 3.8(d). The hole was placed such that it would be positioned between the first and second row of strands in the scenario that a girder being repaired in the field contains more than one row of stands on a 2-in. grid pattern. The depth of these holes was 4 in. Deeper holes are recommended by Orton (2008) and Pudleiner (2016). However, to minimize the risk associated with drilling holes in the bottom flange and considering the successful use of 4-in. deep anchor holes used by Jacobs (2020), a depth of 4 in. was determined to be sufficient.

Due to the 6-in. web width of the test specimens, it was not feasible to drill separate anchor holes for the anchors installed on each side of the girder. Therefore, a modified spike anchorage system different from what is typically implemented in the field was developed by drilling through the entirety of the web. Continuous anchors cut from the FRP rope were then installed in the holes and used to anchor the FRP on both sides of the girder. The installation process for these anchors is described in Section 3.4.3. A similar type of anchorage system was employed in a study conducted by El-Saikaly et al. (2015). In this study, the authors used CFRP rope to anchor CFRP L-strip plates onto reinforced concrete T-beams as shown in Figure 3.9. The T-beam specimens strengthened with the CFRP rope anchorage system exhibited greater shear strength (El-Saikaly et al. 2015). Additionally, the debonding failure mode was prevented in the CFRP rope anchored specimens (El-Saikaly et al. 2015). For the girder specimens in the experimental program of this

thesis, the holes near the bottom of the web had diameters of 1.125 in. to accommodate two anchors, and the remaining holes in the web had diameters of 0.875 in. for a single anchor. The nominal area of the anchors, in the form of a cured laminate, that were inserted through both the 1.125-in. and 0.875-in. diameter holes was approximately 0.31 in.^{2}. This area was achieved by combining 3.1 18-in. long segments of the SikaWrap® FRP rope specified in Table 3.3. A fan angle of 60° was selected for all spike anchors based on research conducted by Kim (2011) and Pudleiner (2016) as well as its successful use in Jacobs (2020). For the current experimental program, the remaining spike anchorage detailing, including number of anchors per sheet, required anchorage area, and anchor hole diameter, followed the recommendations and calculations outlined in Pudleiner (2016). See Appendix B for complete spike anchorage detailing calculations.

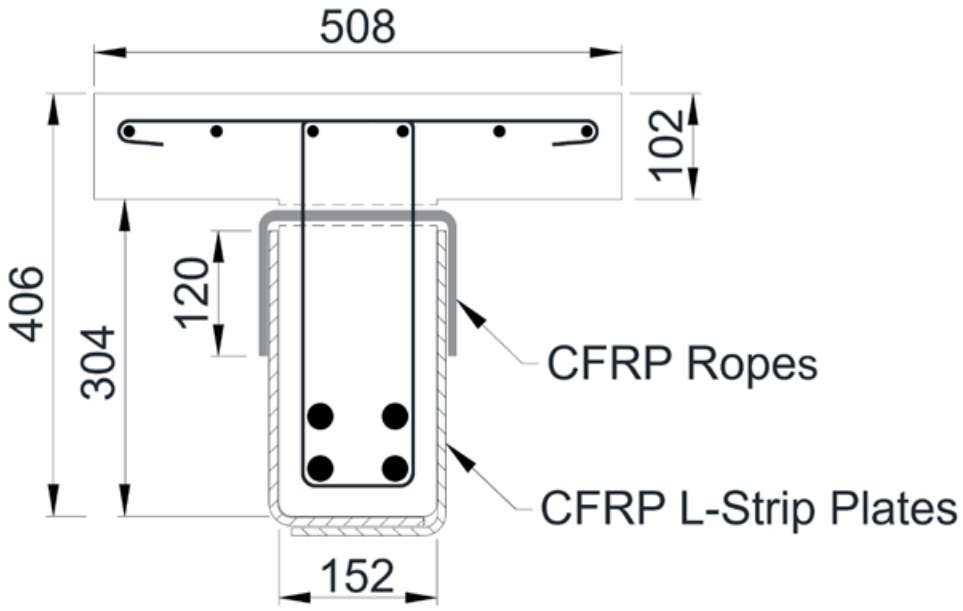

Figure 3.9 CFRP L-Strip Plates Anchored with CFRP Ropes (adapted from El-Saikaly et al. 2015)

The third FRP layer of the repair system consists of externally bonded FRP patch sheets applied over the FRP spike anchors as shown in Figure 3.8(c). Research conducted by Kim et al. (2012) was used as guidance for the design of the patch system. Two layers of externally bonded FRP sheets were placed over the anchors. The fibers of the first layer of the patch sheets were orientated perpendicular to the fibers of the externally bonded sheet/strip of interest, while the fibers of the second layer of patch sheets were orientated parallel to the fibers of the externally bonded sheet/strip. Limited guidelines exist for FRP patch sheet geometry, especially for members

with complex geometries such as I-shaped beams. Therefore, the patch sheet geometries used in this study were based on a combination of successful geometries from previous FRP research (Kim et al. 2012, Pudleiner 2016) and engineering judgement. Typically, the patch sheets are taken as the same width as the corresponding externally bonded FRP sheet/strip. The patch sheet widths for the vertically-oriented face-bonded sheets above the bearing support, the U-wrap sheets, and the longitudinal strip along the web of the girder were therefore selected to match the width of each respective sheet or strip. The patch width for the longitudinal strips along the bottom flange of the girder was increased due to the smaller widths of these strips. More specifically, the patch width was increased to cover the entire width of both the longitudinal strip along the vertical surface of the bottom flange and the strip along the sloped surface of the flange.

The lengths of the patch sheets satisfied the recommendation proposed by Pudleiner (2016) that the patch sheets should extend a minimum of 2 in. beyond the anchorage locations (i.e., beyond the hole into which the anchors are inserted). As such, the patch sheets for the vertically-oriented face-bonded sheets extend over the entirety of the sheets. To meet the recommendation by Pudleiner (2016), the length of the patch sheets corresponding to the U-wraps should extend from the top of the U-wrap sheets to 2 in. beyond the location of the bottom anchor holes. However, because this would result in the patches terminating near a reentrant corner, the patches extend to the end of the sloped surface of the bottom flange as shown in Figure 3.8(c). Finally, the length of the patch sheets at the termination of the longitudinal strips were selected to match the distance from the end of the longitudinal strips to the termination of the splayed fan anchors. The patch sheets are therefore 8.5-in. long.

3.3.3 NSM FRP Repair System

To serve as an alternative FRP repair technique, an FRP NSM repair system was developed. Carbon fiber NSM strips (Hughes Brothers Aslan 500 #2 Carbon Fiber Reinforced Polymer Tape) were selected because of their availability and proven performance in the study conducted by Jacobs (2020). The results from the flexural strengthening program in Jacobs (2020) demonstrated that NSM strips were an effective repair technique for flexural strengthening of damaged reinforced concrete beams. Therefore, the same NSM strips were selected to restore the tensile capacity lost in the bottom flange of the deteriorated end region due to ineffective prestressing strands. Furthermore, NSM FRP strips are relatively easy to install compared to externally bonded

FRP, decreasing the amount of labor required in the field while also eliminating potential sources of error such as uneven saturation of FRP sheets and air voids trapped beneath the sheets. Pertinent mechanical design values of the NSM strips as reported by the manufacturer are shown in Table 3.4. These values apply to the dry FRP strips alone. The nominal cross-sectional dimensions of the strips are 0.079-in. by 0.63-in.

Table 3.4 NSM FRP Repair System Components and Design Values

Repair System	Constituent Materials	A_f (in.^{2})	f_{fu}^* (ksi)	ε_{fu}^*	E_f (ksi)
Near-Surface-Mounted (NSM) Strips	FRP Tape[1] + Epoxy Grout[2]	0.049	325	0.0181	18,000

[1]Hughes Brothers Aslan 500 #2 Carbon Fiber Reinforced Polymer Tape
[2]Pilgrim Permocoat Magmaflow Grout-Pak CF Epoxy Grout

The details of the NSM FRP repair system used for the experimental program are shown in Figure 3.10. The system consisted of four NSM FRP strips on each side of the girder. Two strips were embedded in the vertical surface of the bottom flange and two strips were embedded in the sloped surface of the flange. Like the longitudinal FRP strips in the externally bonded FRP repair system, the NSM strips were installed to restore the tensile capacity lost due to the deterioration of the prestressing strands in the bottom flange of the girder. The groove depth selected (0.875 in.) allows for the system to be implemented on girders which have a clear cover of 1 in., typical of girders with confinement reinforcement enclosing the pretensioned strands in the bottom flange within the end region of the member. The selected clear spacing between the grooves was 1.25 in. It should be noted that the groove depth is less than the depth (1.5 times the greater dimension of the strip) suggested by ACI 440.2R-17. However, the strips used to repair the girder end region were also used in 0.875-in. deep grooves during the flexural strengthening test program conducted by Jacobs (2020) without any noted issues related to the groove depth. Additionally, due to the dimensions of the girder, adhering to the clear spacing (twice the groove depth) and clear edge distance (four times the groove depth) suggested by ACI 440.2R-17 was not practical. The groove width (0.25 in.) is greater than the minimum width (three times the smaller dimension of the strip) suggested by ACI 440.2R-17.

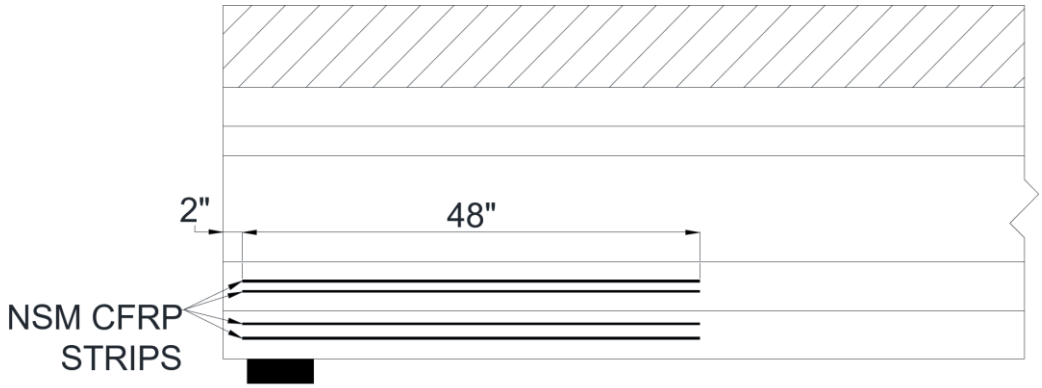

(a) Elevation Detail

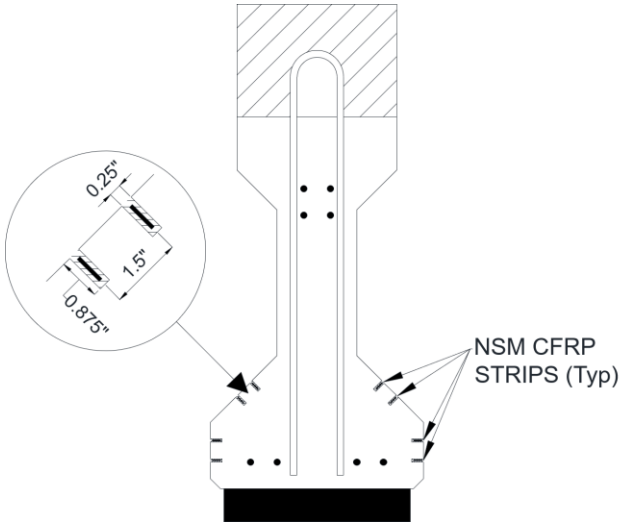

(b) Cross-Sectional Detail

Figure 3.10 NSM FRP Details

3.3.4 Supplemental Diaphragm Repair Systems

The supplemental diaphragm repair technique provides a method that incorporates materials that are more conventional than FRP. The supplemental diaphragm also provides a means to compare the constructability and effectiveness of utilizing traditional materials versus the use of FRP.

The details of the supplemental diaphragm repair system are shown in Figure 3.11. The reinforcement layout was adapted from the reinforcement details utilized in the Needham (2000) and Shield and Bergson (2018) studies presented in Section 2.3. The reinforcing details include two pairs of epoxy-coated No. 3 reinforcing bars (i.e., dowels) inserted through the web to transfer

stresses from the original girder to the repair material. No. 3 reinforcing bars were used for this application, as opposed to No. 4 bars, to aid with the required field bend that is noted in Figure 3.11. The remainder of the reinforcing cage consisted of epoxy-coated No. 4 bars arranged in a manner somewhat similar to the details used in the previous studies described in Section 2.3. While designing the diaphragm, the possibility of casting a diaphragm continuously between adjacent girders in the field was kept in mind. Therefore, transverse reinforcement within the diaphragm in the form of closed stirrups was included. More specifically, as shown in Figure 3.11, one epoxy-coated No. 4 closed stirrup was included in the diaphragm on each side of the girder. Lastly, four U-shaped epoxy-coated No. 4 bars with unequal leg lengths (4.25 in. and 7.25 in.) were included in the diaphragm on each side of the girder. As shown in Figure 3.11(b), these bars were oriented in a manner such that the shorter leg was located at the bottom of the reinforcing cage while the longer leg was located at the top of the reinforcing cage. The repair region extended 24 in. along the length of the girder, which was the minimum length needed to repair the portion of the girder that experienced significant section loss. To account for the possibility of severe deterioration around the original bearing location along with potential concrete consolidation issues near the bottom of the original cross section when implementing the repair in the field, a bearing pad was not placed at the original bearing location during testing. Instead, two bearing pads with lengths equal to half the length of the original bearing pad (measured transverse to the longitudinal axis of the girder) were placed 1.0 in. from the edge of the repair area as shown in Figure 3.11(b). All reinforcement used for the repair was Grade 60 (ASTM A615).

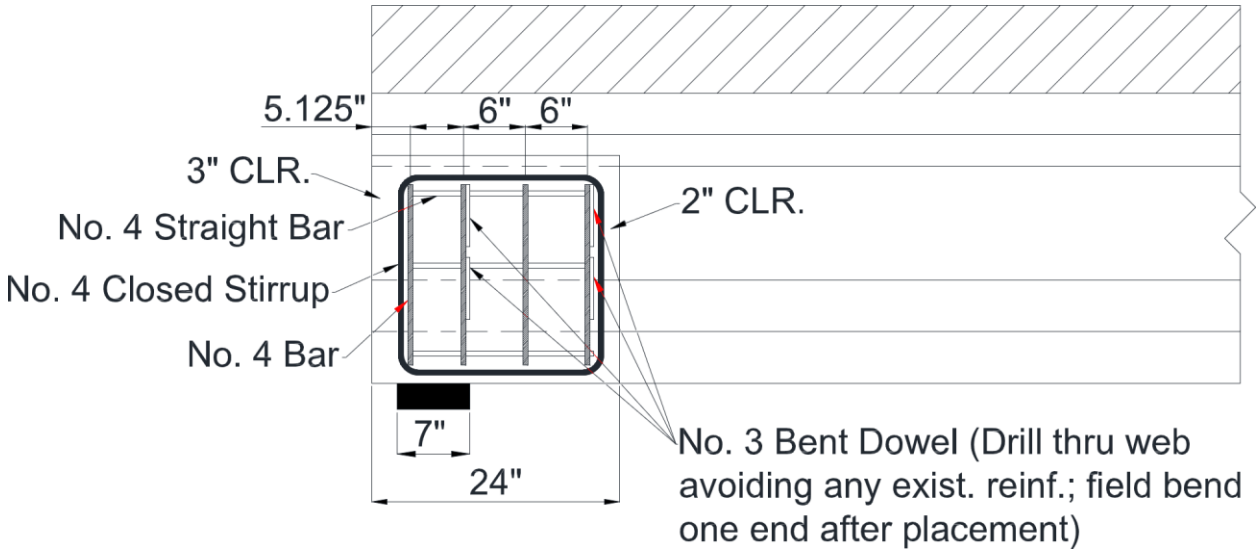

(a) Elevation Detail

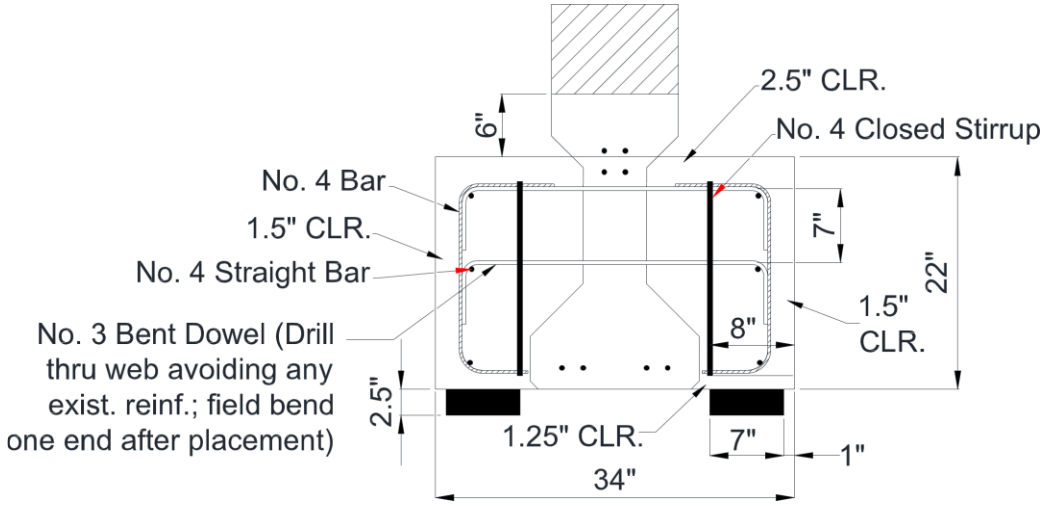

(b) Cross-Sectional Detail

Figure 3.11 Supplemental Diaphragm Details

A self-consolidating concrete (SCC) mixture was used to increase the constructability of the repair. SCC is a flowable concrete that does not require vibration, making it an ideal choice for applications with limited access to the repair region or tightly congested regions. Moreover, SCC is pumpable, giving designers further flexibility when implementing such systems. As a result, a 6-in. clearance was left from the top of the diaphragm to the top surface of the precast girder, allowing for the SCC to be pumped into the forms from below the girder in the field. The mixture

design for the SCC is show in Table 3.5. The specified 28-day compressive strength of the concrete was 6000 psi.

Table 3.5 SCC Mixture Design for Supplemental Diaphragm

Material	Details	Design Quantity	Units
Cementitious Material	Type 1 Cement	580	lb/yd^3 concrete
	Class F Ash	145	
Coarse Aggregate	3/8 in. Pea Gravel	1650	
Fine Aggregate	Natural Sand	1379	
Water	---	279.5	
Admixtures	High-Range Water Reducer	10.00	oz/cwt cementitious material
	Viscosity Modifier	4.00	

Specified f'_c = 6000 psi
Water/Cement Ratio = 0.39
Design Spread = 25.00" +/- 7.0"
High-Range Water Reducer: MasterGlenium 7511
Viscosity Modifier: MasterMatrix VMA 358

3.4 End Region Repair Procedures

In this section, all of the procedures required to prepare the five AASHTO Type I girders for testing are discussed. This discussion includes (1) removal of a drain from the deck of two test specimens and the subsequent repair of the decks; (2) repair of the bearing area on one of the specimens prior to testing; and (3) procedures used to implement the three repair techniques described in Section 3.3.

3.4.1 Drain Removal and Deck Repair

Two of the recovered test specimens, Girders 20-C and 20-A, were fascia girders. Because of their location relative to the roadway, stormwater runoff drains were installed in the concrete deck directly above the girders. As shown in Figure 3.12, the proximity of the drains relative to the desired load point for the load tests required that the drains be removed. Concrete was cast to fill the voids left from the removal of the drains.

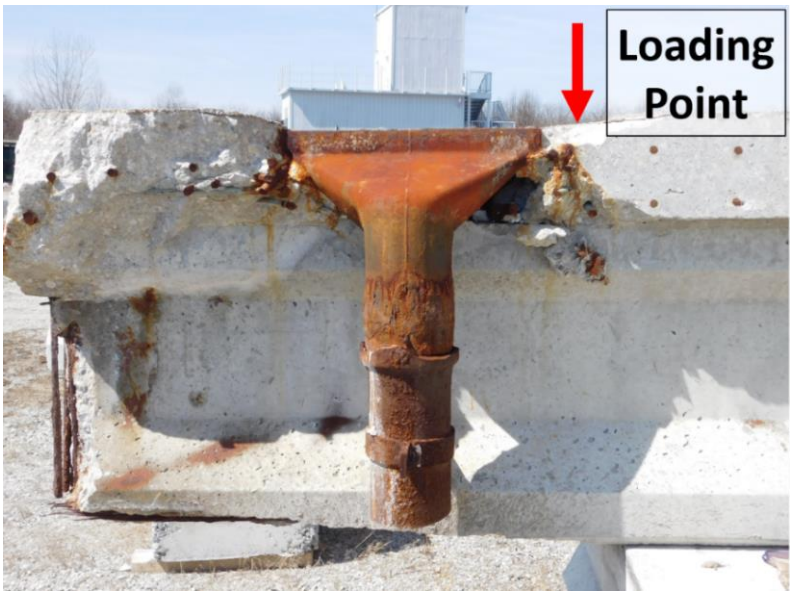

Figure 3.12 Proximity of Load Point to Bridge Drain

The space left within the deck after removal of a drain is shown in Figure 3.13(a). After drain removal, approximately 8 in. of concrete deck, measured from the edge of the former location of the drain toward the midspan of the girder, was removed using a concrete saw and chipping hammer (Figure 3.13(b and c)). Per ICRI Guideline No. 310.1R-2008, concrete was removed from the deck to form a rectangular repair area. A hammer drill with a 0.875-in. drill bit was used to roughen the concrete surface at the ends of the repair area as shown in Figure 3.13(d) to improve the bond between the original deck concrete and the repair concrete.

(a) Void Left After Drain Removal

(b) Sawing Concrete Deck

Figure 3.13 Drain and Deck Concrete Removal and Surface Roughening

Figure 3.13 continued

(c) Removing Concrete to Create Rectangular Repair Area

(d) Roughened Surface at End of Repair Area

Next, reinforcement was added to the region being prepared as shown in Figure 3.14. The reinforcement pattern matched the reinforcement pattern of the original deck: two layers of No. 5 Grade 60 longitudinal reinforcement with a 3.5-in. vertical center-to-center spacing and two layers of No. 5 Grade 60 transverse reinforcement with a 6-in. spacing measured along the length of the girder. The longitudinal reinforcement consisted of pairs of 24-in. long reinforcing bars with one end of each bar doweled into the original girder at the edge of the repair. Each bar was embedded approximately 3 in. into the deck concrete using an epoxy intended for anchoring reinforcing steel in hardened concrete (Figure 3.14(a and b)). This configuration resulted in a 14-in. contact lap splice at the center of the repair area (Figure 3.14(c)). The transverse reinforcement spaced at 6 in. was then positioned after the longitudinal bars were in place (Figure 3.14(d)). At the drain locations, the portion of two stirrups extending into the concrete deck had been either removed or bent to allow for installation of the drain. As such, supplemental reinforcement (No. 4 Grade 60 bars) was also added to replace the portion of the stirrups extending from the top surface of the precast girder to further improve the bond between the repair concrete and the original girder. The supplemental reinforcement was bent to form a U-shape in order to match the original stirrups. Each leg of the U-shaped bars was embedded approximately 4.5 in. into the top surface of the precast girder using epoxy (Figure 3.14(e and f)).

(a) Dispensing Epoxy for Anchorage of Longitudinal Reinforcement

(b) Inserting Longitudinal Reinforcement

(c) Longitudinal Reinforcement After Placement

(d) Transverse Reinforcement

(e) Installing U-Shaped Bars

(f) Completed Reinforcement

Figure 3.14 Reinforcement Installation Procedure for Deck Repair

Finally, formwork was erected on each side of the repair area (Figure 3.15(a)). The formwork was installed such that the top surface of the repair area matched the slope of the original concrete deck. To resist lateral pressure, two 0.25-in. diameter threaded rods where inserted through the sidewalls of the formwork and anchored. Additionally, vertical and diagonal supports were attached to each piece of formwork (Figure 3.15(b)). Upon completion of the formwork, a high-slump INDOT Class C concrete was used to fill the repair area. The completed deck repair is shown in Figure 3.15(c), and the INDOT Class C concrete mixture design is provided in Table 3.6.

(a) Erected Formwork

(b) Formwork Supports

(c) Completed Deck Repair

Figure 3.15 Completion of Deck Repair Procedure

Table 3.6 High-Slump INDOT Class C Mixture Design for Deck Repair

Material	Details	Design Quantity	Units
Cementitious Material	Type 1 Cement	658	lb/yd^3 concrete
Coarse Aggregate	#8 Limestone (INDOT)	1738	
Fine Aggregate	Natural Sand	1242	
Water	---	267	
Admixtures	High-Range Water Reducer	7.00	oz/cwt cementitious material

Specified f'_c = 5000 psi
Water/Cement Ratio = 0.41
Design Slump = 6.50" +/- 1.5"
High-Range Water Reducer: MasterGlenium 7511

3.4.2 Damaged Specimen Bearing Repair

One of the girders with a deteriorated end region was tested with minimal repairs to establish the impact of the end region deterioration on the capacity of the bridge girders. Furthermore, by comparing the strengths of the repaired girders to the capacity of this specimen, the test served as a means by which the effectiveness of the three repair techniques could be evaluated. As such, Girder 20-C was tested in a damaged condition. However, minimal repairs were required in order to perform the test.

While extracting the bridge girders and then transporting them from the bridge site, loose concrete fell from the end regions of the member. Therefore, prior to testing Girder 20-C, reestablishing a bearing area for the girder was necessary. The condition of the girder prior to repairs is shown in Figure 3.16. As shown in Figure 3.5, the centerline of the bearing pad was located 6 in. from the end the member when the girder was in-service. This left 2.5 in. from the end of the girder to the edge of the pad. Restoring the bearing area at this location, however, would have required substantial repairs. Therefore, the bearing location was shifted 4 in. into the span of the girder for testing.

(a) Elevation **(b) Bottom Surface**

Figure 3.16 Condition of Girder 20-C Prior to Bearing Repair

The bearing area was restored using a fast-setting, low-shrinkage, high-strength mortar (CTS Cement Manufacturing Corp. Rapid Set® Mortar Mix). The mortar repair procedure is shown in Figure 3.17. To minimize wasted material, each 55-lb mortar bag was divided into identical 18.3-lb batches. The manufacturer suggested a mixing ratio between 3.0 and 3.75 quarts of water per 55 lbs. After trials were conducted, a mixing ratio of 3.5 quarts of water per 55-lb bag, with the addition of 1/3 of a 25-gram bag of Rapid Set® Set Control® (Figure 3.17(a)), yielded the best results. Dust and debris were removed from the repair area by pressurized air prior to mixing the water and mortar. The Rapid Set® Set Control® admixture was combined with the appropriate volume of water and then added to the proportioned mortar. An electric drill with a mixing paddle was used to mix the mortar until a uniform consistency was achieved (Figure 3.17(b)). The repair surface was wetted using a spray bottle to assist with the mortar application as the manufacturer suggested. Mortar was then placed and packed by hand until an adequate bearing area was restored (Figure 3.17(c)). Relevant properties of Rapid Set® Mortar Mix are displayed in Table 3.7.

(a) Rapid Set® Set Control®

(b) Mixing Mortar

(c) Placing Mortar

Figure 3.17 Mortar Repair Procedure

Table 3.7 Rapid Set® Mortar Mix Properties (CTS Cement Manufacturing Corp. 2018)

Property	Value	ASTM Specification
Initial Set	15 min	C266
Final Set	35 min	C266
1-Hour Compressive Strength[1]	2500 psi	C109 Modified
24-Hour Compressive Strength[1]	5000 psi	C109 Modified
28-Day Compressive Strength[1]	6500 psi	C109 Modified
28-Day Length Change in Air	-0.04	C157 Modified Per C928

[1]Data obtained at flow consistency 100 by ASTM C1437 at 70°F (21°C).

3.4.3 Externally Bonded FRP Repair Specimen

Using the details discussed in Section 3.3.2, a repair procedure was developed for the externally bonded FRP repair system. Careful considerations were made to ensure that the repair procedures were conducted in a manner as similar as possible to an in-field installation. To this end, a board was placed approximately 2 in. from the end of the girder to simulate the presence of a mud wall. Furthermore, a bearing pad was supported against the girder at its original location during the repair procedure. The simulated mud wall and placement of the bearing pad are shown in Figure 3.18.

Figure 3.18 Simulated Mud Wall and Bearing Pad Location for Externally Bonded FRP Specimen

The process followed for repairing the end region with mortar and preparing the specimen for the application of the externally bonded FRP is displayed in Figure 3.19. The repair began by removing delaminated concrete from the end region using an electric chipping hammer until sound concrete was reached (Figure 3.19(a)). Care was taken to keep the regions from which concrete was removed as rectangular in shape as possible, per ICRI Guideline No. 310.1R-2008. To remove corrosion product and mitigate microcracking caused by the impact hammer, as recommended by ICRI Guideline No. 310.1R-2008, the regions where concrete was removed or had previously fallen from the specimen were sandblasted by an outside contractor (Figure 3.19(b)). The end of the specimen after sandblasting is shown in Figure 3.19(c). Next, the original cross section of the girder was restored using Rapid Set® Mortar Mix (Figure 3.19(d)). The mortar repair procedure as

outlined in Section 3.4.2 was again followed. After the mortar cured, the surface of the concrete to which FRP was to be applied was sandblasted to a concrete surface profile (CSP) of 3 per ICRI Guide No. 330.2-2016 and ACI 440.2R-17 (Figure 3.19(e)). A set of CSP chips were used as a reference to verify adequate surface roughness. As shown in Figure 3.19(f), prior to applying FRP to the concrete surface, a hammer drill with a 0.875-in. diameter drill bit was used to drill anchor holes at the locations indicated in Figure 3.8(b). It is recommended that the anchor holes which require drilling through the entirety of the web be drilled from both sides of the girder to mitigate concrete breakout. Based on a trial-and-error approach, a suggested procedure was developed for this process and is provided in Section 5.3 as a recommendation. Per ICRI Guide No. 330-2016 and ACI 440.2R-17, the edges of the anchor holes were rounded to a radius of 0.5 in. using a rotary tool to reduce stress concentrations (Figure 3.19(g)). Similarly, the edges of the girder over which the FRP sheet were applied were rounded to a radius of 0.5 in. (Figure 3.19(h)).

(a) Removing Delaminated Concrete

(b) Sandblasting to Remove Corrosion

Figure 3.19 Mortar Repair, Surface Preparation, and Drilling Anchor Holes

Figure 3.19 continued

(c) Condition After Sandblasting

(d) Specimen After Mortar Repair

(e) Sandblasting for FRP Application

(f) Drilling Anchor Holes

(g) Rounding Edges of Anchor Holes

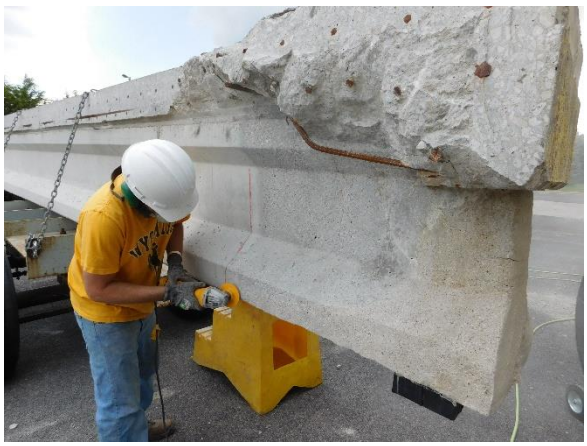

(h) Rounding Girder Edges

As discussed in Sections 3.3.2, the externally bonded FRP was installed using a wet-layup application procedure. The steps followed for the girder specimen are presented in Figure 3.20. As

shown in Figure 3.20(a), paint rollers were used to seal the concrete surface with the appropriate epoxy resin (Sikadur® 330). Sealing the concrete surface with Sikadur® 330 eliminates air voids and ridges in the concrete surface and provides a tack coat to help prevent the fabric from sagging during installation. The longitudinal FRP fabric strips were then saturated with epoxy resin (Sikadur® 300) using plastic laminating rollers (Figure 3.20(b)). Next, the strips were applied to the primed concrete surface (Figure 3.20(c)) at the locations shown in Figure 3.8(a). Once in place, plastic laminating rollers were used to fully impregnate the longitudinal FRP strips and eliminate air voids (Figure 3.20(d)). Squeegees were then used to eliminate excess epoxy (Figure 3.20(e)). Once the longitudinal strips were in place, the vertically-oriented face-bonded sheets above the bearing support and the U-wraps were applied in the same manner to the appropriate locations shown in Figure 3.8(b). The end region of the specimen after all externally bonded strips/sheets were applied is shown in Figure 3.20(f).

(a) Sealing Concrete Surface

(b) Saturating Longitudinal FRP Strips

Figure 3.20 Application of Externally Bonded Strips/Sheets

Figure 3.20 continued

(c) Placing Longitudinal Strips

(d) Rolling FRP to Eliminate Air Pockets

(e) Removing Excess Epoxy with Squeegee

(f) Externally Bonded Strips/Sheets Applied to Specimen

The installation procedure for the FRP spike anchors is shown in Figure 3.21. For the FRP spike anchors that extended through the entirety of the web, a 1/8-in. wooden dowel was fastened within the spike anchors using zip-ties to aid in the installation process, as shown in Figure 3.22. To install the anchors, empty caulk tubes were first filled with the appropriate epoxy resin (Sikadur® 330). A razorblade was then used to separate the fibers of the FRP sheets (Figure 3.21(a)), and the caulk tube was inserted into the anchor hole (Figure 3.21(b)). For the anchors that extended through the web, the anchor hole was first filled half-way with epoxy and the spike anchor was then inserted, as shown in Figure 3.21(c). Next, the wooden dowel was removed from the anchor (Figure 3.21(d)), and the ends of the spike anchors were fanned out at a 60° angle (Figure 3.21(e)) on each side of the girder and saturated with epoxy (Figure 3.21(f)). Using the

filled caulk tube, additional epoxy was injected into the anchor holes to eliminate possible air voids. The same installation procedure was followed for the anchor holes in the bottom flange of the girder, except that the hole was filled entirely with epoxy prior to inserting the anchor and the anchors were folded in half, as shown in Figure 3.23, providing a nominal anchor cross-sectional area of approximately 0.31 in.^{2} (see Section 3.3.2). However, as presented in Appendix B, the amount of material used for each anchor was determined by weight, not by area. Subsequently, the FRP patch sheets were saturated with epoxy (Sikadur® 300) (Figure 3.21(g)) and installed using the same procedure previously described for the externally bonded strips/sheets. Two FRP patch sheets, the first with the fibers orientated perpendicular to the fibers of the FRP sheets and the second with the fibers orientated parallel to the fibers of the FRP sheets, were applied over the installed anchors at the locations shown in Figure 3.8(c) (Figure 3.21(h)). The completed externally bonded FRP repair system installed on the girder specimen is shown in Figure 3.21(i).

(a) Separating Fibers with Razor Blade

(b) Injecting Anchor Hole with Epoxy

Figure 3.21 Spike Anchor Installation Procedure and Completed Externally Bonded FRP Repair System

Figure 3.21 continued

(c) Inserting Spike Anchor

(d) Removing Wooden Dowel

(e) Fanned-Out Anchors

(f) Saturating Anchors

(g) Saturating Patch Sheets

(h) Placing Patch Sheets

Figure 3.21 continued

(i) Completed Externally Bonded FRP Repair System

Figure 3.22 Assembled FRP Spike Anchor for Web Installation

Figure 3.23 Assembled FRP Spike Anchor for Bottom Flange Installation

3.4.4 NSM FRP Repair Specimen

The repair procedure for the specimen tested to evaluate the NSM FRP repair described in Section 3.3.3 consisted of restoring the cross section of the girder with mortar followed by installation of the NSM strips. As with the specimen with externally bonded FRP, a board was placed at the end of the test specimen as shown in Figure 3.24 to simulate a mud wall while the

specimen was prepared for the mortar repair and while the mortar repair was performed. Furthermore, a bearing pad, also shown in Figure 3.24, was placed in its original position during the repair procedures. The procedures that were followed to prepare the end region for the mortar repair and the mortar repair itself were identical to the procedures followed for the specimen with externally bonded FRP. These procedures are outlined in Section 3.4.3. and are shown for the NSM FRP specimen in Figure 3.25. The key stages presented in Figure 3.25 include the removal of delaminated concrete, sandblasting in preparation for the mortar repair, and the end region after the cross section was restored using the same mortar that was previously described. Upon completion of the mortar repair, it was determined that the surface of the repair was too uneven to cut the required grooves at a uniform depth. Therefore, an additional thin layer of mortar was applied over the initial mortar repair to provide a smoother surface.

Figure 3.24 Simulated Mud Wall and Bearing Pad Location for NSM FRP Specimen

(a) Removing Delaminated Concrete

(b) Sandblasting to Remove Corrosion

(c) Condition After Sandblasting

(d) Specimen After Mortar Repair

Figure 3.25 Mortar Repair Procedure for NSM FRP Specimen

NSM FRP systems consist of bars or strips that are embedded into a concrete substrate. The process for installing the NSM FRP strips into the girder specimen of the test program is presented in Figure 3.26. As shown in Figure 3.26(a), a tuckpointing grinder with a 0.25-in. thick diamond cutting blade was used to cut grooves at the locations and with the dimensions specified in Figure 3.10. To ensure the grooves were cut straight and at a constant depth of 0.875-in., a steel angle was temporarily attached to the test specimen. Prior to installation of the FRP strips, compressed air was used to remove dust and debris from the grooves. Then, the installation of the NSM strips was conducted. This process was performed for two grooves (i.e., a pair of grooves on the same repair surface) at a time. First, approximately one-quarter of the grooves was filled with epoxy grout (Figure 3.26(b)). Next, an FRP strip was inserted into each of the two grooves (Figure 3.26(c)). To ensure an adequate bond between the epoxy grout, concrete substrate, and FRP strip,

the strips were inserted into the grooves using a sawing motion until they were centered at approximately the mid-depth of the grooves. The remainder of each groove was then filled with epoxy grout, and squeegees were used to level the epoxy grout to the surface of the test specimen (Figure 3.26(d)). The process was then repeated for the remaining pairs of grooves. The end region of the specimen after the repair was completed is shown in Figure 3.26(e).

(a) Cutting NSM Groove

(b) Filling Groove with Epoxy Grout

(c) Inserting NSM Strip

(d) Leveling Off Excess Epoxy Grout

Figure 3.26 Installation of NSM FRP Strips

Figure 3.26 continued

(e) Completed NSM Repair System

3.4.5 Supplement Diaphragm Repair Specimen

The repair of the specimen with the supplemental diaphragm described in Section 3.3.4 involved minimal surface preparation and concrete chipping, unlike the specimens repaired with the FRP systems. Because the specimen was a fascia girder, one side of the member had been painted. The paint was removed within the end region of the member using a putty scraper. Furthermore, a patch material that had previously been applied to the bottom flange of the member in the field as a measure to mitigate deterioration was also removed. As indicated in Figure 3.27, it was also necessary to remove a large portion of the bottom flange prior to the repair. The portion was only bonded to a single stirrup and had separated from the surrounding concrete. The condition of the girder following the removal of this portion of concrete is shown in Figure 3.28.

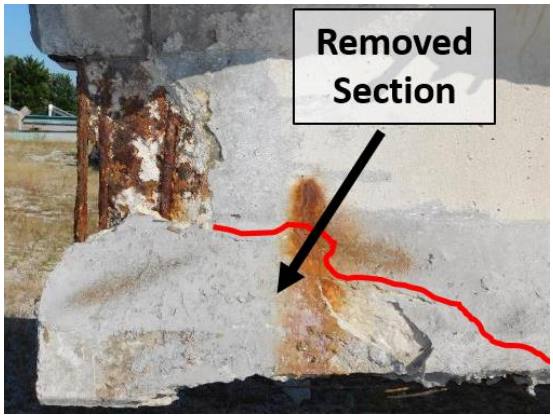

Figure 3.27 Flange Portion Removed from Supplement Diaphragm Specimen

(a) Elevation – Side 1

(b) Elevation – Side 2

(c) End View

Figure 3.28 Condition of Specimen Prior to Supplemental Diaphragm Repair

The procedure followed for the construction of the supplemental diaphragm is presented in Figure 3.29. It should be noted that some of the photographs illustrate the procedure being conducted near the undamaged end of a girder. However, the procedure used at the damaged end of the test specimen was the same. Assembly of the reinforcing cage for the supplemental diaphragm (Figure 3.11) began with drilling holes for the epoxy-coated No. 3 dowel bars. One end of the bar was pre-bent prior to installation, while the other end was bent after the bar was inserted through the girder web. Using a hammer drill with a 0.5-in. diameter drill bit, holes were drilled through the entire thickness of the web, as shown in Figure 3.29(a), at the locations indicated in Figure 3.11. While holding a finger over one end of the hole to plug it, epoxy (Unitex® Pro-Poxy™ 400) was injected into the hole (Figure 3.29(b)). With the No. 3 reinforcing bar marked at the termination point of the field bend and one end of the hole still plugged, the unbent end of the bar

was inserted into the hole (Figure 3.29(c)). When the bar reached the plugged end of the hole, the hole was unplugged, and the bar was pushed through the hole until the mark on the bar was visible (Figure 3.29(d)). To bend the bar, the bar was first rotated so that the hook extension at the pre-bent end of the bar was oriented horizontally and pointing toward the midspan of the girder (Figure 3.29(e)). To perform the 90° field bend, a steel pipe was inserted over the unbent end of the bar and, with the end of the pipe touching the concrete surface of the girder web, the pipe was forced toward the beam (Figure 3.29(f)). Once the end of the bar was bent, the position of the bar was adjusted so that the hooked ends of the bar were centered on the beam (Figure 3.29(g)). The bar was subsequently cleaned to remove excess epoxy. To eliminate air voids in the hole, more epoxy was injected into both sides of the hole (Figure 3.29(h)). The hook extension of the 90° field bend was then cut to the appropriate length (Figure 3.29(i)), resulting in the bar shown in Figure 3.29(j). After all four No. 3 dowel bars were installed, the remaining epoxy-coated No. 4 reinforcing bars were tied to the No. 3 dowel bars to complete the reinforcing cage, as shown in Figure 3.29(k and l). Formwork was then erected around the repair region. A closed-cell polystyrene board was used to form the bottom surface of the diaphragm as shown in Figure 3.29(m). When casting such a supplemental diaphragm in the field, a polystyrene board can be placed on the abutment in a similar manner to form the bottom of the diaphragm. The polystyrene board was used in the lab to simulate such field conditions. The completed formwork is shown in Figure 3.29(n). The SCC concrete mixture provided in Table 3.5 was poured directly into formwork from the concrete truck (Figure 3.29(o)). The completed diaphragm is presented in Figure 3.29(p).

(a) Drilling Holes for No. 3 Bars

(b) Injecting Hole with Epoxy

Figure 3.29 Supplemental Diaphragm Repair Procedure

Figure 3.29 continued

(c) Inserting No. 3 Bar Through Web

(d) No. 3 Bar Inserted Until Mark is Visible

(e) No. 3 Bar Oriented for Bending Operation

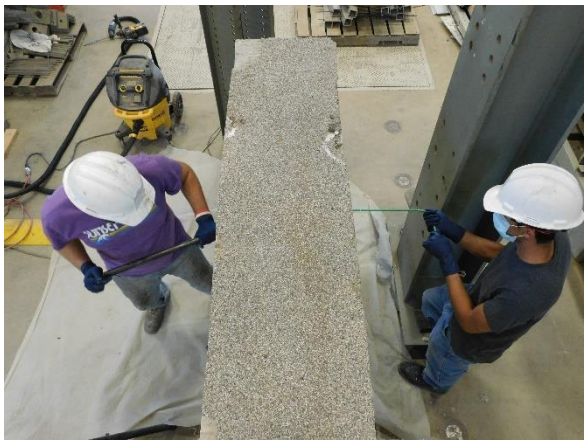

(f) Bending No. 3 Bar

(g) Centering No. 3 Bar

(h) Injecting Additional Epoxy

Figure 3.29 continued

(i) Cutting Hook Extension to Length

(j) Completed Installation of No. 3 Bar

(k) Completed Reinforcing Cage

(l) Completed Reinforcing Cage

(m) Closed-Cell Polystyrene Board

(n) Erected Formwork

Figure 3.29 continued

(o) Casting SCC

(p) Completed Supplemental Diaphragm Repair System

3.5 Test Setup and Procedure

The test specimens were loaded to failure using the loading configuration presented in Figure 3.30. A specimen in the test frame is shown in Figure 3.31. An *a*/*d* ratio of 1.25 (corresponding to a shear span of 45 in. as shown in Figure 3.30) was used for all five test specimens. The relatively short shear span was selected based on the observation that direct compressive stresses transferred from the load to the support would be critical for the end regions. Because the short shear span results in an *a*/*d* ratio less than 2.0, the entire test region is defined as a D-region. Thus, the behavior of the test region will be governed by deep beam behavior rather than sectional behavior. The far end of the girder opposite the test region was supported 60 in. from the end of the member to allowing for testing on the opposite end of the specimen if needed. The original elastomeric bearing pads acquired from the bridge were used to support the specimens. The bearing pads were 14-in. by 7-in. by 2.5-in. For the specimen with the supplemental diaphragm, one of the bearing pads was cut in two, and the member was supported at the supplemental diaphragm as described in Section 3.3.4. A slight modification was made to the test setups for the control and damaged specimens. Although the end region of the control specimen was in relatively good condition, cracking was present in the bottom flange near the end of the member. Therefore, the bearing pad was shifted 3 in. further into the span relative to the original bearing location to avoid the cracks, as shown in Figure 3.32. Moreover, as discussed in Section 3.4.2, the bearing pad for the damaged test specimen was shifted 4 in. further into the span to minimize required

repairs. However, in both of these cases, the shear span of 45 in. remained consistent as did the stirrup spacing (6 in.) within the test region.

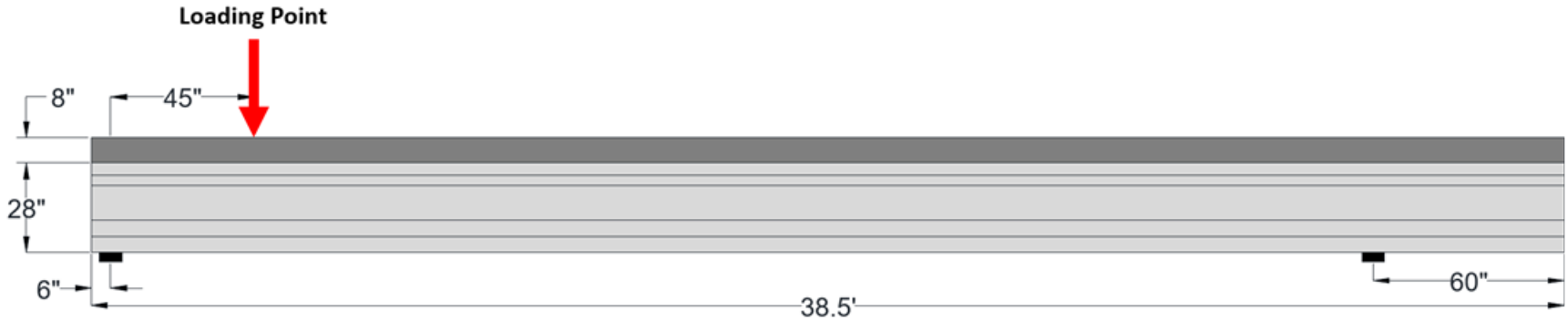

Figure 3.30 Load Configuration

Figure 3.31 Specimen in Test Frame

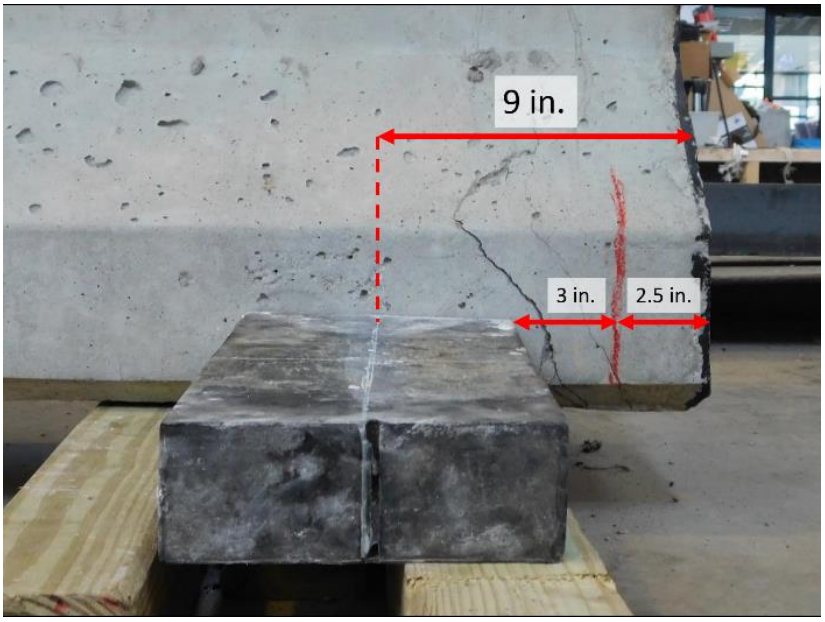

Figure 3.32 Location of Bearing Pad for the Control Specimen

Due to the sloped top surface of the deck, a gypsum concrete wedge was cast at the load point for each girder as shown in Figure 3.33. Using closed-cell polystyrene board, temporary formwork was erected around the loading area. The bottom of the formwork was sealed, and liquid gypsum concrete was poured into the formwork. After self-leveling and curing, the formwork was removed. A 12-in. by 8-in. by 2-in. A36 steel plate was subsequently placed on top of the wedge and centered over the top flange of the test specimen.

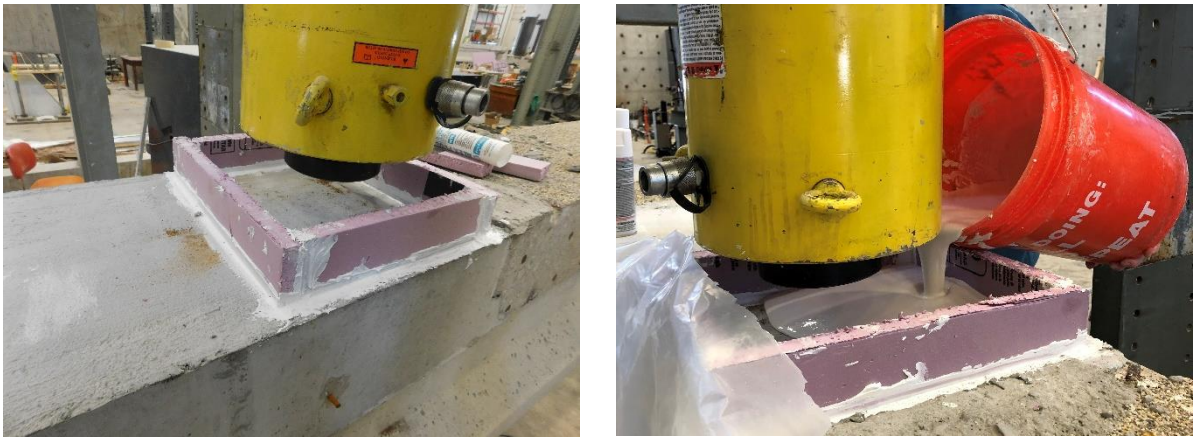

(a) Closed-Cell Polystyrene Formwork **(b) Pouring Gypsum Concrete**

Figure 3.33 Preparing the Load Point

Figure 3.33 continued

(c) Load Plate on Gypsum Concrete Wedge

A hydraulic ram with a capacity of 250 tons was used to apply load to the test specimens at the load point, and a load cell with a capacity of 300 kips was rigidly connected to the hydraulic cylinder to directly measure the load applied to the beam. This assembly is shown in Figure 3.34. At both the load point and at midspan, linear string potentiometers were used to measure displacements throughout each test. At each location, a potentiometer was positioned to measure the displacement at each side of the beam, as shown in Figure 3.35. Additionally, a linear potentiometer was placed on each side of both bearing pads to measure deflections at the supports. The average of the readings from the two linear potentiometers at each location was taken as the deflection at that point. Furthermore, an HD video camera was used during each load test to record video of the experiment.

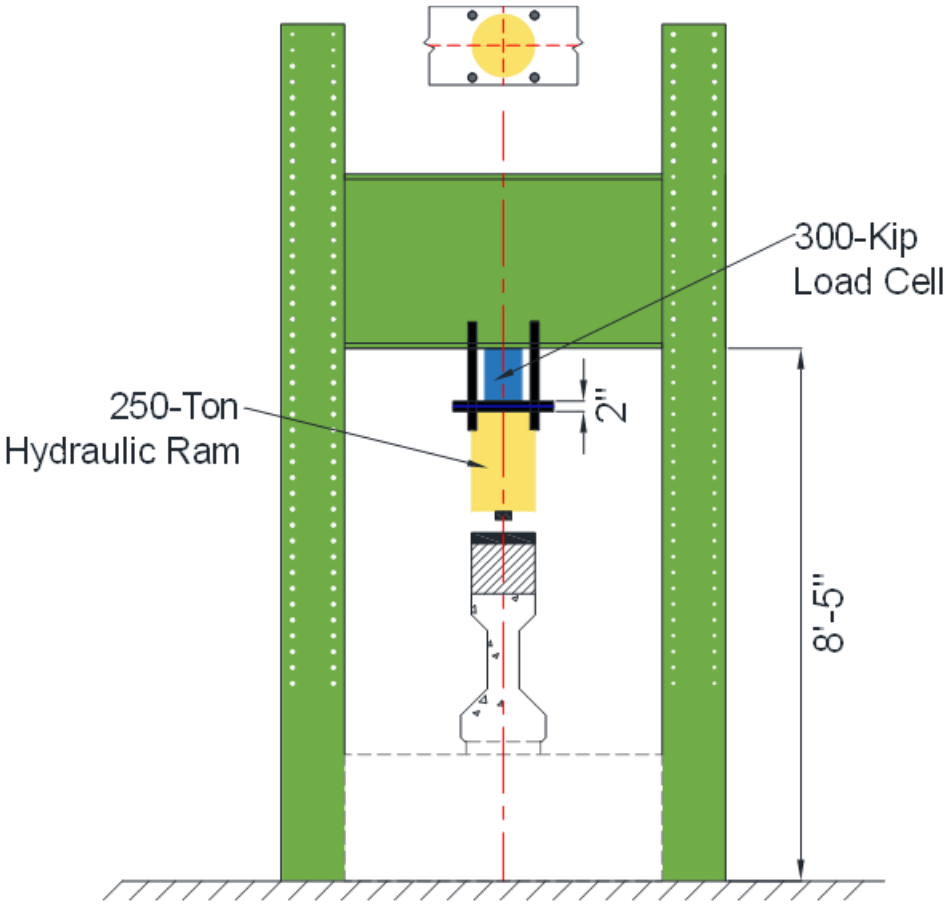

Figure 3.34 Test Frame

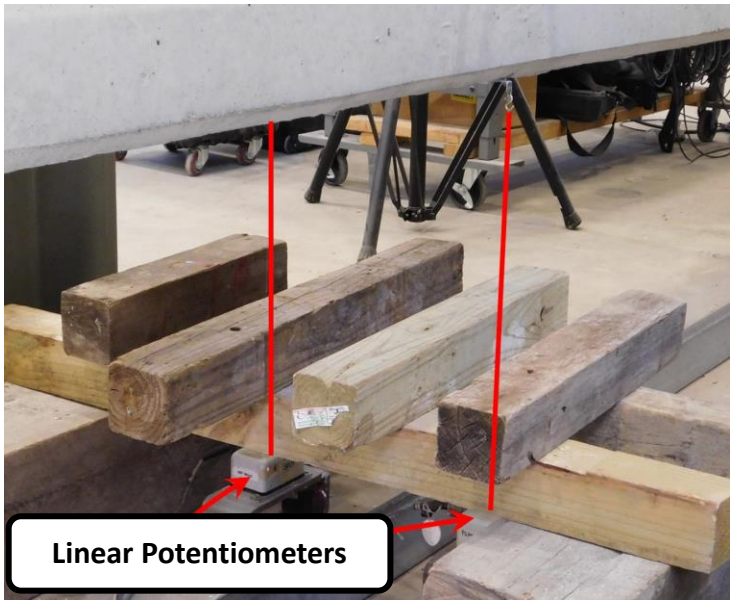

Figure 3.35 Linear Potentiometers

Each specimen was loaded monotonically until failure occurred. The load was increased at 10-kip increments, between which pictures were taken. Cracks were marked with a felt-tipped marker at every load step until failure was imminent, except for the externally bonded FRP specimen due to the presence of the FRP. Failure of the test specimens was defined by either a sudden loss in load-carrying capacity (damaged, externally bonded FRP, and NSM FRP specimens) or when the load-carrying capacity had decreased by 20 kips from its maximum value (control and supplemental diaphragm specimens).

3.6 Summary

This chapter detailed the experimental program focused on developing repair techniques for deteriorated end regions of prestressed concrete bridge girders. The details of three repair techniques (an externally bonded FRP system, an NSM FRP system, and a concrete supplemental diaphragm) were presented. Additionally, the procedures followed to implement each of the repair techniques and prepare two other specimens (a control and damaged specimen) for testing were outlined. Results from the load testing of the five experimental specimens are presented and discussed in Chapter 4. Comparisons between the three repaired specimens, the control specimen, and the damaged specimen are also presented to develop conclusions pertaining to the overall project objectives.

CHAPTER 4. ANALYSIS OF EXPERIMENTAL RESULTS AND OBSERVATIONS

4.1 Introduction

The results of the end region repair experimental program outlined in Chapter 3, consisting of tests on one relatively undeteriorated, one deteriorated, and three repaired AASHTO Type I girders loaded to failure, will be presented in this chapter. Additionally, the overall behavior of each of the five test specimens will be discussed. Then, the results and observations obtained from the tests on the three repaired specimens will be used to establish the effectiveness of each repair technique.

4.2 Experimental Results

The experimental results for the five girders tested are presented in the following subsections. For each specimen, a load-deflection curve is provided to better understand the specimen behaviors. Each curve is a plot of the shear force caused by the applied load within the 45-in. long test region (i.e., shear span) indicated in Figure 3.30 versus the deflection of the girder measured at the location of the load point (see Section 3.5). For consistency, the range of values along the y-axis for each load-deflection plot is 0 to 220 kips, and the range of values along the x-axis is 0 to 3 in. Shear force due to self-weight is not reflected in the load-deflection response curves. The shear force due to self-weight at the middle of the shear span is estimated to be 6.5 kips. It should also be noted that the linear potentiometers positioned to measure the deflection at the support locations (i.e., bearing pads) of the specimens were used to determine the deflection at the load point due to deformation of the bearing pads. As an example, this deflection at the load point was 0.039 in. for the control specimen when the maximum load was applied. This small deflection due to deformation of the bearing pads is not considered in the load-deflection plots provided in the following sections.

4.2.1 Control Specimen

As explained in Chapter 3, one AASHTO Type I girder (3-C) with an end region in good condition acted as the control specimen, providing a baseline performance to which the repaired specimens were compared. The results of the test on the control specimen allowed for the effectiveness of each of the three repair techniques included in the experimental program to be established. The load-deflection response curve for the control specimen is shown in Figure 4.1. Initial cracking of the specimen was observed at a shear force, V_{cr}, of 98 kips (applied load of 110 kips). The first crack observed was a diagonal shear crack that appeared in the web of the specimen. This crack would eventually become one of the primary cracks that characterized the failure of the member. The specimen reached a maximum shear force, V_{test}, of 141 kips (applied load of 158 kips).

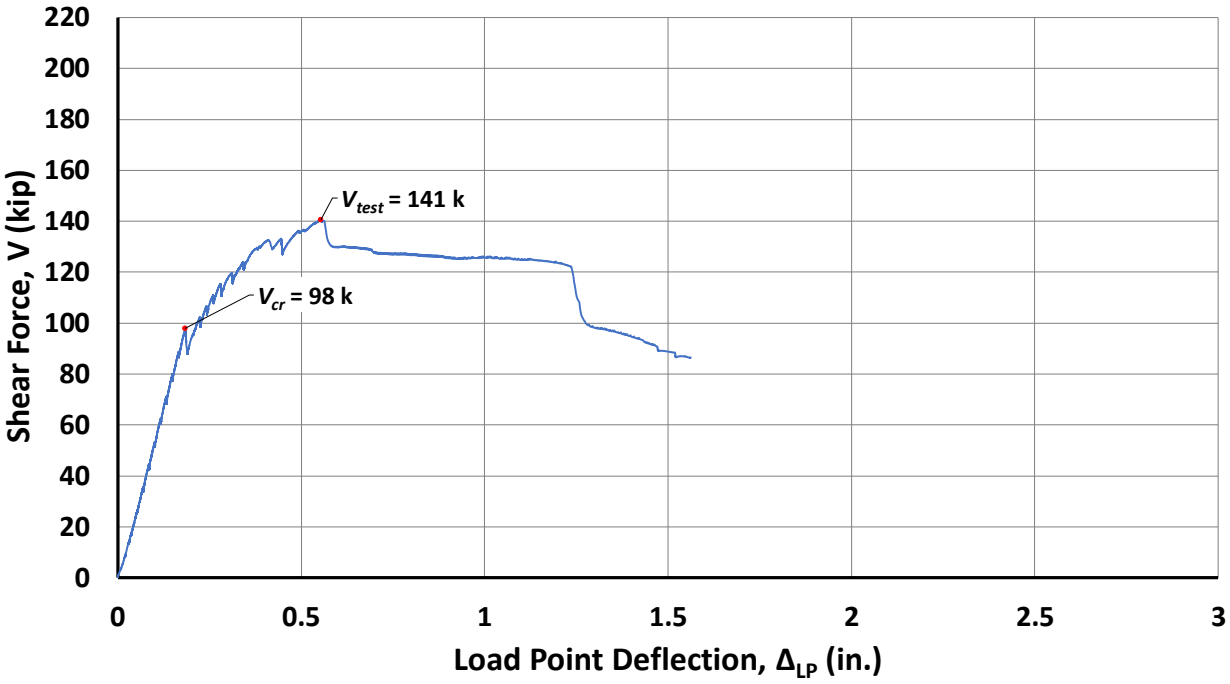

Figure 4.1 Shear vs. Deflection at Load Point for Control Specimen

The condition of the girder prior to testing is displayed in Figure 4.2, and the condition of the girder after failure is shown in Figure 4.3. As discussed in Section 3.3.1, the failure of the control specimen was characterized by the formation of a diagonal strut within the test region, corresponding to a crack angle of approximately 43° measured from the horizontal, as shown in

Figure 4.3. The formation of the strut is consistent with D-region shear behavior. Failure of the specimen was defined by a gradual decrease in load-carrying capacity along with the progressive widening of the diagonal cracks that formed along the strut. Furthermore, as the cracks widened and the specimen continued to deflect, the prestressing strands in the bottom flange experienced slippage. The ends of the strands slipped approximately 1.25 in. into the girder by the end of the test, measured using a caliper after completion of the test. The sudden loss in load-carrying capacity shown in Figure 4.1 at a beam deflection of 1.24 in. is believed to be due to strand slip.

Figure 4.2 Control Specimen Prior to Testing

Figure 4.3 Control Specimen After Failure

After testing the girder, 4-in. by 6-in. cores where removed from the web of the specimen to determine the compressive strength of the concrete at the time of testing. As shown in Figure 4.4, the test specimen was rotated to allow for the cores to be taken vertically. Cores were removed from an undamaged portion of the web located as close as possible to the test region. This procedure was followed for all five girders of the test program. The four cores from the control specimen were tested in compression in accordance with ASTM C42 and yielded an average compressive strength of 7270 psi, as provided in Table 4.1.

Figure 4.4 Coring Web of Test Specimen

Table 4.1 Material Compressive Strength Test Results for Control Specimen

Material	Compressive Strength (psi)
Cored Concrete	7270

4.2.2 Damaged Specimen

To further determine the effectiveness of the three repair techniques described in Chapter 3, Girder 20-C was tested without repairing the damaged end region to better understand the strength and performance of the deteriorated girders in their field condition. The load-deflection response curve for the damaged specimen is shown in Figure 4.5. Due to the existing damage,

cracking was observed early in the test within the region of the bottom flange as a portion of the flange separated from the specimen. However, the first crack that developed during the test and corresponded with a notable change in the load-deflection behavior was observed at a shear force of 61 kips (69 kips of applied load). For the purposes of comparing specimen behaviors, this shear force is taken as the cracking shear force, V_{cr}, for the girder. This crack became the vertical crack which characterized the failure of the specimen, as discussed in more detail below. The specimen resisted a maximum shear force of 80 kips (90 kips of applied load).

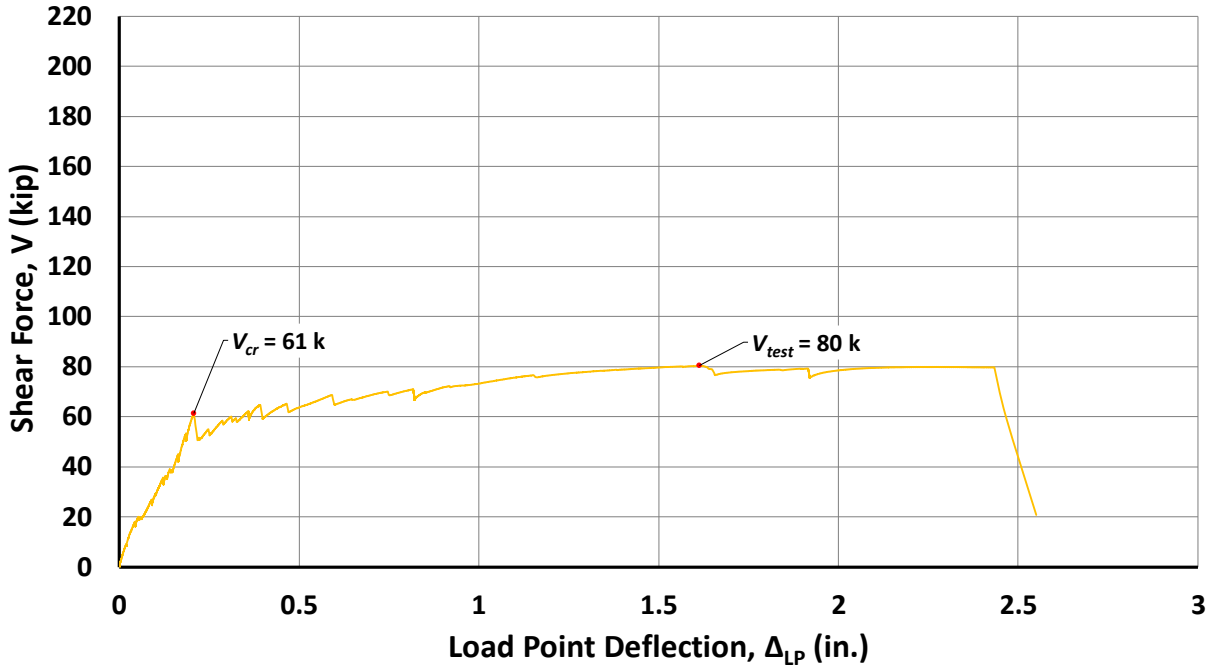

Figure 4.5 Shear vs. Deflection at Load Point for Damaged Specimen

The condition of the specimen prior to testing is shown in Figure 4.6, and the condition of girder following testing is displayed in Figure 4.7. Unlike the control specimen, load was not transferred within the test region through a diagonal strut extending from the load point to the support. Instead, a vertical crack initiated at the bottom of the member approximately 3.5 ft from the end of the specimen. Upon further loading, the crack propagated vertically through the web of the member. Then, the crack propagated diagonally through the top flange and deck toward the load point. Additionally, unlike the control specimen, the failure of the damaged specimen was defined by an abrupt drop in the load-carrying capacity. Comparing Figure 4.7(a and b) with Figure 4.3, the failure mechanisms between the control and damaged girders are significantly different,

with the primary failure crack(s) oriented at approximately 43° from the horizontal for the control specimen and at approximately 90° for the damaged specimen. The behavior of the damaged specimen was a result of the lost tensile capacity within the bottom flange due to the deteriorated and ineffective prestressing strands. Furthermore, as shown in Figure 4.7(c), the portions of the bottom flange outside of the web detached from the specimen at the support. Through destructive evaluation after the test, it was discovered that the individual wires of one of the harped strands had untwisted from one another.

(a) West Side

(b) East Side

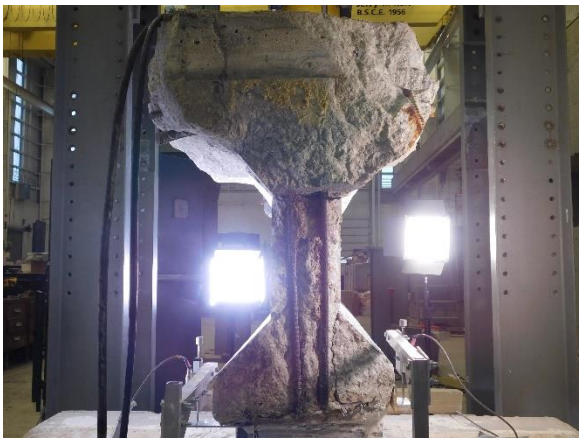

(c) Girder End

Figure 4.6 Damaged Specimen Prior to Testing

(a) West Side

(b) East Side

(c) Girder End

Figure 4.7 Damaged Specimen After Failure

As with the control specimen, 4-in. by 6-in. cores were removed from the web of the specimen following testing. Compression tests on three cores yielded an average strength of 9240 psi. The compressive strength of the concrete used to repair the deck (see Section 3.4.1) was obtained by testing 4-in. by 8-in. cast concrete cylinders. The compressive strength of the cylinders was determined in accordance with ASTM C39 and yielded an average compressive strength of 7220 psi on the day of the girder test (97 days after casting). Moreover, mortar cubes were cast in accordance with ASTM C109 (as shown in Figure 4.8) to determine the compressive strength of the mortar used to repair the bearing area as described in see Section 3.4.2. The average compressive strength of the mortar cubes on test day (32 days after casting) was 9130 psi. The

compression test results of the concrete cores, concrete cylinders, and mortar cubes for the damaged test specimen are summarized in Table 4.2.

Figure 4.8 Casting Mortar Cubes

Table 4.2 Material Compressive Strength Test Results for Damaged Specimen

Material	Compressive Strength (psi)
Cored Concrete	9240
Concrete Cylinders (Deck)	7220
Mortar Cubes	9130

4.2.3 Externally Bonded FRP Repair Specimen

The first repaired specimen to be discussed is the girder restored with the use of externally bonded FRP. The load-deflection response curve for the specimen is shown in Figure 4.9. The development of the first crack that was visually observed during the test was noted at a shear force of 140 kips (158 kips of applied load). The crack was a flexural crack located at the end of the longitudinal FRP sheets. Due to the brittle nature of FRP, however, a close examination of the specimen was not conducted past a shear force of 106 kips due to safety concerns. Thus, it is probable that a crack formed at a lower shear force. Therefore, for the purposes of comparing specimen behaviors, the cracking shear, V_{cr}, of this specimen will be defined by the first notable change in slope of the load-deflection response curve in Figure 4.9. This change in slope occurs at

a shear force of 115 kips (130 kips of applied load). The specimen resisted a maximum shear force of 189 kips (214 kips of applied load).

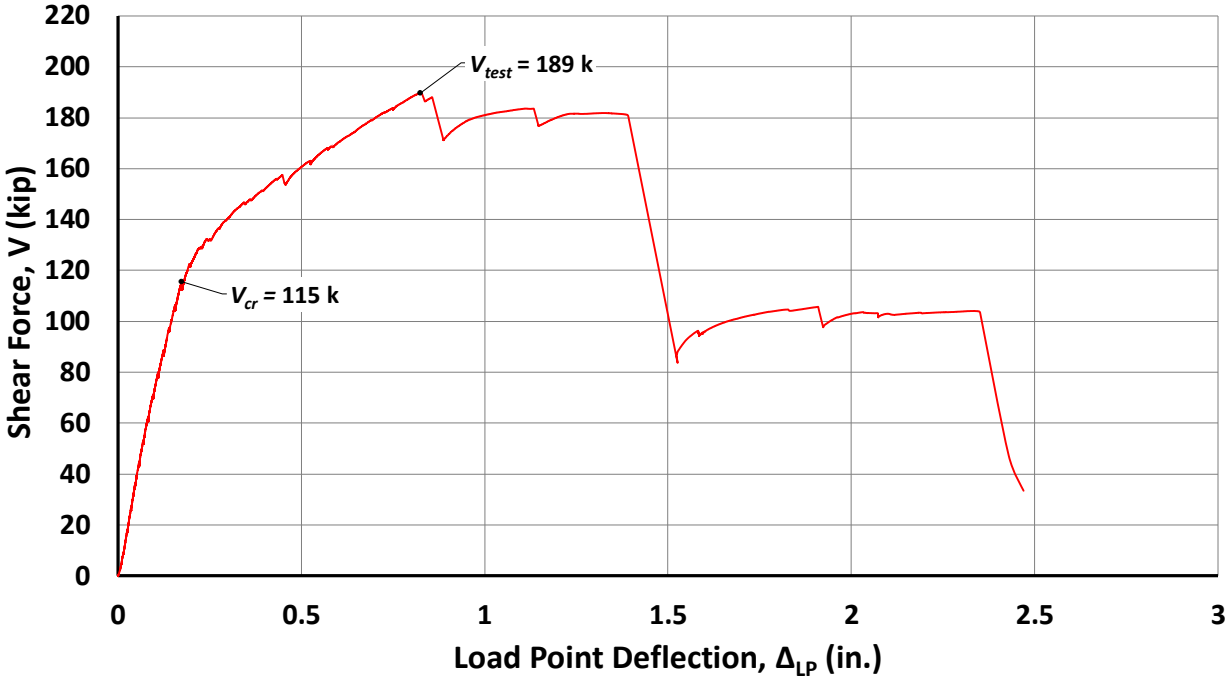

Figure 4.9 Shear vs. Deflection at Load Point for Externally Bonded FRP Specimen

The condition of the specimen prior to testing is presented in Figure 4.10, and the condition of the girder after failure is shown in Figure 4.11. The specimen experienced a flexural failure characterized by the fracture of two prestressing strands in the bottom flange (see Figure 4.12) at the termination of the FRP sheets. The strands fractured at the location of a wide flexural crack at the end of the repaired region as shown in Figure 4.13. The red lines in Figure 4.13 indicate the termination of the FRP strips. The sudden loss in load-carrying capacity at a deflection of 1.39 in. is believed to coincide with the fracture of one of the prestressing strands. The specimen continued to be loaded after this event and maintained a shear force of approximately 100 kips until it is believed another strand in the bottom flange fractured at a deflection of 2.35 in. Concrete crushing was observed in the deck beneath the load point. During the test, minor diagonal cracking was observed near the load point in the region not covered by FRP sheets. The crack was oriented at an angle of approximately 46° from the horizontal. The crack did not widen significantly after formation, however, and the propagation of the crack toward the support is unknown due to the presence of the FRP. Considering the failure behavior of the specimen, the repair system restored sufficient shear capacity so that a flexural failure outside of the damaged region occurred. The FRP

wrap also provided sufficient confinement to prevent the separation of portions of the bottom flange of the member as observed during the test on the damaged specimen. Furthermore, the confinement provided by the FRP allowed the strands to reach their ultimate capacity within their calculated development length. This is unlike the strands of the control specimen which experienced slippage observed at the end of the member as described in Section 4.2.1. Based on Equation 5.9.4.3.2-1 of AASHTO LRFD (2020), the development length of the strands is calculated using Equation 4.1. In the calculation, the value of f_{ps} is replaced with the specified ultimate strength of the strands, f_{pu}, in consideration of the observed fracture of the strands, and f_{pe} is assumed to be 160 ksi, within the typical range of effective prestress after losses.

$$l_d = \kappa\left(f_{ps} - \frac{2}{3}f_{pu}\right)d_b = 1.6\left[270\ ksi - \frac{2}{3}(160\ ksi)\right](0.5\ in.) = 130.7\ in. \qquad \textbf{Equation 4.1}$$

The strands fractured approximately 49 in. from the end of the member, giving evidence of the benefits provided by the FRP confinement. Based on the observed failure behavior and strength achieved by the specimen, the externally bonded FRP repair system is believed to have effectively restored the tie force in the bottom flange that was assumed to be lost due to deterioration as observed for the damaged specimen.

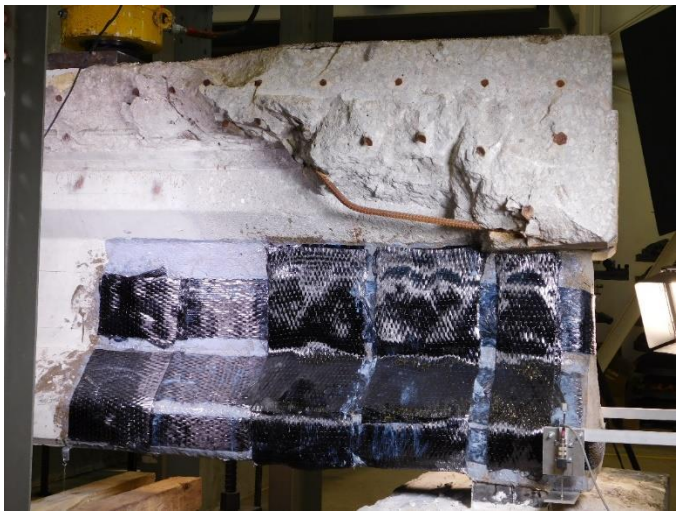

Figure 4.10 Externally Bonded FRP Specimen Prior to Testing

Figure 4.11 Externally Bonded FRP Specimen After Failure

Figure 4.12 Fractured Prestressing Strands in Bottom Flange After Testing

Figure 4.13 Critical Flexural Crack of Externally Bonded FRP Specimen After Failure

Minimal FRP delamination was observed during testing, further indicating a successful FRP repair. Indications of delamination were first noted at a shear force of 106 kips when minor popping sounds were heard. At the end of the test, the delamination was confined to the area along the longitudinal strips between the termination of the patch sheets located at the ends of the strips and the first U-wrap sheet, as indicated by the red areas in Figure 4.11. No other damage to the FRP within the repaired region was observed.

The compressive strength of the specimen was determined by removing 4-in. by 6-in. cores from the web of the specimen following testing. The average compressive strength of the three cores was 7440 psi. Mortar cubes were cast to measure the strength of the mortar used to restore the original cross section of the girder. The average compressive strength of the mortar cubes on the day of the girder test (326 days after casting) was 16,100 psi. The average compression test results of the concrete cores and mortar cubes for the specimen with externally bonded FRP are presented in Table 4.3.

Table 4.3 Material Compressive Strength Test Results for Externally Bonded FRP Specimen

Material	Compressive Strength (psi)
Cored Concrete	7440
Mortar Cubes	16,100

4.2.4 NSM FRP Repair Specimen

The focus of the specimen strengthened with NSM FRP strips was the potential benefits of restoring the tensile capacity along the bottom flange of the girder. The load-deflection response curve for the specimen is shown in Figure 4.14. The shear force corresponding to the development of the first crack observed during the test was 31 kips (35 kips of applied load). As explained next, this shear force was also the maximum shear force resisted by the specimen. Therefore, both V_{cr} and V_{test} are shown to be equal to 31 kips (35 kips of applied load) in Figure 4.14.

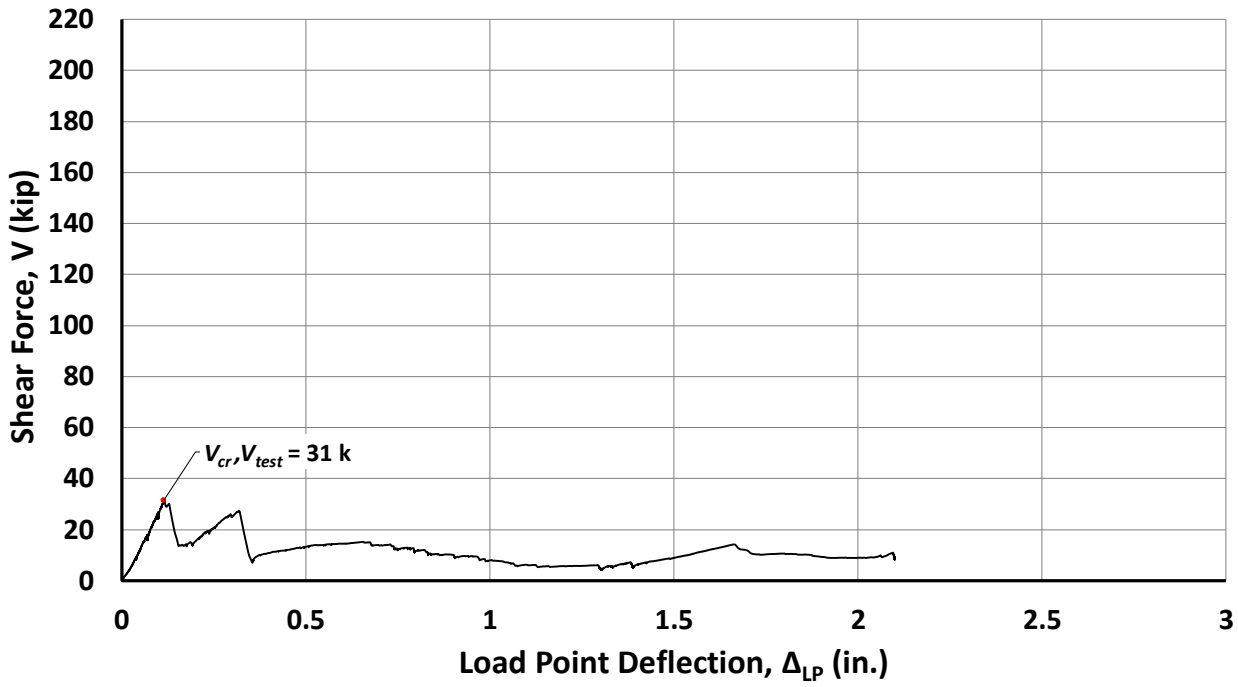

Figure 4.14 Shear vs. Deflection at Load Point for NSM FRP Specimen

The condition of the specimen prior to testing is presented in Figure 4.15, and the condition of the specimen following testing is displayed in Figure 4.16. The hairline cracks marked in Figure 4.15 were preexisting. At a shear force of 31 kips, the portion of the web located above the support

bearing experienced a splitting crack that effectively caused the end of the specimen to separate from the rest of the member. The splitting crack appeared suddenly along the depth of the member, intersecting with the reentrant corner at the notch located along the top flange of the girder. This produced a sudden loss in load-carrying capacity. Once the end of the member that separated from the beam was no longer effective in transferring load to the bearing, load was primarily transferred to the bearing through the outer portions of the bottom flange in contact with the bearing pad. This resulted in the outer portions of the flange separating from the girder as shown in Figure 4.17, preventing load from being transferred to the NSM strips. In other words, because of the failure at the end of the girder, the NSM strips were not engaged. As indicated by the load-deflection plot in Figure 4.14, the load carried by the specimen increased after the development of the splitting crack at a shear force of 31 kips, but load-carrying capacity was again lost when portions of the bottom flange of the girder separated from the member at a shear force of 27 kips.

Figure 4.15 NSM FRP Specimen Prior to Testing

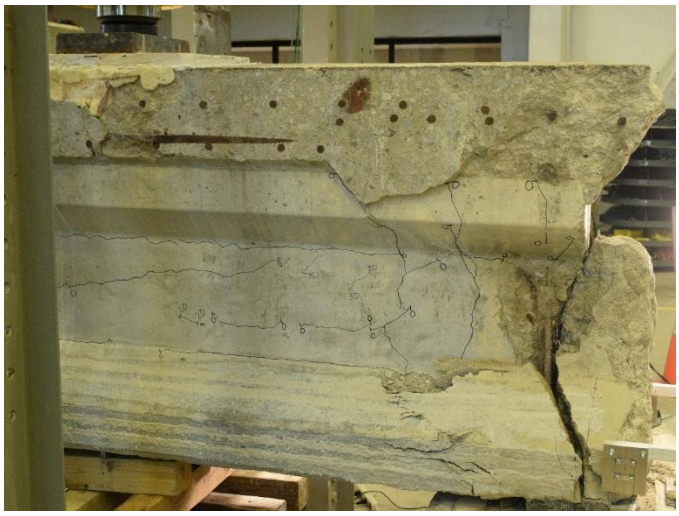

Figure 4.16 NSM Specimen After Failure

(a) Elevation View

Figure 4.17 Flange Separated from NSM Specimen

Figure 4.17 continued

(b) Girder End

The bridge from which the test girders were extracted included a transverse edge beam located within the notch at the ends of the girders. This edge beam was cast monolithically with the bridge deck. As shown in the previous figures of the specimen with the NSM strips (e.g., Figure 4.15 and Figure 4.16), the transverse edge beam was not intact but separated from the girder at some point during the extraction of the beam from the bridge or during transportation. At least a portion of the edge beam remained intact for the other specimens of the test program. The lack of the edge beam on the specimen with NSM strips may have contributed to the splitting in the vicinity of the notch observed during the test.

As with the other specimens, the compressive strength of the girder with NSM strips was determined by removing 4-in. by 6-in. cores from the web of the specimen. The average compressive strength of three cores was 9070 psi. Like the specimen with externally bonded FRP, mortar cubes were cast to measure the strength of the mortar used to restore the original cross section of the girder. The average compressive strength of the mortar cubes on the day of the girder test (310 days after casting) was 12,170 psi. The average compression test results of the concrete cores and mortar cubes for the specimen repaired with NSM FRP strips are displayed in Table 4.4.

Table 4.4 Material Compressive Strength Test Results for NSM FRP Specimen

Material	Compressive Strength (psi)
Cored Concrete	9070
Mortar Cubes	12,170

4.2.5 Supplemental Diaphragm Repair Specimen

The final specimen to be described is the girder repaired with the addition of a supplemental diaphragm at its end. The load-deflection response curve for this specimen is provided in Figure 4.18. During the test, the first crack observed was within the supplemental diaphragm. The end face of the diaphragm began to experience minor cracking at a shear force of 8.9 kips (10 kips of applied load). At a shear force of 44 kips (50 kips of applied load) cracking had propagated along the entirety of both the end face and the bottom surface of the diaphragm, causing the reduction of stiffness indicated by the load-deflection plot. Therefore, as with the externally bonded FRP specimen, the cracking shear, V_{cr}, of this specimen will be defined by the first notable change of slope in the load-deflection curve in Figure 4.18, which corresponds to a shear force of 44 kips (50 kips of applied load). The specimen achieved a maximum shear force of 81 kips (91 kips of applied load).

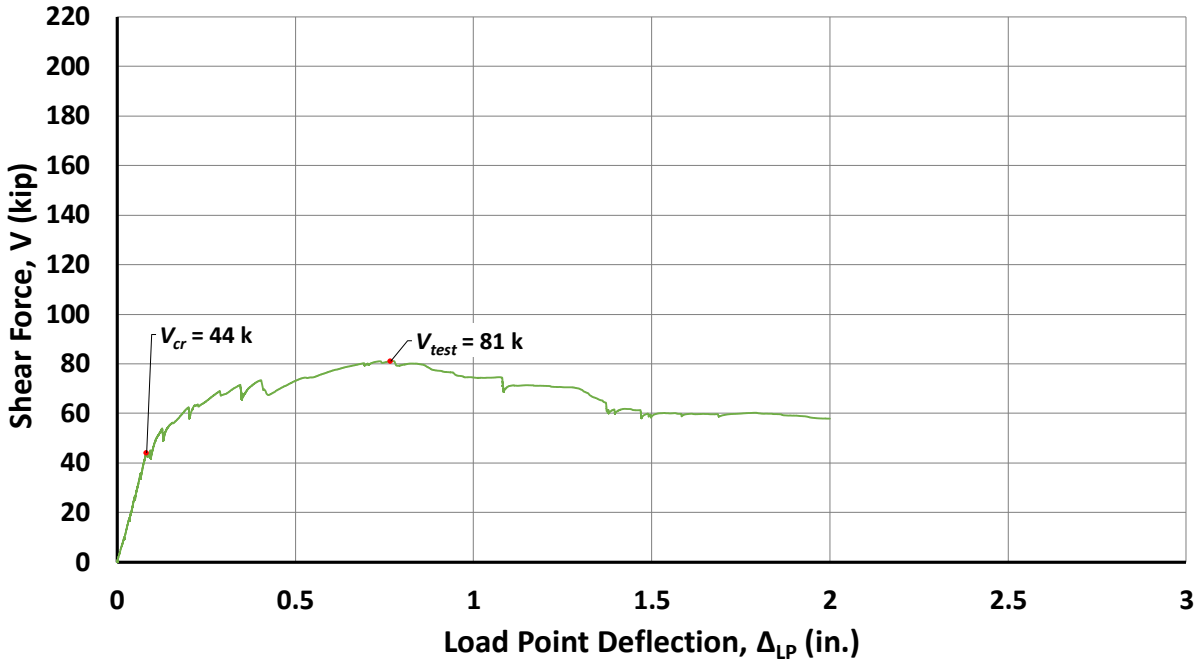

Figure 4.18 Shear vs. Deflection at Load Point for Supplemental Diaphragm Specimen

The condition of the girder prior to the test is shown in Figure 4.19. The hairline cracks marked in Figure 4.19 were present before testing. As discussed above, at shear forces as low as 8.9 kips, cracking was observed on the end face of the supplement diaphragm, and cracking was observed on the bottom surface of the supplemental diaphragm at a shear force of 35 kips. As shown in Figure 4.20, at a shear force of 44 kips, these cracks had propagated along the entire length of both faces. The formation of the cracks at a relatively low shear force (less than half of V_{cr} for the control specimen) was caused by the transfer of load through the diaphragm to the two bearing pads. In other words, the behavior resulted from the elimination of the original center bearing pad of the girder. Furthermore, the absence of continuous reinforcement near the bottom (i.e., tension face) of the diaphragm caused the splitting of the diaphragm along the cracks shown in Figure 4.20 to quickly increase in severity upon further loading. Such reinforcement is needed to restrain the cracks and provide tensile capacity in order to transfer loads to the two bearing pads. Additionally, as the test continued, the interface between the supplemental diaphragm and the original girder concrete failed (i.e., the supplemental diaphragm separated from the original girder concrete), and rotation of the diaphragm was observed, as shown in Figure 4.21(a through d). The end of the girder after the test is shown in Figure 4.21(e). Outside of the supplemental diaphragm, a diagonal crack (see Figure 4.22) initiated at a shear force of approximately 53 kips. The crack extended from the bottom of the diaphragm toward the load point at an angle of approximately 55° from the horizontal. This indicated the general orientation of compressive stresses in this portion of the member.

(a) West Side Interface **(b) East Side Interface**

Figure 4.19 Supplemental Diaphragm Specimen Prior to Testing

Figure 4.19 continued

(c) West Side

(d) East Side

(e) Girder End

(a) End Face of Diaphragm at Shear Force of 44 Kips

(b) Bottom Surface of Diaphragm at Shear Force of 44 Kips

Figure 4.20 Splitting Behavior of Supplemental Diaphragm

(a) West Side Interface

(b) East Side Interface

(c) West Side

(d) East Side

(e) Girder End

Figure 4.21 Supplemental Diaphragm Specimen After Failure

Figure 4.22 Diagonal Cracking of Supplemental Diaphragm Specimen at Shear Force of 80 Kips

Without continuous reinforcement along the bottom of the supplemental diaphragm to help transfer stresses to the two bearing pads and control the splitting cracks, the diaphragm was ineffective. Continuous reinforcement with proper development was identified as being essential for a successful repair with such a diaphragm. Furthermore, if the supplemental diaphragm were cast continuously between girders in the field, the early failure of the diaphragm observed during the test is expected to be prevented. More detailed suggestions for the implementation of a repair using a continuous diaphragm are provided in Chapter 5.

To determine the compressive strength of the girder at the time of testing, 4-in. by 6-in. concrete cores were removed from the web of the specimen for compression tests. The results of test on three cores provided an average strength of 7850 psi. As with the damaged girder specimen, 4-in. by 8-in. concrete cylinders were cast to determine the compressive strength of the concrete used to repair the deck (see Section 3.4.1). The average compressive strength on the day of the girder test (104 days after casting) of the deck repair concrete cylinders was 6410 psi. Similarly, 4-in. by 8-in. concrete cylinders were cast to determine the compressive and tensile strengths of the SCC used for the supplemental diaphragm. The average compressive strength on test day (52 days after casting) of the cylinders was 7070 psi, and the average splitting tensile strength on test day (52 days after casting) was 630 psi. The splitting tensile tests were conducted in accordance with ASTM C496. The results of the compressive and tensile strength tests are displayed in Table 4.5.

Table 4.5 Material Compressive and Tensile Strength Test Results for Supplemental Diaphragm Specimen

Material	Compressive Strength (psi)	Splitting Tensile Strength (psi)
Cored Concrete	7850	-
Concrete Cylinders (Deck)	6410	-
Concrete Cylinders (Diaphragm)	7070	630

4.3 Discussion of Test Results

Within the following subsections, the results of all five experimental specimens are analyzed and discussed. A summary of the test results is first presented for easy comparison. Then, the results for each of the three repair techniques (externally bonded FRP, NSM FRP, and supplemental diaphragm) are compared to the results of the control and damaged specimens to establish the effectiveness and viability of each repair method.

4.3.1 Summary of Test Results

The measured material strengths corresponding to the five girder specimens of the test program are summarized in Table 4.6. All material testing was conducted according to the appropriate ASTM standards. The properties of the FRP systems as reported by the manufacturer are provided in Sections 3.3.2 and 3.3.3. Although some variations in the compressive strengths of the concrete and mortar are evident among the girder specimens, these differences are not believed to be significant in consideration of the failure modes observed during the tests and the overall value provided by the comparisons between the overall performance of the girders.

Table 4.6 Summary of Material Test Results

	Cored Concrete, f_c (psi)[1]	Deck Concrete, f_c (psi)[2]	Mortar, f_m (psi)[3]	Supp. Dia. Concrete, f_c (psi)[2]	Supp. Dia. Splitting Tensile, f_t (psi)[4]
Control	7270	-	-	-	-
Damaged	9240	7220	9130	-	-
Ext. Bonded	7440	-	16,100	-	-
NSM	9073	-	12,170	-	-
Supp. Dia.	7850	6410	-	7070	630

[1]ASTM C42
[2]ASTM C39
[3]ASTM C109
[4]ASTM C496

The results of the load tests performed on the specimens are summarized in Table 4.7. In the table, $V_{Control}$ is the maximum shear force resisted by the control specimen, and $V_{Damaged}$ is the maximum shear force resisted by the damaged specimen. The values of $V_{test}/V_{Control}$ and $V_{test}/V_{Damaged}$ are the ratios of the experimental capacity of a specimen to the experimental capacity of the control and damaged specimens, respectively. As observed in Table 4.7, only the externally bonded FRP specimen resisted a higher maximum shear force than the control specimen (34% increase). The damaged, NSM FRP, and supplemental diaphragm specimens achieved peak shear values equal to 57%, 22%, and 57% of the capacity of the control specimen, respectively.

Table 4.7 Summary of Load Test Results

	V_{cr} (kip)	V_{test} (kip)	$V_{test}/V_{Control}$	$V_{test}/V_{Damaged}$
Control	98	141	1.00	1.76
Damaged	61	80	0.57	1.00
Ext. Bonded	115	189	1.34	2.36
NSM	31	31	0.22	0.39
Supp. Dia.	44	81	0.57	1.01

The load-deflection response curves for the five girders are plotted together in Figure 4.23. This plot will be referenced in the following subsections as the performance of the repaired specimens are compared to the performance of the control and damaged specimens.

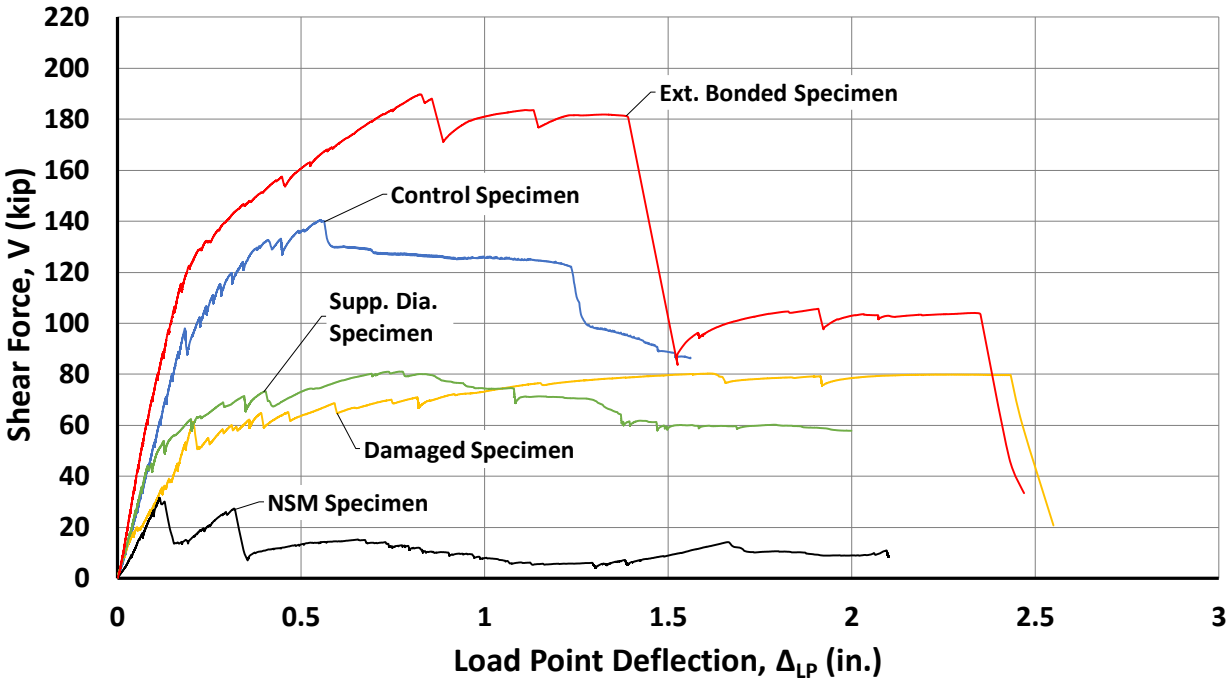

Figure 4.23 Shear vs. Deflection at Load Point for All Girder Specimens

4.3.2 Comparison of Repaired Specimens to Control and Damaged Specimens

4.3.2.1 Externally Bonded FRP Repair Specimen

When the experimental results of the specimen with externally bonded FRP are compared to those of the control and damaged specimens, it can be observed that the externally bonded repair system adequately restored the behavior of the damaged end region. As indicated by the load-deflection response curves in Figure 4.23 and the test data in Table 4.7, the maximum shear force, V_{test}, resisted by the specimen with externally bonded FRP exceeded that of the control specimen by 34%. Furthermore, the shear force, V_{cr}, defined previously, increased by 17% for the repaired specimen compared to the control specimen. It can also be observed from the plots that the externally bonded system resulted in a greater initial stiffness than the control specimen, indicating that, due to the relatively high stiffness of the FRP laminate material, the externally bonded FRP system was able to restore the stiffness lost due to the deterioration of the end region.

As discussed in Section 4.2.3, the specimen repaired with externally bonded FRP failed due to flexure at the termination of the repair. This failure mode differed from the observed failure mode of the control specimen. Considering that the failure of the control specimen can be described as being caused by a combination of D-region shear and strand slip, this change in failure mode

indicates that the repair system successfully restored any lost shear capacity due to the deterioration of the end region and resulted in a shear strength greater than that of the control specimen. Furthermore, the confinement provided by the FRP wrap allowed two strands to reach their ultimate strength at the end of the repaired region. With the tensile capacity in the bottom flange effectively restored, the externally bonded FRP system prevented the failure mode experienced by the damaged specimen. Moreover, the repair system helped to prevent the vertical splitting at the end of the member as was observed for the specimen repaired with NSM strips. It should be noted, however, that the presence of the transverse edge beam (see Section 4.2.4) may have also contributed to eliminating this behavior. Lastly, the specimen did not experience the detachment of the portions of the bottom flange from the web as exhibited by the damaged specimen and the specimen with NSM strips. The confinement and tensile resistance provided by the longitudinal FRP strips that wrapped around the end of the girder helped to strengthen the member against vertical splitting at its end and the failure of the bottom flange. The vertically-oriented sheets above the support bearing also likely contributed to confinement at the end of the member. Based on the test results and above comparisons, it can be concluded that the use of externally bonded FRP is a viable repair technique for prestressed girders with end region deterioration. Furthermore, the chosen details for the repair resulted in behavior superior to that of the control specimen.

4.3.2.2 NSM FRP Repair Specimen

Unlike the externally bonded repair system, the NSM repair system did not adequately restore the behavior of the member to that of the control specimen. Considering the load-deflection response curves for the control, damaged, and NSM specimens in Figure 4.23 and the test data in Table 4.7, the maximum shear force, V_{test}, resisted by the NSM specimen was only 22% of the shear strength of the control specimen. Furthermore, the maximum shear force was only 39% of the shear force carried by the damaged specimen. The initial stiffness of the NSM specimen was also significantly less than that of the control specimen but was similar to the initial stiffness of the damaged specimen.

As noted in Section 4.2.4, the NSM strips installed in the bottom flange of the girder specimen were not engaged due to the failure mode experienced by the member. Therefore, the behavior of the girder essentially represents a member only repaired with mortar. The low strength exhibited by the specimen provides additional information on the potential strengths of members

with deteriorated end regions and emphasizes the need to provide strengthening measures beyond simply restoring the cross section of the girder using a repair material (e.g., mortar).

The NSM specimen failed due to the development of a splitting crack that effectively caused the end of the specimen to separate from the rest of the member. Adequate confinement within the region repaired with mortar, such as that provided by the longitudinal strips that wrapped around the end of the girder in the externally bonded FRP system, is needed to prevent this failure mode. The results indicate that the NSM FRP repair system consisting only of the placement of NSM strips along the vertical and sloped surfaces of the bottom flange is not a reliable repair technique for prestressed girders with end region deterioration. Nevertheless, considering the satisfactory performance of the specimen with externally bonded FRP wrap and the performance of the flexurally-strengthened test specimens with NSM reinforcement tested by Jacobs (2020), it is believed that a hybrid repair system that includes both NSM strips in the bottom flange combined with the confinement, tensile capacity, and stiffness provided by externally bonded FRP sheets is a viable technique for restoring the strength and stiffness of a deteriorated end region. In this hybrid system, any shear strengthening through the use of FRP sheets that is needed within the end region should be considered.

4.3.2.3 Supplemental Diaphragm Repair Specimen

Similar to the NSM FRP system, the supplemental diaphragm repair system was unable to restore the overall behavior of the control specimen. As presented in Figure 4.23 and the test data in Table 4.7, the cracking shear force, V_{cr}, for the specimen with the supplemental diaphragm was 72% of the value of V_{cr} for the damaged specimen due to the crack that developed in the diaphragm as it transferred load to the two bearing pads. The maximum shear forces carried by the specimen with the supplemental diaphragm and the damaged specimen only differed by 1 kip. The values of V_{cr} and V_{test} for the repaired specimen were only 45% and 57% of the corresponding values for the control specimen. However, the initial stiffness of the supplemental diaphragm specimen prior to the reduction in stiffness due to cracking was equivalent to the initial stiffness of the control specimen.

As discussed in Section 4.2.5, the failure of the specimen was characterized by the splitting of the supplemental diaphragm, separation of the diaphragm from the original girder concrete, and rotation of the diaphragm. This resulted in the post-cracking behavior of the specimen more closely

resembling the behavior of the damaged specimen than the control specimen. Consistent with the discussion in Section 4.2.5, the behavior of the specimen with the supplemental diaphragm was a result of the elimination of the original center bearing pad for the load test and the absence of continuous, transverse reinforcement along the bottom of the diaphragm. If the diaphragm were cast continuously between girders in the field and properly detailed, the observed failure behavior would likely be eliminated. Proposed detailing for a continuously cast diaphragm is provided in Chapter 5. While the experimental results indicate the supplemental diaphragm repair system did not adequately restore the behavior of the girder to that of the control specimen, the pre-cracking behavior did demonstrate the same stiffness as the control specimen. With modifications, the repair system could potentially be a viable technique to restore the behavior of prestressed girders with end region deterioration. Further research, however, is needed to assess the viability of this repair system.

4.4 Summary

Five AASHTO Type I girders were loaded to failure according to the experimental program outlined in Chapter 3. One girder in good condition was tested to serve as a control specimen. Another specimen was tested in a damaged state to provide a baseline for the expected behavior of a deteriorated, yet unrepaired, girder. The final three girders were tested after being repaired with either the externally bonded FRP system, the NSM FRP system, or the supplemental diaphragm system described in Chapter 3.

The results and observations from the load tests conducted on the control and damaged specimens influenced the development of the three repair techniques and allowed for the effectiveness of each technique to be established. The comparison of the two specimens indicated that restoring the tensile capacity along the bottom flange of the girder is a key consideration for the development of a successful repair.

The NSM FRP repair system failed prematurely as a result of the formation of a splitting crack in the portion of the web located above the bearing. This behavior emphasized the importance of providing adequate confinement around the repair region when designing repair solutions. In contrast, the externally bonded repair system provided adequate confinement around the repair region and restored the lost tensile capacity, resulting in a shear capacity that exceeded that of the control specimen. Based on these results and observations, it was concluded that the

externally bonded FRP repair system is a viable repair technique for prestressed girders with end region deterioration. Lastly, the specimen with a supplemental diaphragm experienced a premature failure due to inadequate detailing and the elimination of the original bearing pad. Nevertheless, providing a continuous diaphragm between adjacent girders in the field could potentially be a viable solution. The recommendations and conclusions gathered during the experimental program are presented in Chapter 5.

CHAPTER 5. SUMMARY, OBSERVATIONS, CONCLUSIONS, AND RECOMMENDATIONS

5.1 Summary

To assist INDOT in establishing repair techniques for prestressed concrete bridge girders with end region deterioration, an experimental program was conducted. The experimental program focused on developing and evaluating the effectiveness of various repair techniques for prestressed concrete bridge girders with end region deterioration. The three repair techniques examined in this experimental program were (i) an externally bonded FRP system, (ii) a near-surface-mounted (NSM) FRP system, and (iii) a concrete supplemental diaphragm. The main objectives of the two experimental programs included:

1. Evaluating the effects of end region deterioration on the behavior of prestressed concrete bridge girders.
2. Determining effective repair techniques for restoring the behavior of prestressed concrete bridge girders with end region deterioration.
3. Evaluating anchorage details for externally bonded FRP sheets applied to an I-shaped girder.
4. Developing and verifying installation procedures and recommendations for end region repair techniques.

5.2 Conclusions

Based on observations and results from the experimental program, conclusions pertaining to the repair of prestressed concrete bridge girders with end region deterioration were generated. These conclusions are presented below.

1. The deterioration of the end regions of prestressed concrete girders due to leaking expansion joints can result in significant reductions in strength (43% shear strength reduction considering results of the experimental program).

2. Restoring the tensile capacity lost due to deteriorated and ineffective prestressing strands in the bottom flange of prestressed concrete girders is a critical factor when designing end region repair systems. As discussed in Section 3.3.1, the inability of the prestressing strands in the bottom flange to develop tensile forces controlled the failure behavior of the unrepaired specimen. Without adequate tensile capacity in the bottom flange, a diagonal strut could not form between the load and support, resulting in a premature failure mechanism and decreased capacity.

3. Ensuring adequate confinement of the repair region is also a critical factor when designing end region repair systems. End confinement, such as the confinement provided by the longitudinal FRP strips included in the externally bonded FRP repair system, is needed to prevent the premature failure mode observed during the test on the specimen with NSM FRP reinforcement. Providing confinement around the repair region also mitigates some concerns about the condition of the concrete at the repair interface and the resulting bond between the original concrete and mortar used to restore the member cross section.

4. The externally bonded FRP repair system developed for the experimental program proved to be a viable technique for restoring the strength and stiffness of the prestressed concrete bridge girder with end region deterioration. The repaired specimen achieved a greater shear capacity and a greater initial stiffness than the control specimen. Additionally, minimal FRP debonding was observed during testing.

5. The NSM FRP repair system developed for the experimental program did not provide adequate confinement of the repair region, and therefore, the strength and stiffness of the prestressed concrete bridge girder was not restored. The lack of the edge beam on the specimen may have also contributed to the poor performance of the member (see Section 4.2.4). If combined with externally bonded FRP laminate that properly confines the end region, the use of NSM strips may be a viable repair solution.

6. The supplemental diaphragm system developed for the experimental program did not restore the strength of the member. The use of a continuous diaphragm between adjacent girders may provide a viable repair technique for restoring the strength and stiffness of prestressed concrete bridge girders. Suggested details are included in the next section.

5.3 Recommendations

Based on observations and results from the experimental program, recommendations for the design and installation of end region repair techniques were generated. These recommendations are listed below.

1. The use of FRP systems in Indiana for the repair of deteriorated end regions of bridge girders is recommended.
2. When designing repair systems for prestressed concrete bridge girders with end region deterioration, special attention should be placed on restoring tensile capacity in the bottom flange of the girder and providing confinement to the repair area.
3. Considering the success of the externally bonded FRP repair system for restoring the strength and stiffness of the test specimen, similar details as those incorporated into the repair system of the experimental program are recommended when implementing the system in the field. These details include the use of a combination of longitudinal strips and vertical sheets, utilizing FRP spike anchors for the anchoring of both longitudinal and vertical strips/sheets, and wrapping longitudinal strips around the end of the girder. For the vertical sheets, U-wraps should be used where possible.
4. Simply restoring the cross section of a girder with end region deterioration using a repair material (e.g., mortar) is an insufficient technique for recovering the overall behavior of the member. As discussed in Section 4.3.2.2, the low strength exhibited by the specimen with NSM FRP reinforcement emphasizes the need to provide strengthening measures beyond restoring the cross section of the girder.
5. To prevent the premature failure mode observed during the test on the specimen with the supplemental diaphragm, it is recommended a diaphragm be cast continuously between girders. The details described below are suggested with the understanding that tests have not been conducted to verify the resulting performance of the repair system.

Suggested detailing for a continuously cast diaphragm is shown in Figure 5.1. The details of the diaphragm consist of nine reinforcing bars that extend along the length of the diaphragm. Five of the bars are continuous and are installed through the web of the girders. These bars are mechanically spliced halfway between adjacent girders. Although a mechanical splice is preferred,

a lap splice could be used as an alternative if the required lap splice length can be achieved. Two more continuous reinforcing bars are installed below the original bottom surface of the girder and can be spliced as needed. The final two reinforcing bars extend between the bottom flanges of adjacent girders. Closed-cell polystyrene board is placed around and between the bearing pads. Away from the bearing locations, the depth of the diaphragm increases to accommodate the two bars installed below the original bottom surface of the girder. Depending upon the spacing of the girders, multiple bearings may need to be placed between adjacent girders. Pairs of closed stirrups are spaced evenly between the girders. All reinforcing bars in the diaphragm should be epoxy coated.

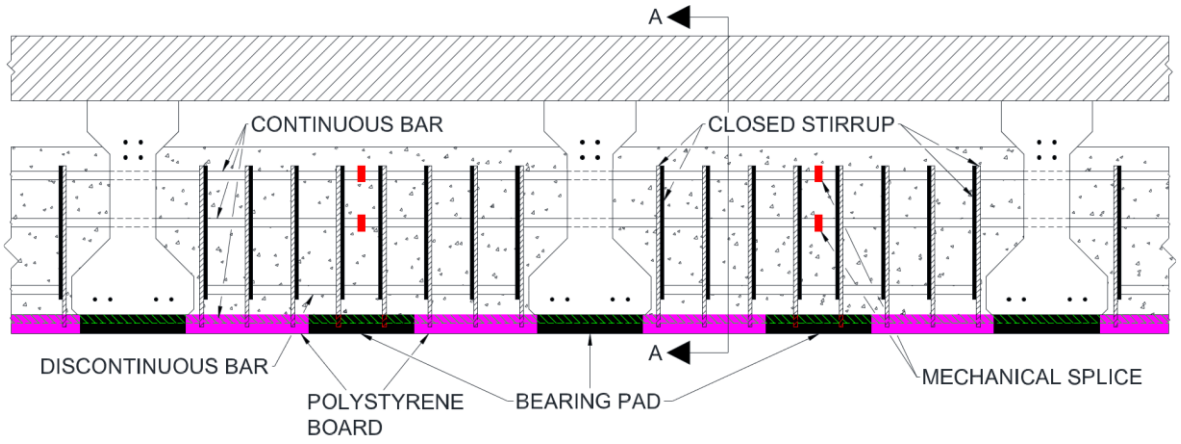

(a) Diaphragm Details

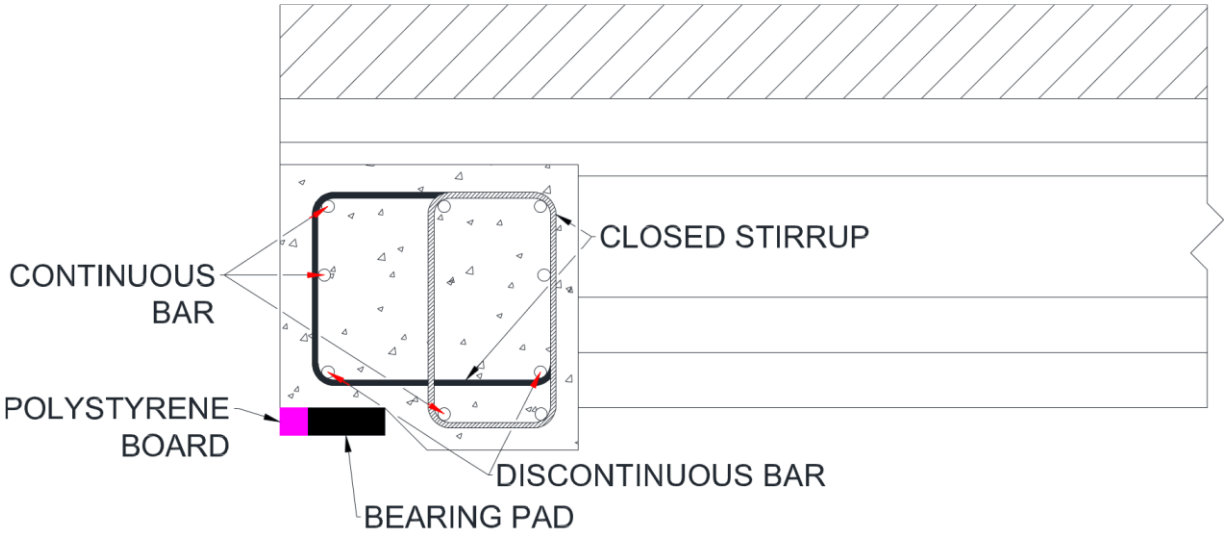

(b) Cross Section A-A

Figure 5.1 Continuous Diaphragm Details

Based on first-hand experience of conducting the end region repairs of the test girders, recommendations were developed for implementing procedures in the field for the repair of girder end regions. These recommendations are listed below.

1. As environmental conditions, such as temperature and humidity, can cause drastic changes in the curing behavior of different materials, a trial batch of the repair material (e.g., mortar) used to restore the cross section of the girder should be cast under similar environmental conditions as those that are expected at the time of the repair. This will provide the installation team a better understanding of the pot life and finish time of the repair material under the expected conditions. The amount of water and set retardant that are used can then be adjusted as necessary for installation.

2. When it is necessary to drill a hole through the entire web for the installation of an FRP spike anchor, the hole should be drilled from both sides of the web to avoid concrete breakout. To ensure that a straight hole is drilled, the following steps outline the recommended drilling procedure:

    i. Using a drill bit with the desired diameter of the hole, drill through the majority of the web, stopping approximately 0.75 in. short of the other side of the web.

    ii. From the same side of the girder, use a smaller diameter drill bit to drill through the remainder of the web. This will indicate the location of the hole on the other side of the girder and greatly reduce concrete breakout.

    iii. From the other side of the girder, use the drill bit with the desired diameter of the hole to finish drilling the hole.

3. When installing FRP spike anchors through the entire width of a member, special care should be taken to ensure that the anchor does not pull the FRP sheet away from the concrete surface. As the anchor is inserted into and pushed through the anchor hole on one side of the member, it should be ensured that the anchor does not snag or catch on the FRP sheet on the other side of the member. Prior to fanning and saturating the anchors, check all edges and surfaces on both sides of the member to ensure the FRP sheet has not shifted during installation of the anchor.

4. When restoring the cross section of a damaged region located overhead, support for the mortar along the bottom surface of the member is recommended. While it is possible to repair overhead sections without supporting some repair materials, sagging and even total failure of the material prior to curing is common. Furthermore, supporting the material in this manner will decrease the repair time, providing more time to achieve an even finished surface.

Recommendations for future areas of research pertaining to the repair of prestressed concrete bridge girders with end region deterioration were also generated. One area requiring further research is the development of an NSM FRP repair system. While NSM systems can be successfully utilized in flexural strengthening applications (Jacobs 2020), no NSM system has been successfully developed for end region repair applications. This may include investigating hybrid-type FRP systems where both NSM FRP strips and externally bonded FRP sheets are used to adequately restore the behavior of damaged end regions. Another concept that requires further investigation is the application of externally bonded FRP systems to complex geometries such as I-shapes. Most of the past FRP research has been performed on beams with simple geometries, such as T-shaped beams. I-shaped members present different challenges than T-shaped members, including thin web sections, frequent and abrupt changes in cross-section geometry, and more complicated anchorage and patch requirements. Therefore, while the results of the experimental program described in this thesis strongly indicate that the externally bonded FRP system that was developed is a viable repair option for I-shaped girders, further research should be conducted to explore details that optimize the resulting structural performance with the ease of implementing the repair.

5.4 Concluding Remarks

The results and observations obtained from the experimental program provided helpful insight for the proper repair of deteriorated end regions of prestressed concrete bridge girders. Of the three repair techniques examined, the externally bonded FRP system was determined to be an effective repair solution for restoring the structural behavior of bridge girders with end region deterioration. While the two other repair techniques did not successfully restore the behavior of the girders, alterations were proposed which may lead to improved performance upon further

investigation. The hope is that the information gathered from this experimental program will increase familiarity with these repair techniques and help facilitate the continued investigation, and ultimately, the successful use of repair systems as a cost-effective solution for extending the service life of bridges.

APPENDICES

APPENDIX A. END REGION REPAIR EXPERIMENTAL PROGRAM EXTERNALLY BONDED FRP REPAIR SYSTEM DETAILS

The following figures provide detailed drawings of the externally bonded system (see Section 3.3.2) with complete dimensions. It should be noted, however, that the 6-in. fan anchors have been removed from the figures below for clarity.

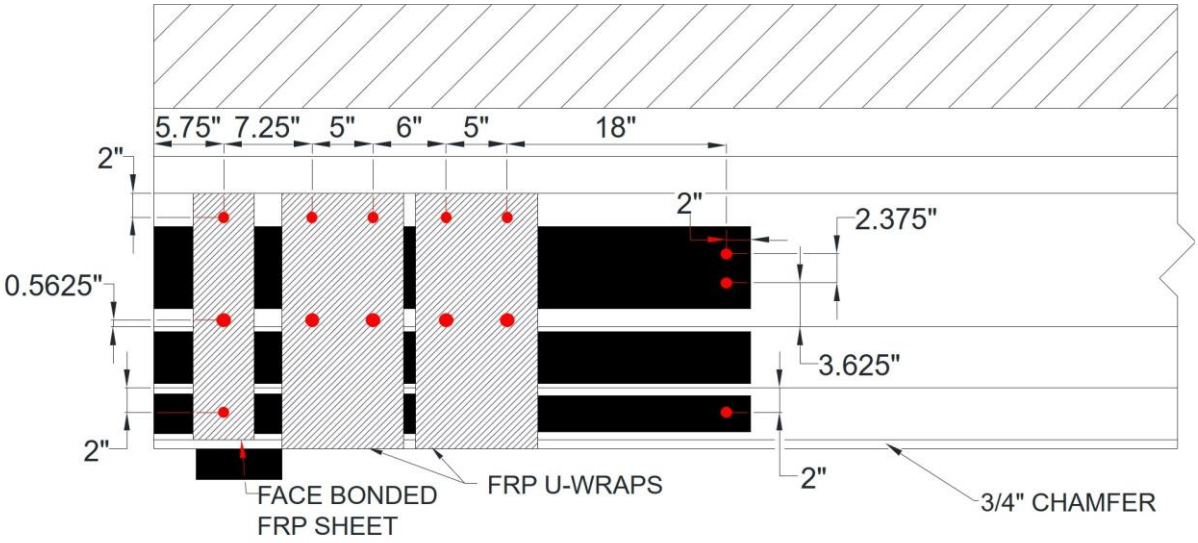

Figure F.1 Externally Bonded FRP Repair System Hole Locations

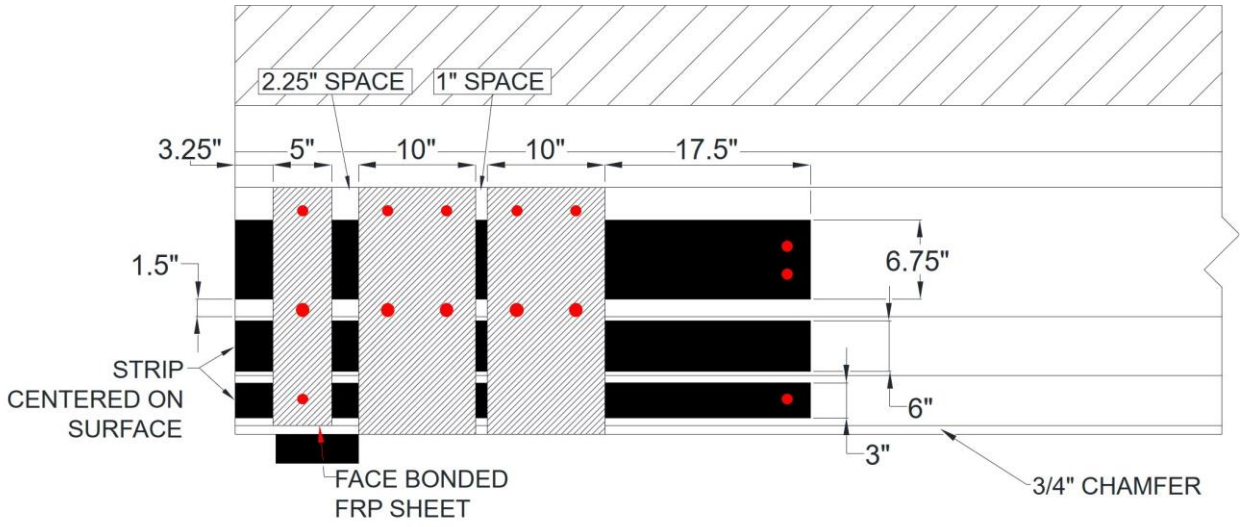

Figure F.2 Externally Bonded FRP Repair System FRP Dimensions

APPENDIX B. SPIKE ANCHOR DESIGN CALCULATIONS

The design procedure and calculations for the FRP spike anchors used in the end region repair experimental program are presented in this appendix. The variable names, procedures, and equations used below follow those developed by Pudleiner (2016).

B.1 Variable Notation and Definitions

A_{Eqv} = equivalent anchor laminate cross-sectional area, in.^{2}

AMR_A = actual anchor material ratio provided (the ratio, by weight, of fiber material in the anchor to the FRP sheet or strip it is developing)

AMR_D = design anchor material ratio (the ratio, by weight, of fiber material in the anchor to the FRP sheet or strip it is developing)

d_e = embedment depth, in.

d_h = diameter of the anchor hole, in.

l_{af} = fan overlap length, in.

n_a = number of rope segments per hole

n_A = number of anchors per FRP sheet or strip

n_l = number of laminate layers in the FRP sheet or strip

R_c = anchor edge chamfer radius, in.

t_f = specified thickness of the FRP laminate being developed, in.

w_f = width of FRP strip, in.

$w_{f,A}$ = anchor tributary width, in.

$\gamma_{s,Exp}$ = expected fiber weight per surface area of the FRP sheet or strip being developed, oz/in.^{2}

$\gamma_{s,Sp}$ = manufacturer-specified dry fiber weight per surface area of the FRP sheet or strip being developed, oz/yd^2

λ_A = manufacturer-specified dry fiber weight of the anchor per length, oz/in.

$\lambda_{A,A}$ = actual weight of the anchor fibers provided per anchor hole, oz/in.

$\lambda_{A\text{-}Req}$ = required weight of the anchor fibers per length, oz/in.

θ_{anchor} = anchor fan angle, degrees

B.2 Anchorage Design Example

The following design example presents the procedure used to design the anchorage details for the anchors installed in the 0.875-in. diameter holes drilled through the entirety of the web (see Section 3.3.2). However, the same general procedure was used to design all the anchorage details used during the experimental program. These anchors were designed to provide anchorage for the 10-in. wide externally bonded U-wraps used in the experimental program.

The material properties of the SikaWrap® – 103 C FRP sheet and the SikaWrap® FX-50 C FRP rope needed to carry out the design calculations are:

- SikaWrap® – 103 C

  Thickness of the FRP laminate, t_f = 0.04 in.

  Specified dry fiber weight of the FRP sheet or strip per surface area, $\gamma_{s,Sp}$ = 18.0 oz/yd^2 = 0.0139 oz/in.^{2}

- SikaWrap® FX-50 C

  Manufacturer-specified dry fiber weight of the FRP anchor per length, λ_A = 0.045 oz/in.

To determine the expected dry fiber weight of the externally bonded U-Wraps, $\gamma_{s,Exp}$, Pudleiner (2016) suggests increasing the specified dry fiber weight, $\gamma_{s,Sp}$, by 25% to account for observed underestimates in the weight of the FRP. However, this underestimate in the weight was not observed with the SikaWarp – 103 C sheets used. Therefore, this factor was neglected, resulting in $\gamma_{s,Exp} = \gamma_{s,Sp}$ = 0.0139 oz/in.^{2}.

As discussed in Section 3.3.2, the design of the externally bonded U-wraps consisted of a single layer (n_l = 1) of FRP, with a sheet width, w_f, of 10 in. Based on the recommendations in Pudleiner (2016), it was determined that two anchors would be used to anchor each U-wrap (n_A = 2). Therefore, the anchor tributary width, $w_{f,A}$, was calculated using Equation B.1.

$$w_{f,A} = \frac{w_f}{n_A} = \frac{10\ in.}{2} = 5\ in. \qquad \textbf{Equation B.1}$$

Next, Equation B.2 was used to calculate weight of the anchor fibers needed, $\lambda_{A\text{-}Req}$, to anchor the U-wrap. Per recommendations from Kim et al. (2012) and Pudleiner (2016), a design anchor material ratio, AMR_D, of 2.0 was assumed. The number of rope segments required per hole, n_a, was then calculated using Equation B.3. Here, a rope segment refers to a piece cut from the continuous FRP rope as received from the manufacturer (SikaWrap® FX-50 C).

$$\lambda_{A-req} = \gamma_{s,Exp}\left(w_{f,A} n_l AMR_D\right) = 0.0139\ oz/in.^2 * 5.0\ in. * 1 * 2.0 = 0.139\ oz/in. \qquad \textbf{Equation B.2}$$

$$n_a = \frac{\lambda_{A-req}}{\lambda_A} = \frac{0.139\ oz/in.}{0.045\ oz/in.} = 3.1\ rope\ segments \qquad \textbf{Equation B.3}$$

Once the number of rope segments needed per hole was established, the actual weight of the anchor provided per hole, $\lambda_{A,A}$, was calculated using Equation B.4. Once the actual weight of the anchor fibers provided per hole was determined, the actually anchor material ratio, AMR_A, was calculated using Equation B.5, and the equivalent anchor laminate cross-sectional area, A_{Eqv}, was calculated using Equation B.6.

$$\lambda_{A,A} = \lambda_A n_a = 0.045\ oz/in. * 3.1\ rope\ segments = 0.139\ oz/in. \qquad \textbf{Equation B.4}$$

$$AMR_A = \frac{\lambda_{A,A}}{n_l \gamma_{s,Exp} w_{f,A}} = \frac{0.139\ oz/in.}{1 * 0.0139\ oz/in.^2 * 5\ in.} = 2.0 \qquad \textbf{Equation B.5}$$

$$A_{Eqv} = t_f AMR_A w_{f,A} n_l = 0.04\ in. * 2.0 * 5.0\ in. * 1 = 0.40\ in.^2 \qquad \textbf{Equation B.6}$$

Finally, the diameter of the anchor hole, $d_{h,}$ was calculated using the equivalent laminate area and Equation B.7. Based on this value, an anchor diameter of 0.875 in. was selected.

$$d_h = \sqrt{\frac{4 * 1.4 * A_{eqv}}{\pi}} = \sqrt{\frac{4 * 1.4 * 0.40\ in.^2}{\pi}} = 0.844\ in. \qquad \textbf{Equation B.7}$$

As discussed in Section 3.3.2, an anchor fan angle, θ_{anchor}, of 60° was used based on recommendations found in Kim (2011) and Pudleiner (2016) as well as its successful application in Jacobs (2020). This fan angle, combined with the number of anchors per sheet and the width of sheet, necessitated that the fan overlap length, l_{af}, be 6 in. for the fan to extend 0.5 in. past the edge of the U-wrap as recommended. Additionally, this was the minimum fan overlap length suggested by Kim et al. (2012). As the anchor holes for the U-wraps were drilled through the entirety of the web, the anchors did not have an embedment depth, d_e. A 0.5-in. anchor edge chamfer radius, R_c, was used based on the recommendations from Quinn (2009), Kim et al. (2012), and Pudleiner (2016).

REFERENCES

AASHTO. (2020). *AASHTO LRFD bridge design specifications* (9th ed.). Washington, DC: American Association of State Highway and Transportation Officials.

ACI Committee 440. (2007). *ACI 440R-07: Report on fiber-reinforced polymer (FRP) reinforcement for concrete structures*. Farmington Hills, MI: American Concrete Institute.

ACI Committee 440. (2017). *ACI 440.2R-17: Guide for the design and construction of externally bonded FRP systems for strengthening concrete structures*. Farmington Hills, MI: American Concrete Institute.

Andrawes, B., Shaw, I. D., & Zhao, H. (2018). *Repair & strengthening of distressed/damaged ends of prestressed beams with FRP composites* (Illinois Center for Transportation Rep. No. FHWA-ICT-18-001). Urbana, IL: University of Illinois at Urbana-Champaign. https://doi.org/10.36501/0197-9191/18-001

ARTBA. (2020). *ARTBA bridge report*. Washington, DC: The American Road & Transportation Builders Association.

ASTM. (2013). *ASTM C928/C928M-13: Standard specification for packaged, dry, rapid-hardening cementitious materials for concrete repairs*. West Conshohocken, PA: ASTM International doi: 10.1520/C0928_C0928M-13

ASTM. (2015). *ASTM C1437-15: Standard test method for flow of hydraulic cement mortar*. West Conshohocken, PA: ASTM International doi: 10.1520/C1437-15

ASTM. (2017). *ASTM C157/C157M-17: Standard test method for length change of hardened hydraulic-cement mortar and concrete*. West Conshohocken, PA: ASTM International doi: 10.1520/C0157_C0157M-17

ASTM. (2017). *ASTM C496/C496M-17: Standard test method for splitting tensile strength of cylindrical concrete specimens*. West Conshohocken, PA: ASTM International doi: 10.1520/C0496_C0496M-17

ASTM. (2018). *ASTM A615/A615M-18: Standard specification for deformed and plain carbon-steel bars for concrete reinforcement*. West Conshohocken, PA: ASTM International. doi: 10.1520/A0615_A0615M-18

ASTM. (2018). *ASTM C266-18: Standard test method for time of setting of hydraulic-cement paste by gillmore needles*. West Conshohocken, PA: ASTM International doi: 10.1520/C0266-18

ASTM. (2020). *ASTM C109/C109M-20B: Compressive strength of hydraulic cement mortars (using 2-in. or [50-mm] cube specimens).* West Conshohocken, PA: ASTM International. doi: 10.1520/C0109_C0109M-20B

ASTM. (2020). *ASTM C39/C39M-20: Standard test method for compressive strength of cylindrical concrete specimens*. West Conshohocken, PA: ASTM International. doi:10.1520/C0039_C0039M-20

ASTM. (2020). *ASTM C42/C42M-20: Standard test method for obtaining and testing drilled cores and sawed beams of concrete.* doi: 10.1520/C0042_C0042M-20

Chennareddy, R., & Taha, M. M. R. (2017). Effect of combining near-surface-mounted and U-wrap fiber-reinforced polymer strengthening techniques on behavior of reinforced concrete beams. *ACI Structural Journal,* 114(3), May-June 2017, 719–728. doi: 10.14359/51689443

De Lorenzis, L., & Teng, J. G. (2006). Near-surface mounted FRP reinforcement: an emerging technique for strengthening structures. *Composites: Part B 38,* October 2006, 119–143. doi:10.1016/j.compositesb.2006.08.003

El-Saikaly, G., Godat, A., & Chaallal, O. (2015). New anchorage technique for FRP shear-strengthened RC T-beams using CFRP rope. *Journal of Composites for Construction,* 19(4). doi:10.1061/(asce)cc.1943-5614.0000530

Federal Highway Administration. (1995). *Recording and coding guide for the structure inventory and appraisal of the nation's bridges* (Report No. FHWA-PD-96-001). Washington, DC: U.S. Department of Transportation.

Federal Highway Administration. (2020). *Select Data.* Charts -LTBP InfoBridge. https://infobridge.fhwa.dot.gov/BarStackChart.

fib Task Group 9.3. (2001). *Bulletin 14: externally bonded FRP reinforcement for RC structures*. european fédération international de béton (*fib*).

Garcia, J., Sun, W., Kim, C., Ghannoum, W.M., & Jirsa, J.O. (2014). *Procedures for the installation and quality control of anchored CFRP sheets for shear strengthening of concrete bridge girders* (Rep. No. 5-6306-01-1). Austin, TX: The University of Texas at Austin: Center for Transportation Research.

Grelle, S. V., & Sneed, L. H. (2013). *Review of anchorage systems for externally bonded FRP laminates*. International Journal of Concrete Structures and Materials, 7(1), 17-33. doi: 10.1007/s40069-013-0029-0

Hughes Brothers. (2011). *Carbon fiber reinforced polymer (CFRP) tape – Aslan^{TM} 500 Series*. Seward, NE: Hughes Brothers, Inc.

ICRI. (2008). *ICRI Guideline No. 310.1R: Guide for surface preparation for the repair of deteriorated concrete resulting from reinforcing steel corrosion.* Saint Paul, MN: International Concrete Repair Institute.

ICRI. (2013). *ICRI Guideline No. 310.2R: Selecting and specifying concrete surface preparation for sealers, coating, polymer overlays, and concrete repair*. Saint Paul, MN: International Concrete Repair Institute.

ICRI. (2016). *ICRI Guide No. 330.2: Guide specifications for externally bonded FRP fabric systems for strengthening concrete structures.* Saint Paul, MN: International Concrete Repair Institute.

INDOT. (1987). *Bridge plans for spans over 20 feet on State Road No. 24* (Project No. MAF-170-1). Indianapolis, IN: Indiana Department of Transportation.

INDOT. (2019). *Indiana Department of Transpiration 2019 strategic plan*. Indianapolis, IN: Indiana Department of Transportation. www.in.gov/indot/files/INDOTStrategicPlan.pdf

Jacobs, R.R. (2020). *Experimental evaluation of flexural strengthening methods for existing reinforced concrete members using fiber reinforced polymer (FRP) systems.* (Master's thesis), Purdue University, West Lafayette, IN. Retrieved from https://hammer.figshare.com/articles/thesis/Experimental_Evaluation_of_Flexural_Strengthening_Methods_for_Existing_Reinforced_Concrete_Members_Using_Fiber_Reinforced_Polymer_FRP_Systems/13420907

Kalfat, R., Al-Mahaidi, R., & Smith, S. T. (2013). Anchorage devices used to improve the performance of reinforced concrete beams retrofitted with FRP composites: state-of-the-art-review. *Journal of Composites for Construction*, 11(1), Jan.-Feb. 2013. 14-33. doi: 10.1061/(ASCE)CC.1943-5614.0000276

Kang, T. H.-K, Howell, J., Kim, S., & Lee, D. J. (2012). A state-of-the-art review on debonding failures of FRP laminates externally adhered to concrete. *International Journal of Concrete Structures and Materials*, 6(2), June 2012, 123–134. doi: 10.1007/s40069-012-0012-1

Khalifa, A., Alkhrdaji, T., Nanni, A., & Lansburg, S. (1999). Anchorage of Surface Mounted FRP Reinforcement. *Concrete International*, 21(10), 49-54. Retrieved from https://www.researchgate.net/publication/251767051_Anchorage_of_Surface_Mounted_FRP_Reinforcement

Kim, S. (2008). *Use of CFRP to provide continuity in existing reinforced concrete members subjected to extreme loads* (Doctoral dissertation). The University of Texas at Austin, Austin, TX. Retrieved from http://hdl.handle.net/2152/17915

Kim, Y. G. (2011). *Shear behavior of reinforced concrete T-beams strengthened with carbon fiber reinforced polymer (CFRP) sheets and CFRP anchors* (Doctoral dissertation). The University of Texas at Austin, Austin, TX.

Kim, Y., Quinn, K., Satrom, N., Garcia, J., Sun, W., Ghannoum, W.M., & Jirsa, J.O. (2012). *Shear strengthening of reinforced and prestressed concrete beams using carbon fiber reinforced polymer (CFRP) sheets and anchors* (Center for Transportation Research Rep. No. 0-6306-1). Austin, TX: University of Texas at Austin. Retrieved from https://ctr.utexas.edu/wp-content/uploads/pubs/0_6306_1.pdf

National Academies of Sciences, Engineering, and Medicine (NASEM). (2011). *Design of FRP systems for strengthening concrete girders in shear*. Washington, DC: The National Academies Press. doi.org/10.17226/14465

Needham, D. E. (2000). *Prestressed concrete beam end repair: final report* (Michigan Department of Transportation Rep No. R-1380). Lansing, MI: Michigan Department of Transportation. https://www.michigan.gov/documents/mdot_c&t_r-1380_67568_7.pdf

Ortega, C. A., Belarbi, A., & Bae, S. W. (2009). Proceedings from the 9th International Symposium on Fiber Reinforced Polymer Reinforcement for Concrete Structures, FRPRCS-9: *End anchorage of externally bonded FRP sheets for the case of shear strengthening of concrete girders*. Sydney, Australia.

Orton, S. L. (2007). *Development of a CFRP system to provide continuity in existing reinforced concrete buildings vulnerable to progressive collapse* (Doctoral dissertation). The University of Texas at Austin, Austin, TX. Retrieved from http://hdl.handle.net/2152/3241

Petty, D. A., Barr, P. J., Osborn, P. G., Halling, M. W., & Brackus, T. R. (2011). Carbon fiber shear retrofit of forty-two-year-old AASHTO I-shaped girders. *Journal of Composites for Construction*, 15(5), 773-781. doi:10.1061/(ASCE)CC.1943-5614.0000208

Pevey, J.M. (2018). *A review of FRP repair and strengthening methods for applications to Indiana bridges.* (Master's thesis), Purdue University, West Lafayette, IN. Retrieved from https://docs.lib.purdue.edu/dissertations/AAI10793809/

Pham, L. T. (2009). *Development of a quality control test for carbon fiber reinforced polymer anchors* (Master's Thesis). The University of Texas at Austin, Austin, TX. Retrieved from http://hdl.handle.net/2152/ETD-UT-2009-12-688

Pilgrim. (n.d.). *Magmaflow Grout-Pak CF*. Tampa, FL: Pilgrim Permocoat, Inc.

Pudleiner, D. K. (2016). *Design consideration based on size effects of anchored carbon fiber reinforced polymer (CFRP) system.* (Master's thesis). The University of Texas at Austin, Austin, TX. Retrieved from http://hdl.handle.net/2152/39031

Quinn, K.T. (2009). *Shear strengthening of reinforced concrete beams with carbon fiber reinforced polymer (CFRP) and improved anchor details.* (Master's thesis), The University of Texas at Austin, Austin, TX. Retrieved from http://hdl.handle.net/2152/ETD-UT-2009-12-508

Ramseyer, C., & Kang T. H.-K. (2012). Post-damage repair of prestressed concrete girders. *International Journal of Concrete Structures and Materials*, 6(3). doi: 10.1007/s40069-012-0019-7

Rapid Set. (2018). *Mortar mix: high-strength structural repair mortar product datasheet*. Garden Grove, CA: CTS Cement Manufacturing Corp.

Shekarchi, W. A. (2016). *Shear behavior of reinforced concrete bridge pile cap girders strengthened with carbon fiber reinforced polymer (CFRP) strips and CFRP anchors* (Doctoral dissertation). The University of Texas at Austin, Austin, TX. Retrieved from http://hdl.handle.net/2152/41611

Shekarchi, W.A., Pudleiner D.K., Alotaibi, N.K., Ghannoum, W.M., Jirsa, J.O. (2020). Carbon fiber-reinforced polymer spike anchor design recommendations. *ACI Structural Journal*, 117(6). doi: 10.14359/51728065

Shield, C., & Bergson, P. (2018). *Experimental shear capacity comparison between repaired and unrepaired girder ends* (Minnesota Department of Transportation Rep No. MN/RC 2018-07). Minneapolis, MN: University of Minnesota. http://www.dot.state.mn.us/research/reports/2018/201807.pdf

Sika Corporation. (2015). *Product data sheet Sikawrap® FX-50C: carbon fiber rope for structural connection and anchoring of Sikawrap® strengthening systems* (Edition 5.16.2015). Lyndhurst, NJ: Sika Corporation.

Sika Corporation. (2018). *Product data sheet Sikadur®-300: high-modulus, high-strength, impregnating resin* (Version 01.01). Lyndhurst, NJ: Sika Corporation.

Sika Corporation. (2018). *Product data sheet Sikadur®-330: high-modulus, high-strength, impregnating resin* (Version 03.01). Lyndhurst, NJ: Sika Corporation.

Sika Corporation. (2019). *Product data sheet Sikawrap® Hex-103C: carbon fiber fabric for structural strengthening* (Version 01.04). Lyndhurst, NJ: Sika Corporation.

Unitex. (2018). *Technical data sheet Pro-Poxy® 400 epoxy gel anchor*. Miamisburg, OH: Dayton Superior.